IMPACT IONIZATION PROCESSES AND DEEP CENTRES IN ZnSe AND ZnS

A thesis presented by

Nan Ding (BSc, MSc)

to the

University of St. Andrews

in application for the degree of

Doctor of Philosophy

April, 1992

DECLARATION

I hereby certify that this thesis has been composed by me, and is a record of work done by me, and has not previously been presented for a higher degree.

The research was carried out in the Wolfson Institute of Luminescence within the School of Physical Sciences in the University of St. Andrews under the supervision of Professor J. W. Allen.

Nan Ding

CERTIFICATE

I certify that Nan Ding has spent nine terms at research work in the Wolfson Institute of Luminescence within the School of Physical Sciences in the University of St. Andrews under my direction, that she has fulfilled the conditions of the Resolution of the University Court, 1967, No.1, and that she is qualified to submit the accompanying thesis in application for the degree of Doctor of Philosophy.

Professor J. W. Allen
(Research Supervisor)

CAREER

I first matriculated in the Physics Department of Beijing Normal University, P. R. China, in September 1981. In July 1985, I graduated with the degree of Bachelor of Science in Physics and in September of the same year I matriculated in the Physics Department of Beijing Normal University again. In July 1988, I obtained the degree of Master of Science in Physics.

In December 1988, following the ORS Award and the University Scholarship, I was enrolled as a research student in the University of St. Andrews under the Resolution of the University Court, 1967, No.1, as a candidate for the degree of Doctor of Philosophy.

ACKNOWLEDGEMENTS

First of all, I would like to express my sincere thanks to my supervisor Professor J. W. Allen for his invaluable guidance, continuous encouragement and help throughout this work.

I wish to thank the Committee of Vice-Chancellors and Principals of the Universities of the United Kingdom for the ORS Award, and the University of St. Andrews for the University Scholarship. Their financial supports enabled me to undertake the work for this project.

I would also like to thank my colleagues, Dr. Jiazhen Zheng and Mr. Jorma Talas, for their help and advice at work.

I like to thank all my friends who have been giving me a wonderful time in St. Andrews. Their friendship stimulated me to fulfil my work.

Finally, I own debts of gratitude to my husband and my parents for their encouragement and understanding over the last few years.

ABSTRACT

We have re-examined theoretically and experimentally the theories of two-stage impact ionization and band-to-band impact ionization. It is found that there is not much difference in the variations of the multiplication with electric field in the two theories. They are both very rapid multiplication processes with electric field when the thresholds are reached. However, the multiplication process could be controlled in some materials with special band structures and special state density distributions. For the two-stage impact ionization process to be measurable, the deep centre concentration is required to be at least as high as 10^{19} cm^{-3}. Experimentally, the behaviour of the photocurrent has been investigated over a wide range of electric fields on various ZnSe samples. The photoconductivity process with recombination at lower fields has been identified. One multiplication process was observed in our samples at higher fields. It is attributed to the band-to-band impact ionization.

We have investigated the deep levels in Co-doped ZnSe and in MOCVD grown epitaxial ZnS by junction techniques. By comparing with the data in the literature, four unintentionally-doped deep levels (labelled L1, L2, M, L4 respectively) in ZnSe and a deep level (labelled M') in ZnS have been characterized by their distinctive photoionization cross-section spectra. The identification of the self-activated luminescent centres in ZnSe and ZnS with those deep centres found by junction techniques is further made by the comparison of the optical quenching spectra, the photoionization cross-section spectra and the relevant EPR results. We have better understood the optical quenching process in terms of hole transfer between different centres when many deep levels are present in the same sample.

The heterojunction interface between n-ZnSe epilayer and n-GaAs substrate was studied by conventional I-V and C-V measurements. An insulating layer has been found at the interface. Its thickness increases with the increase of the annealing temperature.

CONTENTS

page

Chapter 1

Introduction

This thesis is concerned with the mechanisms of electroluminescence in semiconductors and the deep levels in the wide band-gap II-VI semiconductors. In this chapter some relevant background information is introduced, combined with an introduction to the structure of this thesis.

1.1 Electroluminescence in semiconductors

The first observation of electroluminescence was obtained in silicon carbide (SiC) by Round in 1907 [1]. However, in 1936 the useful electroluminescence device was first achieved by Destriau [2]. He discovered that light could be generated by applying an alternating voltage to a layer of insulator in which a luminescent material, usually ZnS doped with copper, had been embedded. Since that time, the phenomenon of electroluminescence eventually attracted a great interest for physicists and manufacturers. A lot of effort has been made in the investigation of the mechanisms of electroluminescence and its applications.

The mechanisms of electroluminescence in a solid are various. Different mechanisms raise different requirements for device materials and device designs. One is in light-emitting diodes (LED's) with a pn junction. When carriers are injected across a forward-biassed pn junction, the current can cause the injection of minority carriers into the regions of the crystal where they can recombine with majority carriers, resulting in the emission of recombination radiation. This effect is called carrier injection electroluminescence.

Since the first light emitting pn junction appeared in 1952, it has provided an important application of devices as generators of light. In 1968, the first integrated solid-state displays appeared on the market. Nowadays the name of

"semiconductor laser" is not unfamiliar for people as compact disks (CD), played with an infrared GaAs laser, are becoming more and more popular. Many applications of carrier injection electroluminescence have been developed in displays, optical communications and other areas. However, the visible electroluminescence efficiency of these devices is still low. This, and the expensive cost of large devices limit visible LED's to be acceptable only for simple displays but not for illumination.

At present, most commercial colour LED's and semiconductor lasers are made of III-V compounds, such as $GaAs_{1-x}P_x$ or $Al_xGa_{1-x}As$. The emitting photon energy can be varied by changing the composition x, but is finally limited by the biggest band-gap of these solid solutions. For the $GaAs_{1-x}P_x$ system, when x is small, the colour can be changed simply by changing x; when x is bigger than 0.44, the band-gap becomes indirect and an impurity, such as N, has to be incorporated to increase the radiative efficiency. For the II-VI compounds, such as ZnSe and ZnS with a wider band-gap which blue LED's require, it is difficult to produce p-type materials. Therefore, so far this carrier injection mechanism has not been commercially applied in these materials.

Another mechanism acts in the high-field-thin-film electroluminescence devices. These devices have a sandwich structure consisting of a thin phosphor layer, usually ZnS: Mn, in the centre, coated with two thin insulating layers on both sides, followed by two conducting films on the two resulting sides, finally bound with glass plates outside. They are driven with a high ac voltage, for example, 200 V and 400 Hz. The electrons are first released from the interface between the insulating layer and the phosphor layer, then are accelerated at the high electric field. The accelerated electrons with energy between 2 eV and 3 eV give up their kinetic energy to the luminescent centre Mn by exciting an electron from the Mn ground state to its first excited state. This process is called the impact excitation process. When the excited

electrons return from the excited state to the ground state, orange-yellow light is emitted.

These devices were first successfully produced by Inoguchi in 1974 [3]. They were found to have a longer lifetime, better brightness and stability than the previous dc high-field electroluminescence powder panel, usually ZnS: Cu. The cheap cost of ZnS makes large area displays feasible. However, choosing a suitable luminescent centre is very important in the production of devices with a wide range of colour. At present, the commercial production of high-field electroluminescence devices is mainly based on ZnS: Mn and ZnS: Cu.

Electroluminescence has also been observed from metal-insulator-semiconductor (MIS) structures, eg Al-oxide-ZnSe (n-type), when the MIS diode is driven in either forward bias or reverse bias [4,5]. The "forward bias" and "reverse bias" here correspond to the metal biassed positively and negatively. The mechanism of electroluminescence for a reverse-biassed MIS diode is interpreted [5] in terms of an impact ionization process. That is: electrons hop from the metal through the defects in the insulating layer into the n-type semiconductor, eg n-ZnSe, then gain kinetic energy by being accelerated at the high electric field in the depletion layer. The hot electrons impact ionize electrons from the valence band to the conduction band. The following recombination may give off radiative emission. The mechanism of electroluminescence for a forward-biassed MIS diode is still not well understood. Several possibilities have been proposed in the literature [4,5,6,7,8]. Among them, the more likely interpretation [8] is that the electrons tunnel from the valence band of ZnSe to the metal by hopping through defects or impurity centres in the insulator so that the holes, which are required for the recombination radiation, are left behind in the semiconductor near the interface. Since the electroluminescence efficiency and stability of MIS structures is very poor, the study of them still remains at the experimental stage.

Nowadays, with more advanced growth techniques, such as metalorganic chemical vapour deposition (MOCVD) and molecular beam epitaxy (MBE), efforts are being made to make better visible LED's, especially blue LED's, using eg ZnSe or ZnS, so far not with great success. In the meantime, new mechanisms are being sought. It has been known that the impact processes, for instance, the impact excitation process and the impact ionization process, produced by hot carriers can produce the carrier production which the high-field electroluminescence requires. Our interest is then encouraged in the further investigation of the impact ionization processes.

1.2 Impact ionization processes in a solid

In analogy with gas discharge lamps or fluorescent tubes, in a solid the energetic electrons can give up their energy by the impact ionization processes.

The band-to-band impact ionization is well known by the avalanche breakdown phenomenon. In this process, the electrons are impact ionized directly from the valence band to the conduction band. Then the created electron-hole pairs can recombine radiatively through some centre. The theories of band-to-band impact ionization of Wolff [9], Shockley [10] and Baraff [11] have been used to quantify experimental observation in many materials. The band-to-band impact ionization cross-section can be very large so that the current increases extremely rapidly with voltage when the band-to-band impact ionization occurs. Therefore, special circuits or structures are required for stable operation, and the field, 1-10 $MVcm^{-1}$, can in the long term damage materials with an ionic component in their bonding.

Another similar process whose possibilities were first investigated by Livingstone and Allen [12] in 1973 is the two-stage impact ionization process. In this process, an incident hot carrier ionizes a deep centre by an electron transition to the conduction band, and then another hot carrier raises an

electron from the valence band to the deep centre. The total effect is to produce free electrons and holes. Appreciable carrier generation by this process is expected to occur at fields lower than those required for band-to-band impact ionization. In addition, the current increase with voltage is also expected to be less steep than those by the band-to-band impact ionization. These features were observed in ZnSe: Mn diodes with a Schottky contact by Livingstone and Allen [12]. Thompson [13] did similar experiments in ZnS.

However, because the relevant path-lengths for carriers to gain high energy are small, according to the two-stage impact ionization model proposed by Livingstone and Allen [12], the concentration of luminescent centres must be high and eventually a limit is set by solubility or concentration quenching. To counter these factors, a large impact ionization cross-section of the deep level is also required.

In chapter 2, two theories of the band-to-band and the two-stage impact ionization processes are reviewed. The multiplication equations derived from the two theories are compared. The possibilities of these two impact ionization processes taking place are discussed in detail. Experimentally, the behaviour of the photocurrent in ZnSe was measured in a wide range of electric fields (from 10^4 Vcm^{-1} to 10^5 Vcm^{-1}). It is found that the required deep level concentration for two-stage impact ionization is very high, at least greater than $1*10^{19}$ cm^{-3} when the thickness of the active layer is of order of 1μm. This is difficult to be realised generally by doping impurities, for instance the transition-metal impurities, because of their solubility, although the manganese impurity can be doped in very high concentration, for example 30% Mn, in ZnSe. For the unintentionally-doped deep centres in ZnSe and ZnS, the reletvant information, for example, their concentrations, energy levels and so on, is limited. This then turned our interest to the field of deep centres in ZnSe and ZnS.

1.3 Deep centres in semiconductors

Semiconductors are the backbone of the electronic industry because their properties can be manipulated over wide ranges through the control of impurities and other imperfections. Shallow impurities introduce minor perturbations in the crystal and generally contribute extra charge carriers, electrons or holes. Their role, therefore, is mainly to control the type and magnitude of conductivity. Other impurities and a variety of lattice defects constitute a more severe local perturbation, and give rise to bound states which are more localized, and often have energies deep in the band-gap. They are called deep centres.

Unlike shallow impurities, deep centres often behave as carrier traps or recombination centres. Thus deep centres can control the lifetime of charge carriers. In devices where carriers must have a long life-time, eg solar cells, they are undesirable. When the carrier concentration needs to be reduced sharply in time, as in a fast switch, they are useful. In addition, luminescent deep centres are used in making light-emitting diodes.

In addition to shallow impurities and deep centres, a semiconductor may contain extended defects, such as dislocations, grain boundaries, stacking faults or precipitates. The dislocations and stacking faults are quite common at lattice mismatched heterojunction interfaces. Though these defects sometimes affect the electrical properties of the crystal in the same way as deep centres, they generally have a more peculiar effect on the more microscopic properties. Thus, all types of imperfections have both useful and detrimental features.

The microscopic properties and the role of shallow impurities were already quite well understood by the end of the 1950's through a combination of the theory (effective-mass theory) and experiments (primarily electrical conductivity and optical absorption) in silicon and germanium. Deep centres

and extended defects, on the other hand, proved far more difficult to investigate. The study of deep centres in semiconductors has been an important field in semiconductor physics.

In the field of deep centres, an advance in the development of experimental techniques was the development of junction techniques around 1970. The key feature of these techniques is their ability to decouple deep centres from the shallow dopants and focus on signals arising from deep centres only. In addition, junction measurements can determine many important physical parameters of deep centres, for instance, the concentration, ionization and capture cross-sections, and energy levels of deep centres even when several centres are present in the same sample.

Since the semiconductors ZnSe and ZnS have direct band-gaps of 2.7 eV and 3.7 eV at room temperature, in principle they can provide a wide spectral range of visible light up to ultra-violet light. So they are potential materials for optoelectronic devices. However, at present, because of the presence of unintentionally-doped deep centres, the emission bands from these two materials are mainly in the energy range much less than their band-gaps. A lot of work has been done in the investigation of deep levels in ZnSe by junction techniques. However, the understanding and the analysis of what has been obtained by those experiments are not always easy and obvious. The development of the understanding of the characteristic photoionization cross-section spectrum of the M-centre in ZnSe is an example. It is described in more detail in chapter 3. On the other hand, the presence of unintentionally-doped deep levels could make the analysis of intentionally-doped impurities difficult.

In chapter 3, as an example, the deep levels in a Co-doped bulk ZnSe sample have been investigated by dual-light steady state (DLSS) photocapacitance measurements, which is one of the junction techniques. The peculiar advantage of the DLSS photocapacitance method in the study of

the case of many deep levels is shown in this chapter. Four unintentionally-doped deep centres (labelled L1, M, L2, L4) and two deep centres (one is labelled L3, the other is the Co d^7 ground level) related to the cobalt impurity are characterized by their individual photoionization cross-section spectra by analysing the results obtained in our work and in the literature.

Chapter 4 describes the photocurrent studies of deep levels in ZnS grown by MOCVD. A deep centre, i.e. the M'-centre, is found. Its characteristic hole photoionization cross-section spectrum is in strong analogy with that of the M-centre in ZnSe.

Since several deep centres have been found in ZnSe and ZnS by junction techniques and several luminescent centres have been found in the same materials by photoluminescence measurements, one would like to identify those centres or associate them with each other. In chapter 5, the identification and association of deep levels in ZnSe and ZnS are tentatively done by the analysis of the optical quenching spectra, photoionization cross-section spectra and the relevant EPR results, obtained in our work and in the literature.

The appearance of non-equilibrium crystal growth techniques, such as MOCVD and MBE, has brought a new age of application of semiconductor devices. These techniques allow the improvement of crystal qualities and new device designs to be realized, such as the multiple-quantum-well epilayer system. However, the lattice mismatched heterojunctions raise very important problems to be faced in this area. In chapter 6, the nonlinear I-V characteristics of n-ZnSe/n-GaAs heterojunctions grown by MOCVD are investigated with conventional I-V and C-V measurements.

Finally, a summary of the conclusions in chapter 2 to chapter 6 is presented in chapter 7 in order to outline the main contribution of this thesis. Future work is also prospected.

Chapter 2

Impact ionization processes in zinc selenide

2.1 Introduction

One of the very important applications for solid state physics is to find ways of producing light efficiently by passing electrical current through a solid. At present this can be done by the injection of minority carriers at a forward-biassed pn junction, for example GaAs LED's or $Al_xGa_{1-x}As$ LED's. However, the wavelength of the visible light emitted from the III-V compound pn junction LED (light emitting diode) is limited by its band-gap. Although more efforts are being made to extend to shorter wavelength by using wide band-gap materials, eg. ZnSe and ZnS, it is still difficult to produce a good p-type ZnSe or ZnS, even employing advanced growth techniques such as MOCVD or MBE.

Another approach is to use impact processes produced by hot carriers to realize the carrier reproduction. It is known that in a semiconductor under an electric field electrons and holes gain energy as they move along the direction of the field. At low fields this gain can be balanced by loss via various scattering mechanisms. In this case the movement of electrons is described by the formulas $\mathbf{J}=nq\mathbf{v}$ and $\mathbf{v}=\mu\mathbf{E}$ where $\mathbf{v}$ is the vector of drift velocity, $\mathbf{E}$ is the vector of electric field and μ is the mobility. In general, the most significant scattering mechanisms are lattice collisions (optical and acoustic phonon scattering) and ionized impurity scattering. At high fields (typically greater than $10^3\ Vcm^{-1}$ depending on the material) the drift velocity becomes independent of the electric field. As the electric field increases further some electrons gain energy from the field at a faster rate than they are scattered. Electrons may accumulate energy of a few eV, which can be bigger than the band-gap of the semiconductor, by being accelerated through a certain distance

in the field. Such an energetic electron may impact ionize an electron from the valence band to the conduction band. This process is the well-known avalanche breakdown in a solid in analogy with the Townsend breakdown in gases. It has been found in many semiconductors, eg. silicon, germanium, gallium asenide and gallium phosphide, at fields greater than 10^5 Vcm^{-1}. If there are enough deep centres within the band-gap, Livingstone and Allen [12] in 1973 first proposed that another process can occur. In this, one hot electron could impact ionize an electron from a deep centre to produce a new conduction band electron in one step. Another hot electron may then impact ionize a valence band electron into the resulting empty deep centre in another step. This is called here the two-stage impact ionization via deep centres. Because the threshold energy required for two-stage impact ionization is obviously less than that for band-to-band impact ionization, the two-stage impact ionization could be a potential hole-production mechanism in n-type semiconductors. The band-to-band and the two-stage impact ionization processes are shown diagrammatically in Fig.2.1. Another familiar process is that of impact excitation of a luminescent centre in commercially-available ZnS: Mn electroluminescent devices, wherein the electron located in the ground state of a luminescent centre can be excited by a hot electron to the excited state. In both theoretical and technological aspects, more research needs to be done in the investigation of the impact ionization processes and behaviours, at high fields, of the ZnSe semiconductor with the wide band gap, taking into account the band structure.

In previous work, Livingstone and Allen [12] saw an increase in photocurrent in bulk ZnSe: Mn Schottky diodes at lower fields followed by another steep increase in photocurrent at higher fields. The former increase was attributed to a two-stage impact ionization via deep level manganese impurities [14]. The steep increase was explained as the band-to-band impact ionization. They also worked out a phenomenological theory of the two-stage

impact ionization. Thompson [13] also saw two rises in photocurrent in bulk ZnS Schottky diodes. However, some of his interpretations seem not to be consistent. This will be further discussed in section 2.5 of this chapter. Both Livingstone and Allen and Thompson emphasized the difficulty of making reproducible measurements.

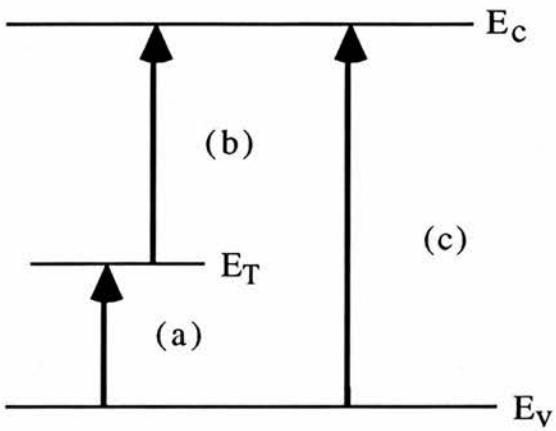

Fig.2.1: The two-stage impact ionization process consists of (a) and (b) via the deep level E_T. The band-to-band impact ionization process is (c).

In this chapter, the two theories of the two-stage and the band-to-band impact ionization processes are reviewed and the multiplication equations derived from the two theories are compared. Experimentally, more detailed measurements were performed on the various ZnSe samples such as epilayer and bulk samples. The electronic behaviours and impact ionization processes of ZnSe in the wide range of electric fields used (from 10^4 Vcm^{-1} to 10^6 Vcm^{-1}) were investigated. The possibilities of the two-stage or the band-to-band impact ionization processes are discussed.

2.2 The background theories

In experiments, the two multiplicative processes are expected to be observed. However, in order to determine if a multiplicative process is due to

two-stage impact ionization or band-to-band impact ionization, first of all, it is necessary to distinguish theoretically the features governed by the different processes.

2.2.1 The theory of the band-to-band impact ionization

McKay [15] has applied a modified form of the Townsend discharge theory for gases to the multiplicative breakdown by band-to-band impact ionization in silicon junctions. Following the notation of McKay, for a Schottky diode as shown in Fig2.2, n_0 is the number of electrons at the edge of the depletion layer at x=0, n_1 is the number of electron-hole pairs produced by an electron between 0 and x, n_2 is the number of electron-hole pairs produced by an electron between x and W. By definition, α is the number of pairs generated in unit length by an electron, similarly β is the number of pairs generated in unit length by a hole. Assume that the loss of carriers in the depletion layer by recombination is negligible and mutual interactions between carriers are negligible too. Then the number of electrons produced between x and x+dx is

$$dn_1=(n_0+n_1)\,\alpha\,dx + n_2\beta\,dx$$

$$\Rightarrow \quad dn_1=(n_0+n_1)(\alpha-\beta)\,dx + (n_0+n_1+n_2)\,\beta\,dx\,. \qquad (2.1)$$

This is integrated with the boundary conditions $n_1=0$ at x=0 and $n_2=0$ at x=W. One then obtains the general expression for the electron multiplication process as following

$$1-\frac{1}{M_n} = \int_0^W \alpha \exp\left[-\int_0^x (\alpha-\beta)\,dx'\right]dx \qquad (2.2)$$

where $M_n=(n_0+n_1+n_2)/n_0$ is the electron multiplication factor. A similar expression for the multiplication initiated by holes can be obtained if α and β are interchanged and M_n is replaced by M_p. In a reverse-biassed Schottky diode made on n-type semiconductors, when it is illuminated with the light

of photon energy greater than the band-gap so that the absorption is mainly at the edge of the depletion layer, the multiplication process is mainly initiated

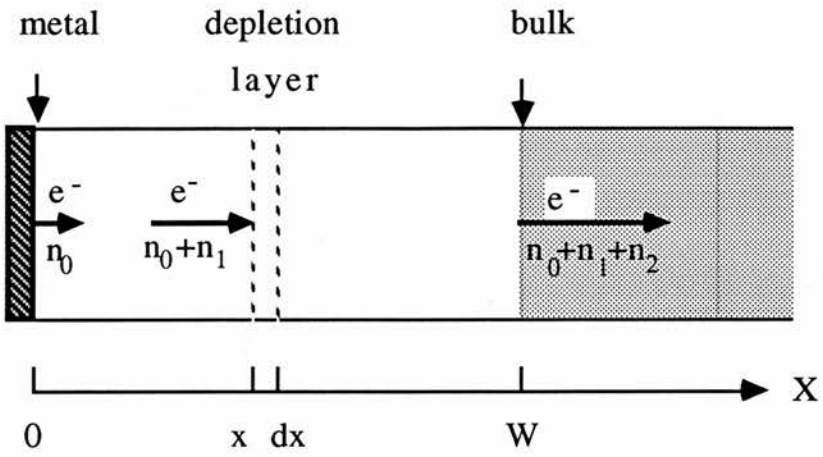

Fig.2.2: The band-to-band impact ionization process in a Schottky diode.

by electrons. So we only consider the electron multiplication process here. For different materials, it has been found that the ionization rates α and β could be very different. For instance, electrons have from three to thirty times the ionization rate of holes in silicon [16,17,18], whereas holes have from two to four times the ionization rate of electrons in germanium [19]. In GaAs [20,21,22] and GaP [23], electrons have approximately the same ionization rate as holes. Because the hole diffusion length L_p in ZnSe is very small it is practically very difficult to realize a pure hole-initiated multiplication process [24]. So far there are not reliable measurements of the ionization rate of holes for ZnSe.

If we suppose $\beta=0$ and α=constant, then equation (2.2) can be simplified as

$$1-\frac{1}{M_n}=\int_0^W \alpha \exp(-\alpha x)\, dx\,,$$

then

$$M_n= \exp(\alpha W)\,. \qquad (2.3)$$

If we suppose $\alpha=\beta$, then equation (2.2) becomes

$$1-\frac{1}{M_n}=\int_0^W \alpha\, dx\,. \tag{2.4}$$

The form of α has to be known before this integral can be evaluated.

The first theoretical calculation of the electric field dependence of the ionization rate was carried out by Wolff [9]. He solved the Boltzmann equation for high fields considering the emission of optical phonons and impact ionization as scattering processes. He assumed that the charge carriers gain energies until some reach the ionization threshold step by step. Then he obtained the equation

$$\alpha=\alpha_0 \exp(-E_0^2/E^2) \tag{2.5}$$

where α_0 is a constant and E_0 is the impact ionization parameter. On the other hand, Shockley [10] assumed that some of the electrons can be accelerated to the ionization energy during one free path. Shockley considered only the high energy charge carriers of the distribution tail and obtained

$$\alpha=\alpha_0 \exp(-b/E) \tag{2.6}$$

where b is now the impact ionization parameter. Baraff [11] proved that these two equations were limiting cases of the general solution. The values of α_0 in equations (2.5) and (2.6) are not necessarily equal, and it is not obvious which form for α should apply.

For a Schottky diode, the position dependence of the electric field is

$$E(x)=-E_{max}\left(1-\frac{x}{W}\right) \tag{2.7}$$

where

$$E_{max}=\frac{2(V+V_d)}{W},$$

E_{max} is the maximum of electric field, W is the width of the depletion layer, V_d is the built-in barrier potential, and V is the applied voltage. Substituting equations (2.6) and (2.7) into equation (2.4), we have

$$1-\frac{1}{M_n}=\alpha_m W_{eff} \tag{2.8}$$

where

$$\alpha_m=\alpha_0 \exp(-\frac{b}{E_{max}}), \tag{2.9}$$

$$W_{eff}=\int_0^W \exp(-\frac{x}{W-x}\frac{b}{E_{max}})\,dx. \tag{2.10}$$

Moll [18] has tabulated values of W_{eff} as a function of E_{max} for various values of the parameter b.

2.2.2 The theory of the two-stage impact ionization

The theory of the two-stage impact ionization was first proposed by Livingstone and Allen [12]. It was based on a simple model which relates the impact ionization parameters of deep centre to the multiplication. The theory that is relevant to the present work is outlined below.

First of all, let us consider a region of semiconductor of width W containing a uniform electric field E. It is supposed that an electron flux, with current density I_0, enters the region by some injection mechanism and that an electron flux with current density $I \equiv M_n I_0$ leaves the region, where M_n is by definition the electron multiplication factor. For simplicity, the notation M is used instead of M_n for the same concept below. In the steady state, there must be a hole current of magnitude $I - I_0$ at the first boundary, as shown in Fig.2.3, in order to maintain current continuity. It is clear that the excitation of deep centres cannot of itself lead to steady-state current multiplication if transitions

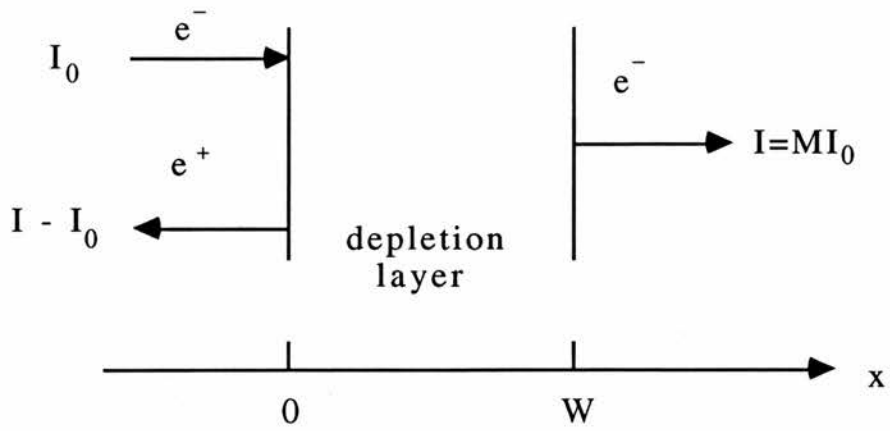

Fig.2.3: The electron and hole currents at the boundaries of the depletion region.

involve only one band, eg. impact ionization to the conduction band followed by recombination from the conduction band. Multiplication requires a two-stage transfer of electrons from the valence band to the conduction band via the deep centre. The four processes of generation and recombination via one deep centre are shown in Fig.2.4.

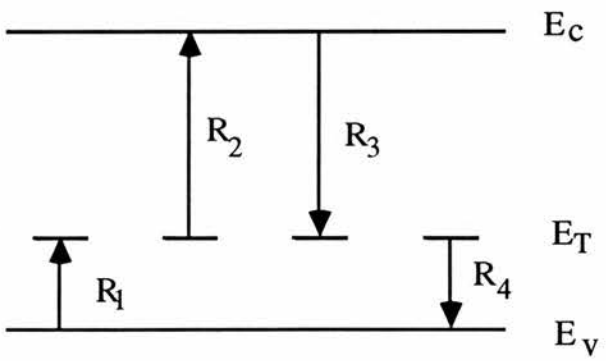

Fig.2.4: The four processes of generation and recombination via one deep centre.

For simplicity, we assume that the energies involved are sufficiently large for thermal processes to be negligible, that impact ionization is by electrons

alone, and that the electrons have a constant drift velocity v_n while the holes have a constant drift velocity v_p. Then the rate R_1 at which electrons in unit volume are raised from the valence band to the deep centre in unit time is

$$R_1=n\sigma_1 v_n(N_T-n_T) \tag{2.11}$$

where σ_1 is the impact ionization cross section, n is the density of free electrons, N_T is the concentration of deep centres, and n_T is the concentration of the filled deep centres. A corresponding relation holds for R_2. The rates R_3 and R_4 for recombination can be written in a similar form, with σ_3 and σ_4 being recombination cross sections. In the steady state, the rate of filling deep centres must equal to the rate of emptying, hence

$$nv_n(\sigma_1+\sigma_3)(N_T-n_T)=(nv_n\sigma_2+pv_p\sigma_4)n_T\,. \tag{2.12}$$

Current continuity requires that

$$I=I_n+I_p=qnv_n+qpv_p \tag{2.13}$$

where I, the total current, has electron and hole components I_n and I_p. Thus equation (2.12) can be written as

$$n_T=N_T\frac{\sigma_1+\sigma_3}{(\sigma_1+\sigma_2+\sigma_3-\sigma_4)+\sigma_4 I/I_n}\,. \tag{2.14}$$

The rate of flow of electrons from the valence band to the conduction band due to the ionization processes involving deep centres is

$$\frac{\partial n}{\partial t}=nv_n\sigma_1(N_T-n_T)-pv_p\sigma_4 n_T. \tag{2.15}$$

Since the continuity equation for electrons is

$$\frac{\partial}{\partial x}(nv_n)=\frac{\partial n}{\partial t}, \tag{2.16}$$

and the drift velocity v_n is assumed to be a constant, one can have

$$\frac{\partial n}{\partial x} = nN_T \frac{\sigma_1\sigma_2+\sigma_3\sigma_4-\sigma_3\sigma_4 I/I_n}{(\sigma_1+\sigma_2+\sigma_3-\sigma_4)+\sigma_4 I/I_n} \quad . \tag{2.17}$$

Integrating between the limits $n=I_0/ev_n$ at $x=0$ and $n=I/ev_n$ at $x=W$, one obtains

$$\ln M = N_T W\sigma_1 \left(\frac{\sigma_2+\sigma_a}{\sigma_2+\sigma_b}\right)+\left[1+\frac{\sigma_1}{\sigma_3}\left(\frac{\sigma_2+\sigma_a}{\sigma_2+\sigma_b}\right)\right] \ln\left[1-(M-1)\frac{\sigma_3\sigma_4}{\sigma_1\sigma_2}\right] \tag{2.18}$$

where $\sigma_a \equiv \sigma_3\sigma_4\sigma_1^{-1}$ and $\sigma_b \equiv \sigma_1+\sigma_3-\sigma_4$. If we neglect the recombination processes ($\sigma_2\sigma_1 >> \sigma_3\sigma_4$) and assume that one of σ_1 and σ_2 is much greater than the other, the equation (2.18) can be simplified as

$$\ln M = N_T W\sigma$$

$$M = \exp(N_T W\sigma) \tag{2.19}$$

where σ is the smaller one of σ_1 and σ_2. Actually, these conditions are expected to be met by deep centres in a reverse-biassed ZnSe Schottky diode at high enough fields. By definition, the relationship between α and σ can be deduced as following

$$\sigma = \alpha N_T^{-1}. \tag{2.20}$$

where α is the number of electrons or holes ionized from a deep centre by a hot electron in unit length, i.e. the ionization rate of deep centres. The impact ionization cross-section σ and the ionization rate α of deep centres are both functions of field. The ionization rate of deep centres can also be described by the equations (2.5) and (2.6) which were originally derived for band-to-band impact ionization. However, the constant α_0 has implicated the probability of impact ionization via deep centres instead of the probability of ionizing electrons from the valence band to the conduction band. Now the constant α_0

is related to the deep level concentration N_T by equation (2.20). Combining equations (2.19), (2.20), (2.5) and (2.6), we have

$$M=\exp(\alpha W)\,, \tag{2.21}$$

or

$$\ln M=W\alpha_0\exp(-b/E) \tag{2.22}$$

and

$$\ln M=W\alpha_0\exp(-E_0^2/E^2)\,. \tag{2.23}$$

2.2.3 Comparisons of the multiplication equations derived from the two theories

Actually, either multiplication process is very complicated, especially as the known information about the electron-energy distribution at differing high fields is so limited. So it is very difficult to describe the multiplication behaviour precisely and theoretically in a wide range of high electric fields. In both the theoretical derivations of the two-stage and the band-to-band impact ionizations, many assumptions have been made. To be clear, we rewrite the main derived equations for the two multiplication processes below.

For the band-to-band impact ionization, under the conditions $\beta=0$, α=constant, we have equation (2.3)

$$M = \exp(\alpha W).$$

under the conditions $\beta=\alpha$, in a Schottky diode, we have equation (2.8)

$$1-\frac{1}{M} =\alpha_m W_{eff.}$$

For the two-stage impact ionization, if the recombination processes are negligible and α is constant, then we have equation (2.21)

$$M = \exp(\alpha W) .$$

It should be noted that equation (2.3) is exactly the same as equation (2.21). No matter which equation, eg. equation (2.3) or equation (2.8), the band-to-band impact ionization follows, once either multiplication process occurs, the number of electrons will increase almost as the exponential of an exponential. In principle, both multiplication processes could take place, if the electron energies are high enough. The threshold energy for the two-stage impact ionization should be smaller than that for the band-to-band impact ionization. However, it is impossible to distinguish the different multiplication processes by fitting the variation of photocurrent with field to either theory if the band-to-band impact ionization process follows equation (2.3). In principle, a process which follows equation (2.8) can be distinguished from the other due to two-stage impact ionization, but this requires measurements at large values of M.

2.3 Experiments

2.3.1 Sample preparation

We carried out the photocurrent measurements on four types of samples.

A. ZnSe epilayer samples K and H7

The ZnSe K and H7 were grown epitaxially on GaAs substrates by atmospheric pressure MOCVD at 280°C in the laboratories of Professor J. O. Williams at UMIST. Because they were grown in different runs we distinguished them by the signs K and H7. The epilayers were 5±0.5 μm thick and had carrier concentrations of about $1.0*10^{18}$ cm^{-3}.

In order to produce deep centres, post-growth annealing was employed. Several dice were cut from the ZnSe H7 slice using a wire saw, followed by cleaning with three organic solvents (toluene, acetone and propanol) and dilute HCl. To minimize copper contamination during thermal annealing they were placed in a container made from high-purity germanium which was then placed in a spectrosil silica tube. They were heat treated at 390°C or 400°C in air for 30 minutes.

B. ZnSe bulk sample Tr1 S1

The high resistivity single crystal was grown from constituent elements by vapour transport, by other workers in this laboratory. The crystal was cut into dice and made conducting by immersion in molten zinc at 950°C for 150 hours. The details of this process have been described in Ref.[13]. Before making a diode, the n-type ZnSe single crystal was polished with cerium oxide and etched in 1% fresh bromine/methanol for $2\frac{1}{2}$ minutes, then left in carbon disulphide for about 30 minutes followed by another etching in 50% caustic soda solution at 50°C for 20 minutes and rinsing with de-ionized water several times.

C. ZnSe bulk sample E30-1

This single crystal sample was also grown in this laboratory in the same way as that described in B. However, this crystal has been treated differently in that it has been doped with the impurity nickel to give deep centres within the band gap. It was made conducting by heating the ZnSe in a molten Zn/Ni alloy. Then the same polishing and etching processes were made on the sample.

D. ZnSe epilayer sample HL2

ZnSe epilayer sample HL2 has the three-layer structure as shown in Fig.2.5. After one conducting n-type ZnSe layer of about 1 to 2 μm thick was grown epitaxially on a very conducting n-type GaAs substrate, another higher resistivity ZnSe layer of about 5 μm thick was further grown epitaxially by MOCVD at UMIST. Because the top ZnSe layer was not insulating enough as expected we heat treated the dice HL2-007, which was cut from the sample HL2, at 380°C in air for 30 minutes. The heat treatment method has been described in A.

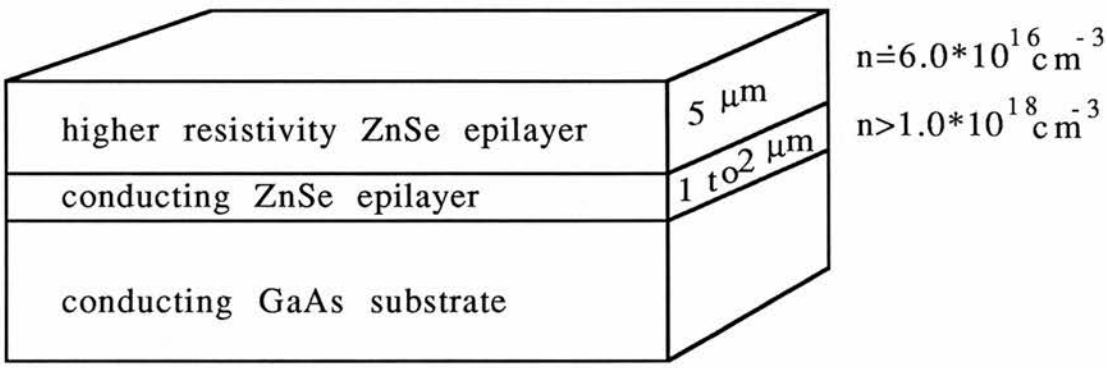

Fig.2.5: The diagram of the three-layer structure for ZnSe HL2.

2.3.2 The making of ohmic and Schottky contacts

In order to get the high electric field, greater than 10^4 Vcm^{-1}, required in this study, we chose Schottky diodes driven in reverse bias. The diagram of an ideal Schottky diode is shown in Fig.2.6. When a Schottky diode is driven in reverse bias, the region of the depletion layer can be approximated as a capacitor. The relevant formulas are written below

$$\frac{1}{C^2} = \frac{2(V+V_d)}{(N_D-N_A)q\varepsilon_0\varepsilon_s A^2} \tag{2.24}$$

$$W = \left(\frac{2\varepsilon_0\varepsilon_s}{q(N_D-N_A)}\right)^{1/2}(V+V_d)^{1/2} \tag{2.25}$$

$$E_{max} = \frac{2(V+V_d)}{W} \qquad (2.26)$$

where C is the capacitance of the depletion layer, W is the width of the depletion layer, V_d is the built-in barrier potential, V is the applied voltage, N_D-N_A is the uncompensated shallow donor concentration, E_{max} is the maximum electric field in the junction, A is the area of the Schottky contact, and ε_o, ε_s are dielectric constants of vacuum and semiconductor respectively. After N_D-N_A has been determined by the capacitance measurements, E_{max} can be deduced from equations (2.25) and (2.26).

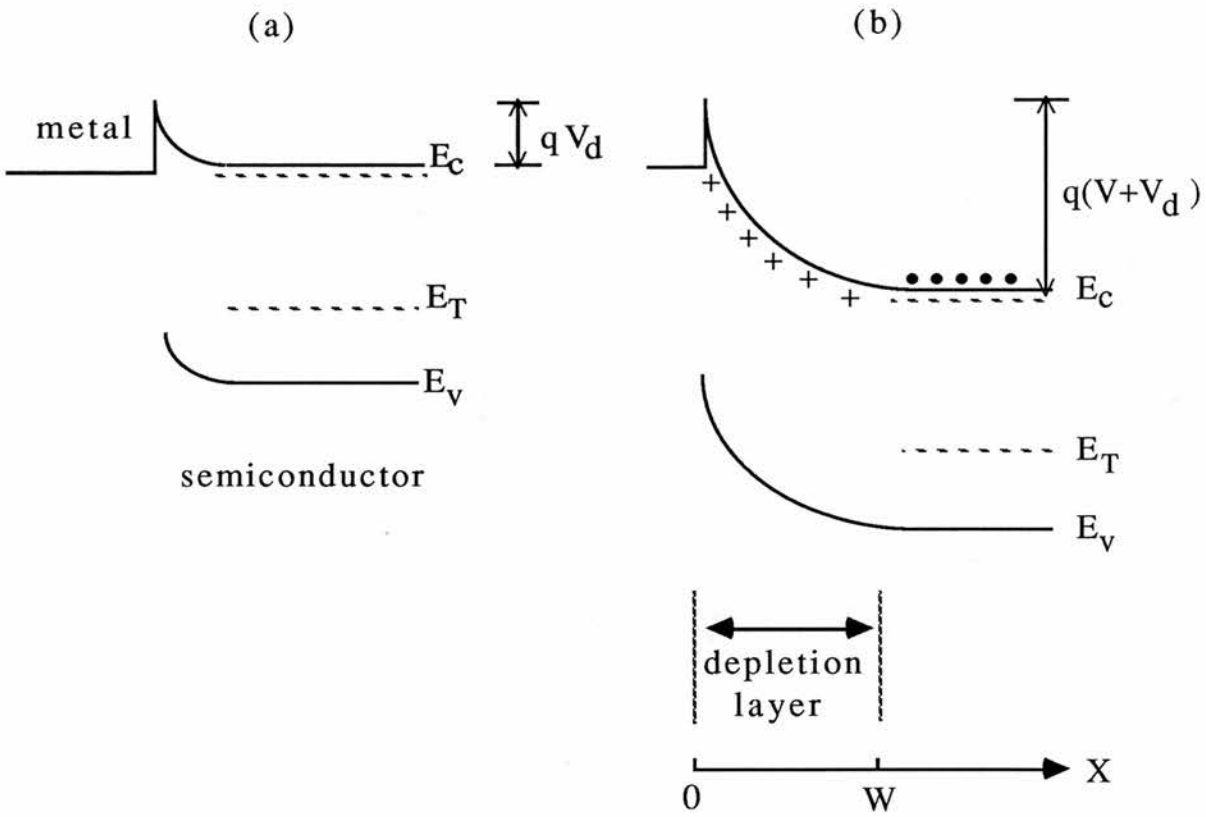

Fig.2.6: The diagrams of an ideal Schottky diode driven in zero bias (a) or reverse bias (b).

Before making ohmic contact, samples were etched with 50% NaOH solution at 50°C for 10 minutes in order to remove the oxide layer from the

surface, followed by rinsing with de-ionized water several times. Ohmic contacts were made on one side with indium dots by heating at 310°C in 90% N_2/10% H_2 for 30 seconds. The I-V characteristics of two indium dots were measured in both directions of current. They showed straight lines which indicated that the contacts were ohmic. Aluminium was evaporated on the clean surface, which was etched in the same way as that for ohmic contacts, to form a semi-transparent metal Schottky contact. For ZnSe epilayer samples K001 and H001,2,3, ohmic contacts and Schottky contact were made on the same side, for other samples ohmic contacts and Schottky contact were on opposite surfaces.

2.3.3 I-V and C-V measurements

Conventional I-V and C^{-2}-V measurements were made in the dark to check the quality of the Schottky diodes and to determine the uncompensated donor concentration. The capacitance characteristics were measured with the Wayne-Kerr 601 Bridge at a frequency of 1 MHz with a peak-to-peak signal of about 30 mV across the junction.

2.3.4 Photocurrent measurements

In the photocurrent measurements, the electrical behaviour is described by different formulas. Mott has given a detailed treatment in Ref.[25]. When a crystal is illuminated by light with suitable photon energies, free carriers can be created. Under electric fields these free carriers will move towards the electrodes, as shown in Fig.2.7, to give a photocurrent. Taking the electron movement as an example, suppose that the electrons created travel an average distance ω before being trapped. Assume ω is proportional to the electric field E. At lower fields, ω is less than X_0. It means recombinations could take place as the electrons are passing through. The charge in an external circuit is proportional to ω/L, where L is the distance of two

electrodes, so the photocurrent increases as the electric field E increases. At higher fields, ω could become greater than X_0. So all electrons can reach the anode without being trapped. In this case, the charge in an external circuit is proportional to X_0/L which is constant, and the photocurrent is independent of the electric field. At very high fields, ω can be of the order of a centimetre. So, in an ideal system, one might expect to observe four processes, which are shown in Fig.2.8, by photocurrent measurements in reverse-biassed Schottky diodes, if we suppose that the two-stage impact ionization process is observable. They are the photoconductivity process with recombination, the photoconductivity process without recombination, the two-stage impact ionization process and the band-to-band impact ionization process. Here it is assumed that light is strongly absorbed near the cathode, so X_0 corresponds with the width of the depletion region.

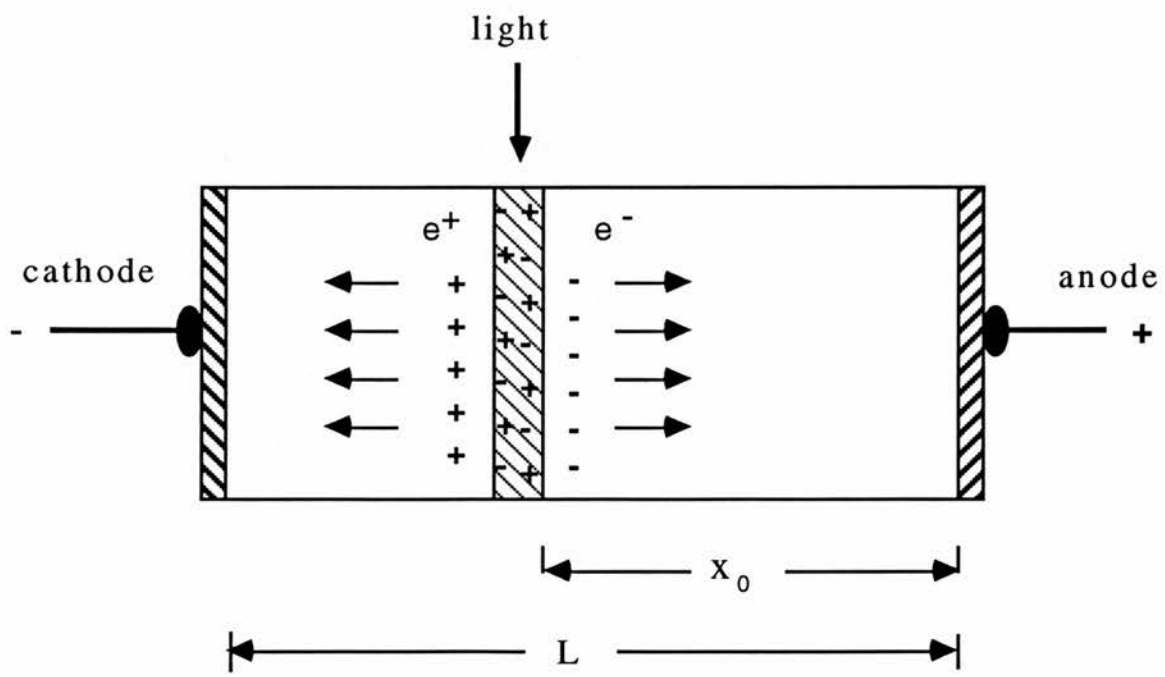

Fig.2.7: The diagram of the movement, in an electric field, of electron-hole pairs generated by illumination.

In order to determine the multiplication factor M and consequently $\alpha(E)$, we need to know the ratio of the number of carriers entering the high field region to that leaving at various fields. No method which simply involves measuring current-voltage characteristics is valid because of the current density formula J=nev where n is the total number of current carriers. The current density is determined by both the number of current carriers and the drift velocity. Another difficulty is that in the junctions used here there can be a thin oxide layer between the metal and the semiconductor, and electrons may be injected from the cathode into the semiconductor through the oxide layer to form the dark current. In this case, because the dark current depends on voltage it is difficult to distinguish the multiplication process from the increase in dark current.

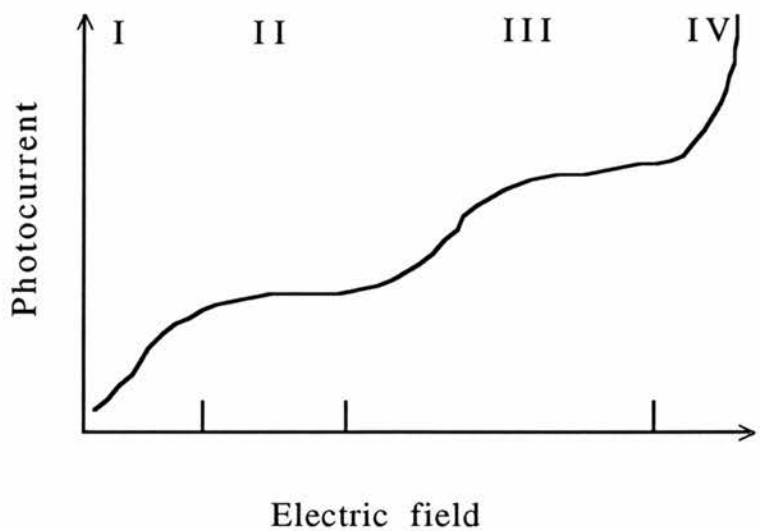

Fig.2.8: I: The photoconductivity process with recombination.

II: The photoconductivity process without recombination.

III: The two-stage impact ionization process.

IV: The band-to-band impact ionization process.

To get round this problem we chose to measure photocurrent generated by chopped light. In this case a fixed photon flux produces a constant number of carriers in unit time. The AC photocurrent obtained from a Schottky diode driven in DC reverse bias is then completely separated from the dark current. If the electric field is high enough so that the recombination process can be negligible, the AC photocurrent is then a measurement of charge and is independent of drift velocity. So any multiplication of photocurrent is only due to the increase in the number of current carriers by some kind of ionization process. A phase sensitive technique was used to amplify the signal, and consequently improve the signal to noise ratio.

A block diagram of the apparatus is shown in Fig.2.9. The ultra-violet lamp, with main wavelength 365 nm (3.397 eV), was employed as light source to generate electron-hole pairs in ZnSe. The band-gap of ZnSe is about 2.7 eV at room temperature and 365 nm (3.397 eV) has photon energy above the band-gap. The light was chopped at a frequency of 90 Hz. The phase of the phase sensitive detector (PSD) was fixed by the biggest photocurrent obtained from a commercial photodiode driven in a certain reverse bias. Careful focussing of the incident light on the chopper and samples ensured a near square light pulse. In this case the capacitance effect which arises from the diode itself was minimized. To protect the Lock-in Amplifier (PSD) and separate the photocurrent from the dark current, the diode was set in an additional circuit shown in Fig.2.10. The signs C and R represent an ordinary capacitor (0.2 μF) and resistor (5 kΩ) respectively. The reason for choosing this value of a resistor is to get a large enough voltage at the Lock-in input. Then the photocurrent was measured with a PSD as the DC reverse bias applied to a diode was changed.

A Schottky diode can be equivalent to a capacitor of the depletion layer and a resistor of the depletion layer in parallel and that combination in series with a bulk resistor. So the total applied voltage is the sum of the voltages

dropped in the depletion layer and the bulk resistor. The differential resistance ($\frac{dV}{dI}$) of the depletion layer decreases as the dark current increases. When the leakage current is large enough and the differential resistance is comparable to the bulk resistance, the voltage dropped in the bulk resistor cannot be ignored. Then the maximum electric field (E_{max}) in the depletion layer is no longer given by equation (2.26). If the dark current is too large, then the depletion layer model might not be suitable. In this case the electric field in the junction might not increase as the applied voltage increases, and the photocurrent might decrease. One example is shown in Fig.2.11 for a leakage Schottky contact. So the method of photocurrent measurement is only suitable for the Schottky diodes with a low enough dark current.

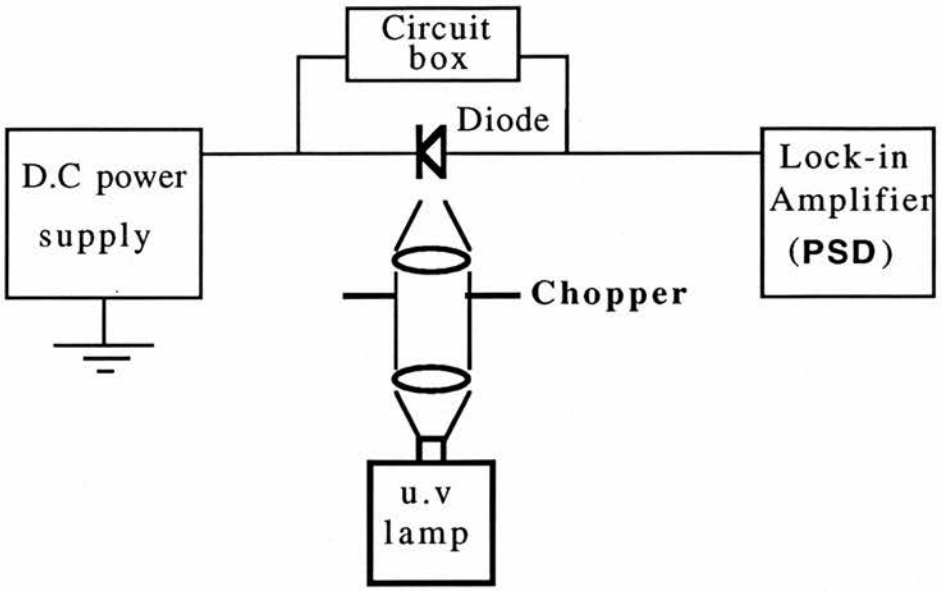

Fig.2.9: The apparatus for photocurrent measurements.

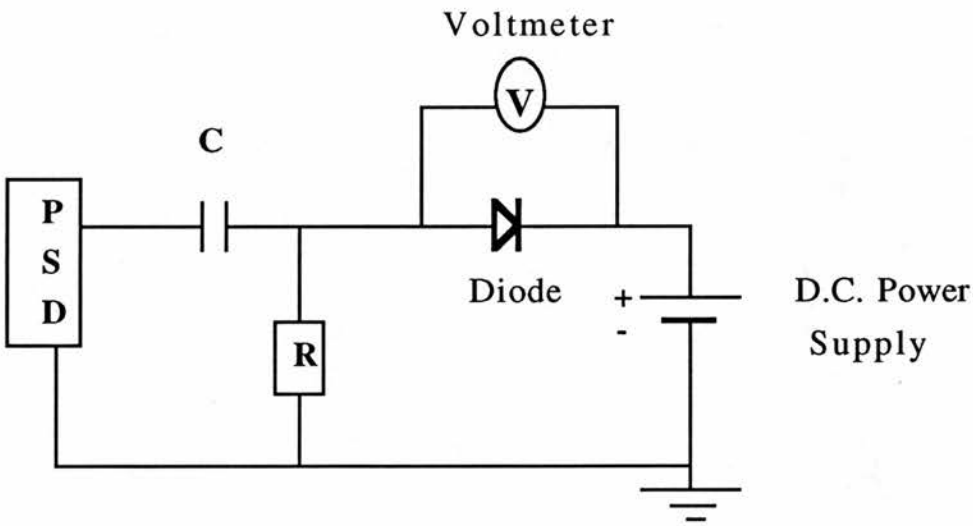

Fig.2.10: The diagram of the additional circuit box.

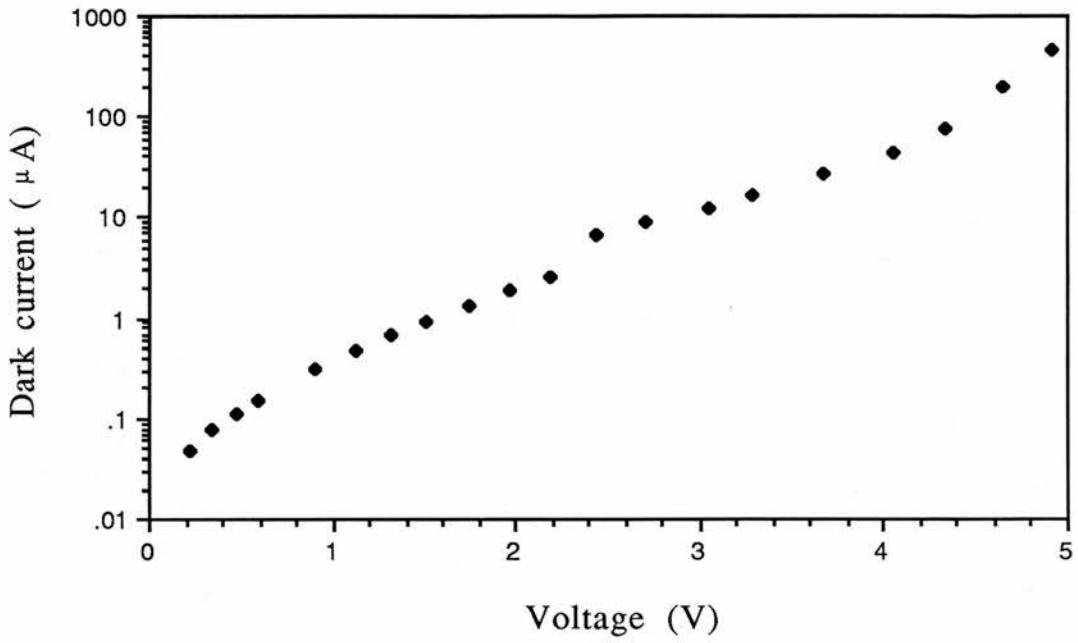

(a)

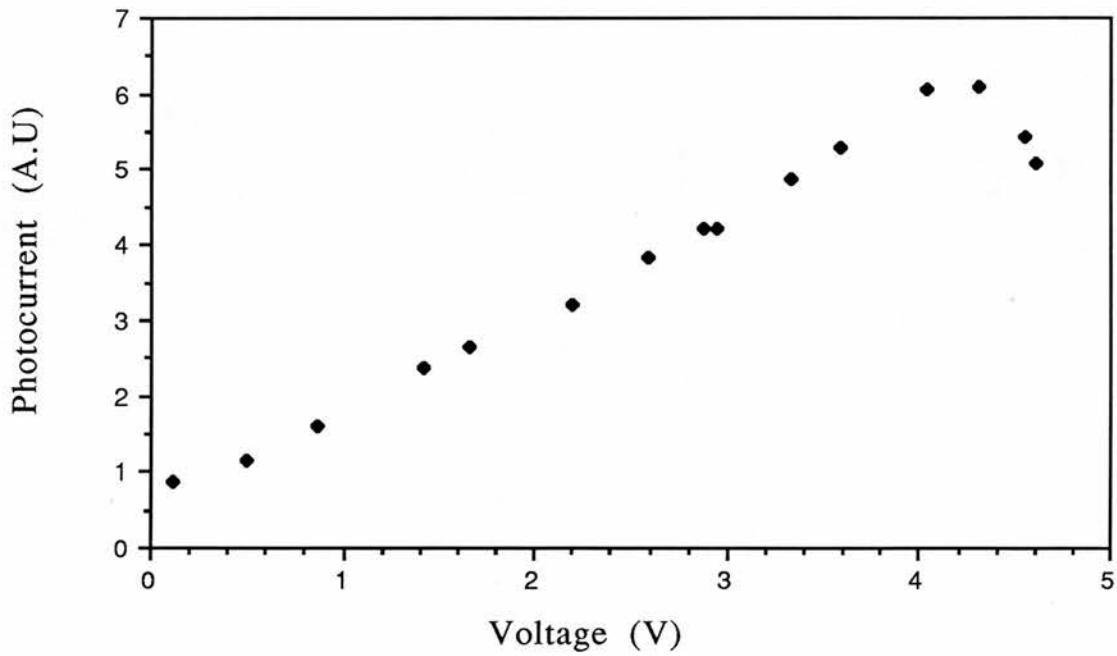

(b)

Fig.2.11: The curves of the dark current (a) and the photocurrent (b) against voltage for a Schottky diode with a large leakage current. In b the photocurrent is in arbitrary units (A.U).

2.4 Results

In order to measure accurately the electric field strength, a good quality of the Schottky diodes is very important in photocurrent measurements. Fortunately, it is fairly easy to make good Schottky contacts on ZnSe with sufficient care. Since diodes were only used in reverse bias for photocurrent measurements, we were more interested in the I-V characteristic of a Schottky diode in reverse bias, and we measured the I-V curve before and after photocurrent measurements.

Fig.2.12 and Fig.2.13 show the I-V characteristics of diodes H7001 and Tr1 S1. The currents in forward and reverse biases are plotted on different scales. For other samples the I-V characteristics are, basically, the same. The I-V characteristics made before and after photocurrent measurements are also similar.

The typical C^{-2}-V characteristics for some samples are shown in Fig.2.14 and Fig.2.15. They are all good enough straight lines. According to equation (2.24), the N_D-N_A can be calculated from the slope of the straight line and the area of contact. The intercepts on the voltage axis are also marked in the figures. They vary in the range 0.9 to 2.5 V depending on the different Schottky diodes. So far the smallest voltage intercept for an aluminium Schottky contact on ZnSe which can be obtained in this laboratory is 0.51 V. The different intercepts are believed to be the result of an oxide layer inevitably introduced during the making of Schottky contacts.

In a word, the I-V and C^{-2}-V measurements indicated that all diodes have good rectification. They ensured the reliability of photocurrent measurements.

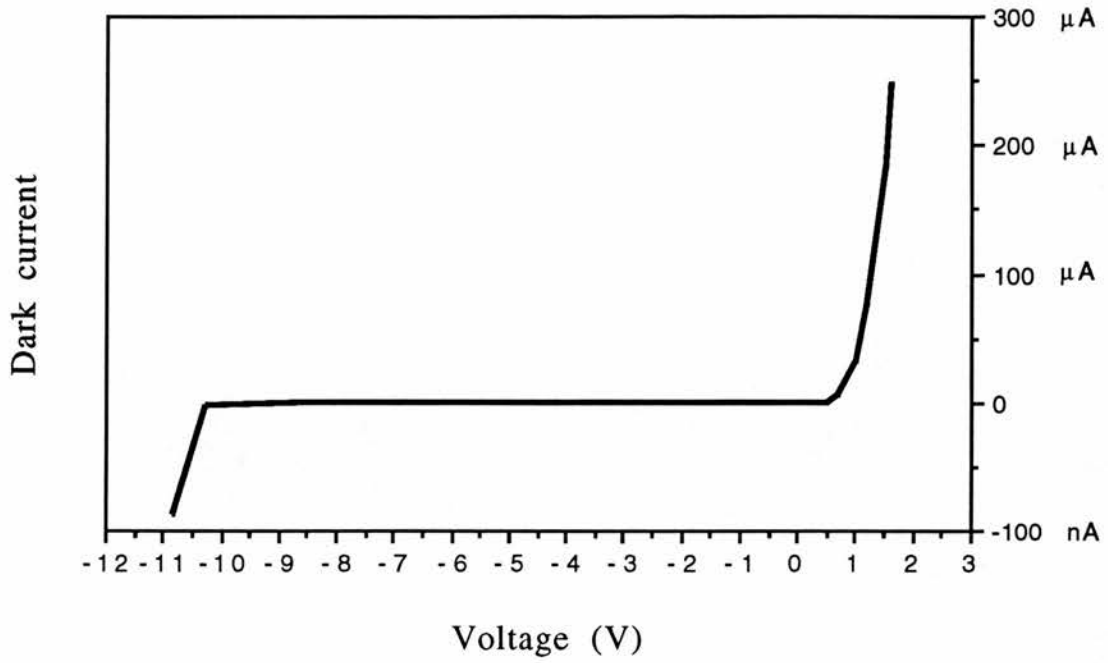

Fig.2.12: The I-V characteristic for H7001.

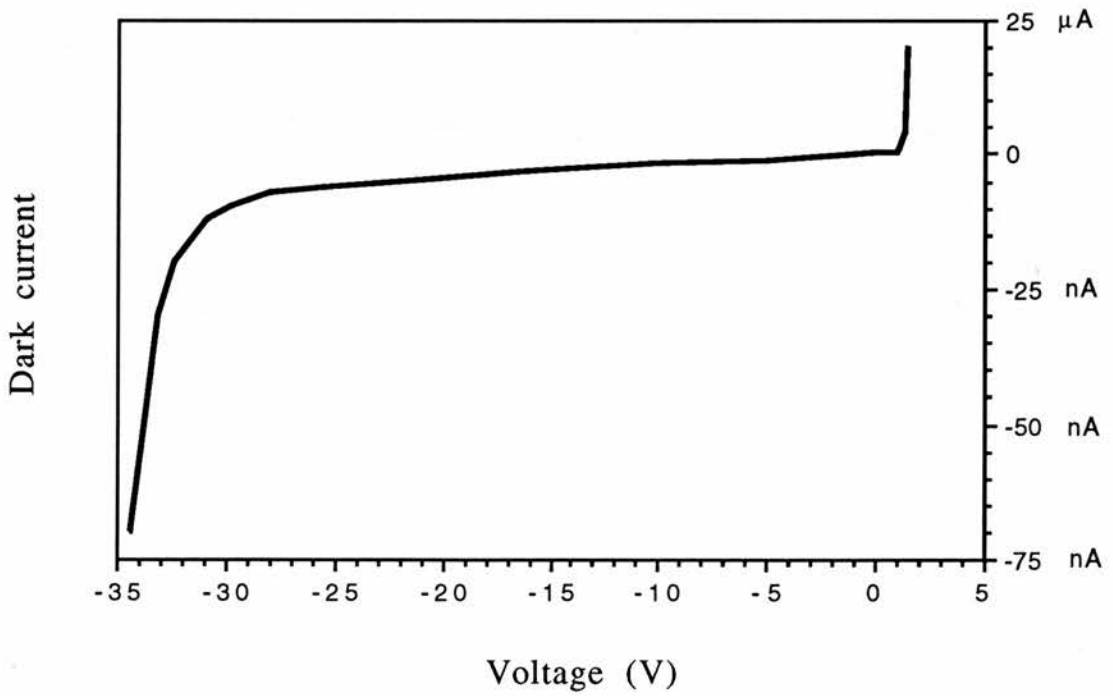

Fig.2.13: The I-V characteristic for ZnSe Tr1 S1.

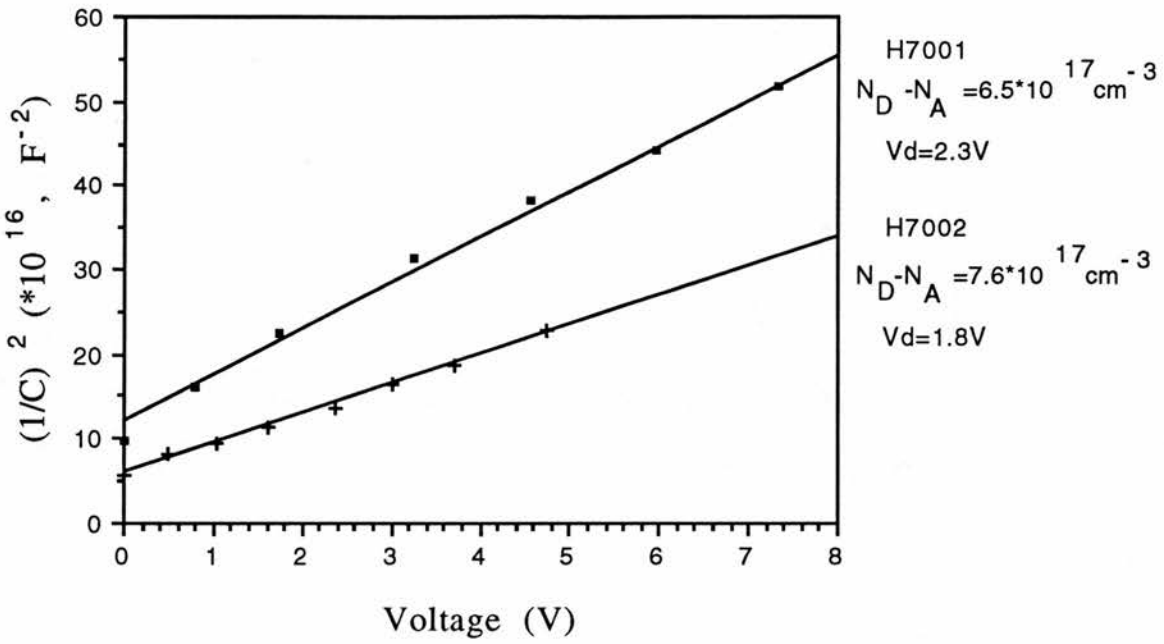

Fig.2.14: The C-V characteristics for H7001, H7002.

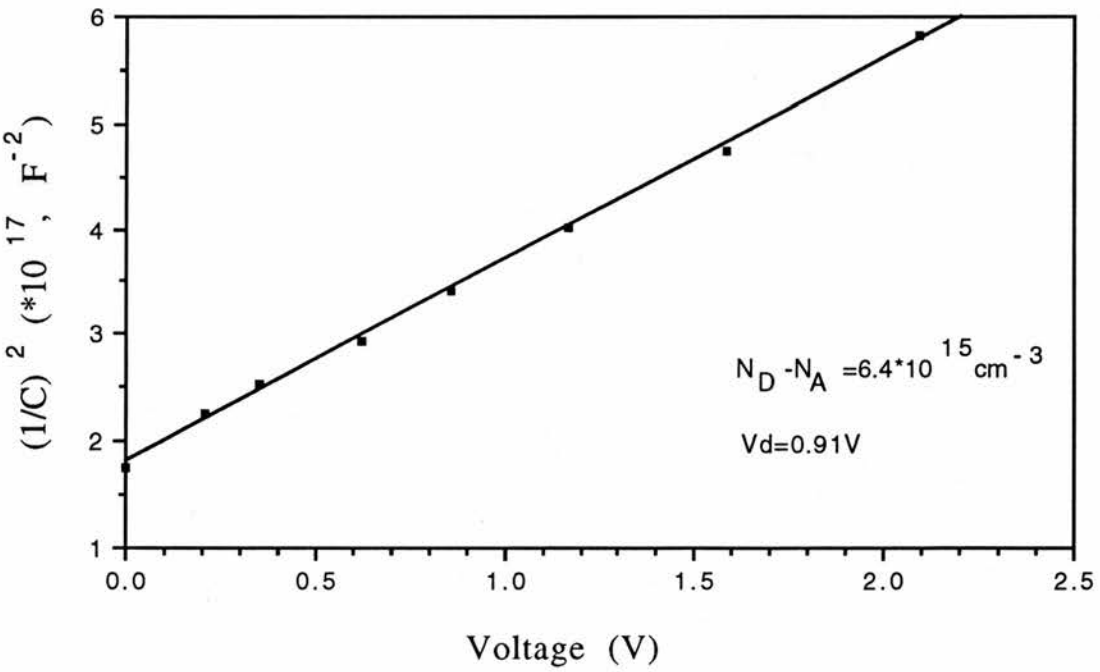

Fig.2.15: The C-V characteristic for ZnSe E30-1.

For the ZnSe epilayer sample HL2-007, the capacitance was a constant for different reverse bias. It means that the first higher resistivity ZnSe epilayer has become a very insulating layer after annealing at 380°C. According to the equation $C=A\varepsilon_0\varepsilon_s/W$, the thickness W of the insulating layer is calculated to be about 5 μm (which agrees with the value estimated by the grower) by using the value of capacitance obtained from the bridge. Then the average electric field is equal to V/W where V is the applied voltage.

The plots of the relative photocurrents against the maximum electric field in the junction (average electric field for HL2-007) are shown in Fig.2.16, Fig.2.17, Fig.2.18 and Fig.2.19. The maximum absolute photocurrent was less than 5 μA throughout the photocurrent measurements except for the sample Tr1 S1 in which the photocurrent could be as high as 36 μA. The data obtained from the Lock-in Amplifier was stable enough and fairly repeatable.

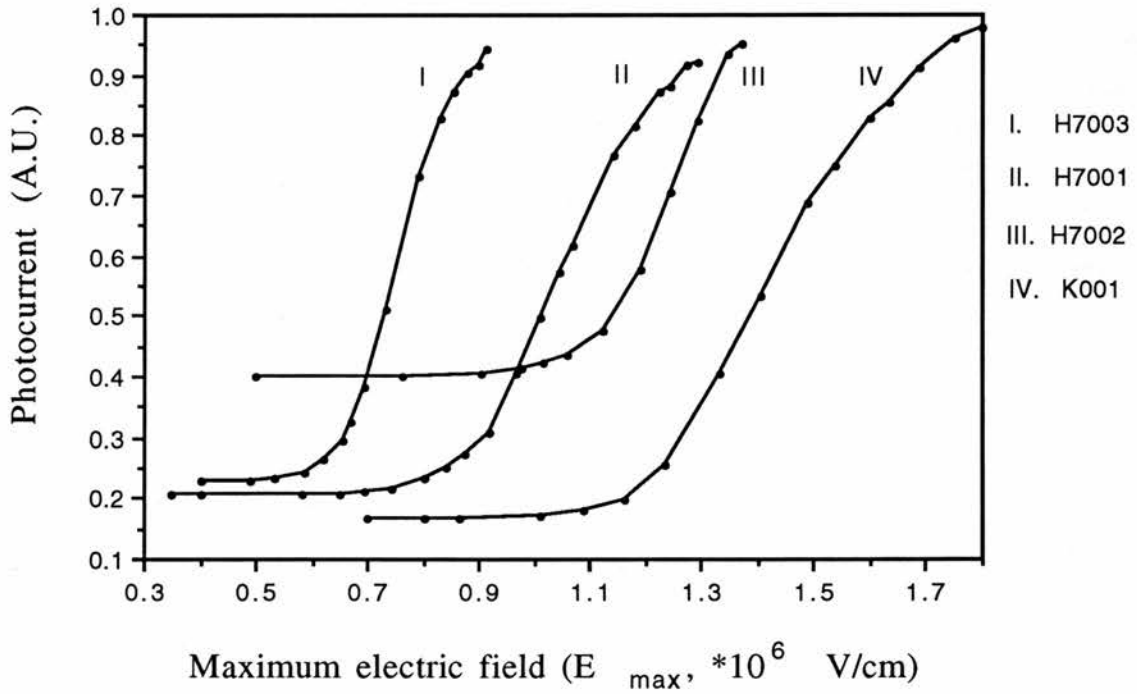

Fig.2.16: The photocurrent vs the maximum electric field for ZnSe H7001,2,3 and K001.

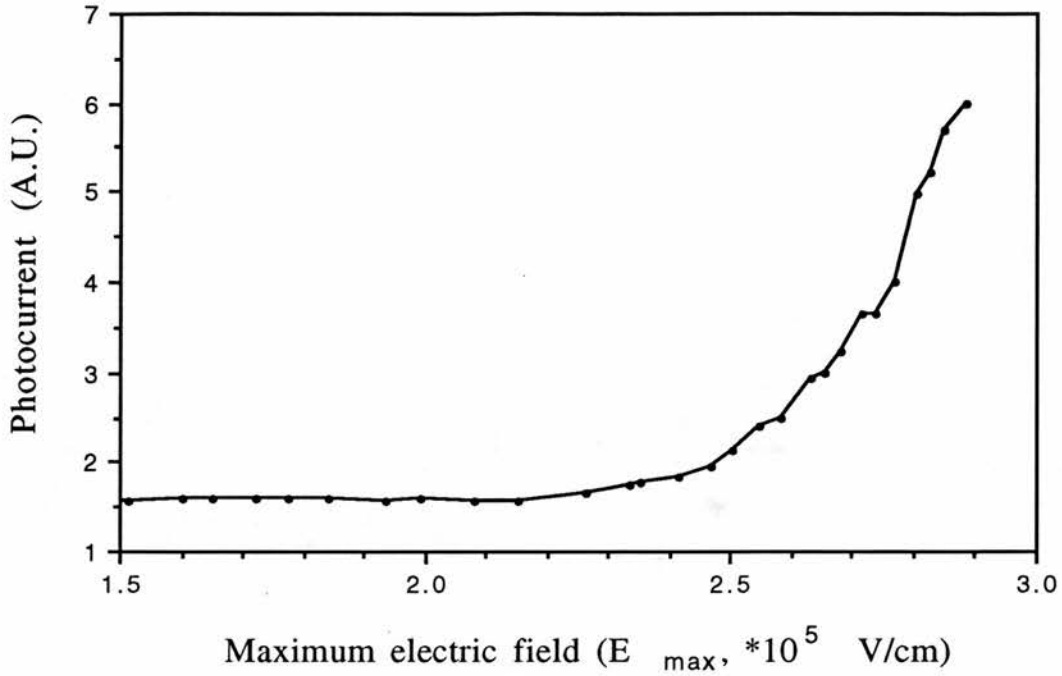

Fig.2.17: The photocurrent vs the maximum electric field for ZnSe E30-1.

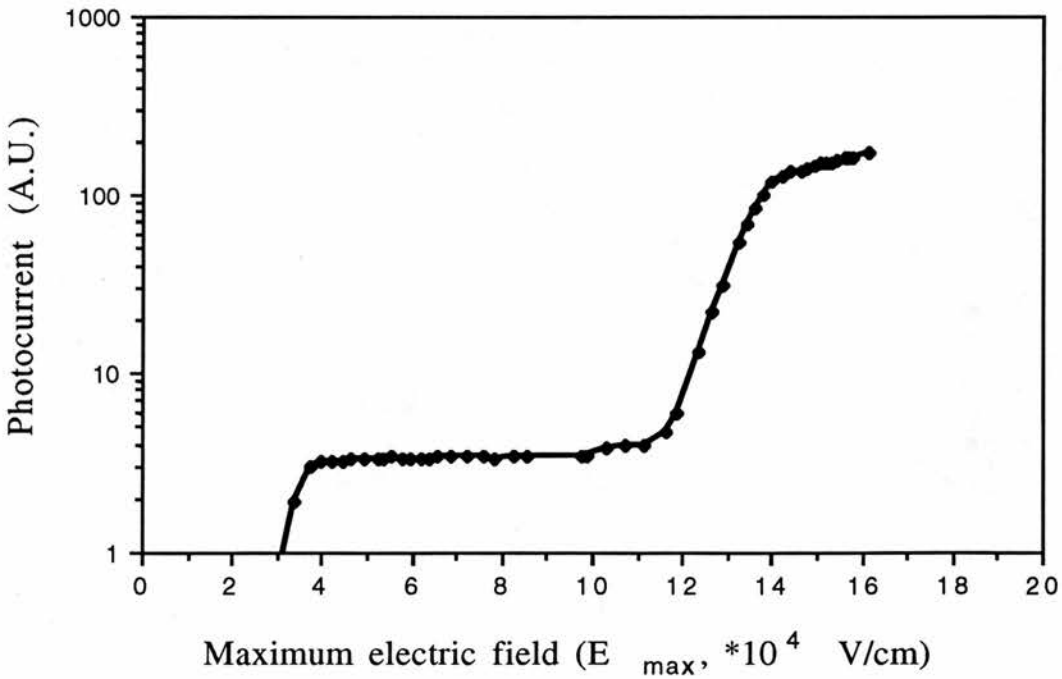

Fig.2.18: The photocurrent vs the maximum electric field for ZnSe Tr1 S1.

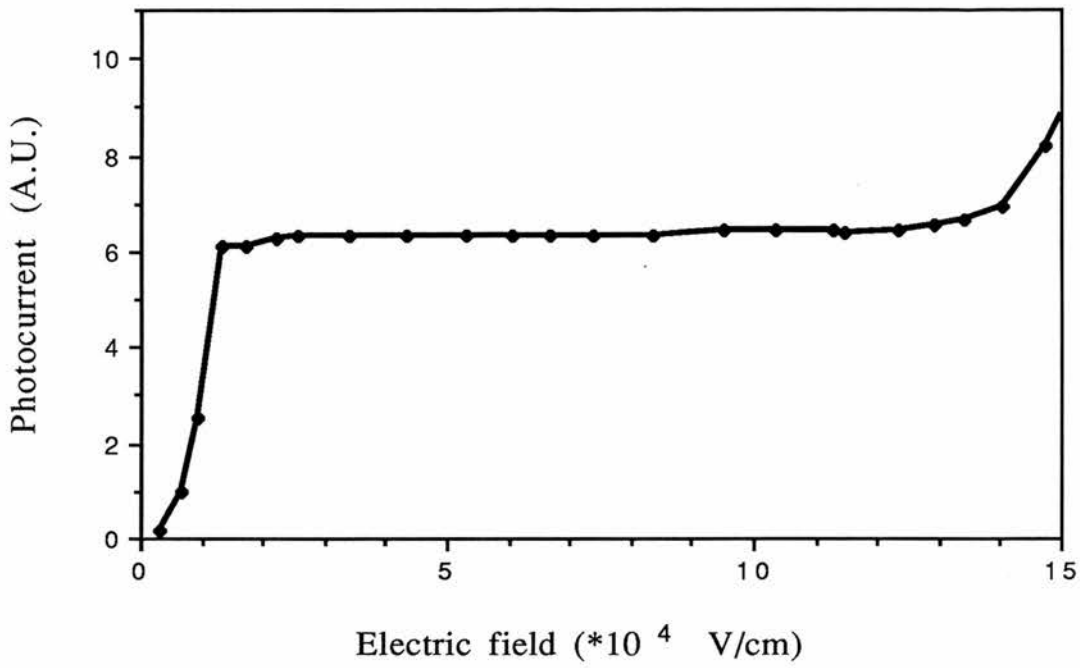

Fig.2.19: The photocurrent vs the average electric field for ZnSe HL2-007.

2.5 Discussion

In Fig.2.16 and Fig.2.17, the photocurrents have a plateau region at lower electric fields. They are followed by a steep multiplication process, and then tend to a slight turn-over, in another word, increase more slowly with fields. In Fig.2.18 and Fig.2.19, there is again a plateau but preceded by an increase occurring at fields less than $4*10^4$ Vcm^{-1}, and followed by another increase occurring at fields greater than $1*10^5$ Vcm^{-1}. In Fig.2.18 the turn-over at high fields is quite strong.

In Fig.2.18 and Fig.2.19, the first increase at lower fields is attributed to the photoconductivity process with recombination in which the transport time from one edge to the other edge of the depletion layer, with much wider thickness, is long enough for recombination to occur. Thompson [13] also observed a similar process in ZnS, but he could not explain it because of a lot of uncertainties. As the applied voltage increases the electric field in the depletion layer increases as well. After the electric field is greater than $1*10^5$

Vcm^{-1} the electron drift velocity can reach the limit of about 10^7 cm/sec. [26]. Because the absorption coefficient of ZnSe in ultra-violet light, especially for 365nm wavelength, is greater than 10^4 cm^{-1} [27], a certain number of electron-hole pairs is generated only at the edge of the depletion layer, which is near the Schottky contact, by a fixed photon flux. All carriers created can pass the depletion region at such high fields. In this case, the photocurrents are independent of the electric fields until the initiation of multiplication. For the samples in Fig.2.16 and Fig.2.17, the carrier concentrations are already high enough to build in an electric field of magnitude of about 10^5 Vcm^{-1} in zero bias, so the photocurrent behaviours start with the plateau, i.e. the photoconductivity process without recombination.

Comparing the measured photocurrent behaviours with those expected in Fig.2.8, we have observed the photoconductivity process with recombination and the photoconductivity process without recombination, then followed by a multiplication process. The multiplication factor M can be obtained by calculating the ratio of the photocurrent in the multiplication region to that in the plateau region. At first sight it looks as if the strong turn-over at high fields in Fig.2.18 is the second plateau in Fig.2.8. However, the turn-over in Fig.2.18 is more likely to be due to the experimental effects.

Actually, the total applied voltage can be divided into two parts. One part is dropped in the depletion layer, the other part is dropped in the bulk resistor. When the dark current is very small, most applied voltage is dropped in the depletion layer. The values of the electric fields at which the multiplication process is taking place can be accurately calculated by taking the applied voltage as the voltage only dropped in the depletion layer. As the dark current increases the resistance of the depletion layer decreases, so the voltage dropped in the bulk resistor can no longer be neglected. In this case, if one still takes the applied voltage as the voltage dropped in the depletion layer to determine the electric field in the depletion layer, then the calculated

electric field would be bigger than the real one. This should account for the turn-over observed at higher electric fields in Fig.2.16 and Fig.2.17, especially in Fig.2.18.

The sample Tr1 S1 in Fig.2.18 has a low carrier concentration, so it has the wider depletion layer. In this case the tunnelling effect cannot occur even at higher fields. The multiplication could reach the much higher value of 40. For the samples in Fig.2.16 and Fig.2.17, with high carrier concentrations, the thicknesses of the depletion layers are of order of magnitude of several hundred angstroms, the tunnelling effect could compete with impact ionization processes and forms the important component of the dark current to damage the diodes so that the higher multiplication factor cannot be measured experimentally.

Therefore, in each sample only one multiplication process was observed. Now the problem is to determine whether the multiplication is due to a two-stage impact ionization process or a band-to-band impact ionization process. As we have discussed in section 2.2.3, it is difficult to determine the origin of multiplication by fitting data to either of the theories as one can see from one example in Fig.2.20 and Fig.2.21, that is, the theoretical fittings to equation (2.3) of $M=\exp(\alpha W)$ (the same as equation (2.21)) and equation (2.8) of $1-\frac{1}{M}=\alpha_m W_{eff}$. This point will be discussed in more detail below. However, it is noted that the multiplication factors in Fig.2.16 and Fig.2.17 are all bigger than 2. If we suppose the multiplication is due to the two-stage impact ionization, then according to equation (2.19) of $M=\exp(N_T W \sigma)$, the deep-level concentration can be estimated. Taking M=2, W=1 μm, and $\sigma=5*10^{-16}$ cm^2, then the deep-level concentration N_T should be greater than $1*10^{19}$ cm^{-3}. Actually, for the samples with high carrier concentrations, used in Fig.2.16 and Fig.2.17, the thicknesses of the depletion layers are all less than 1 μm, the

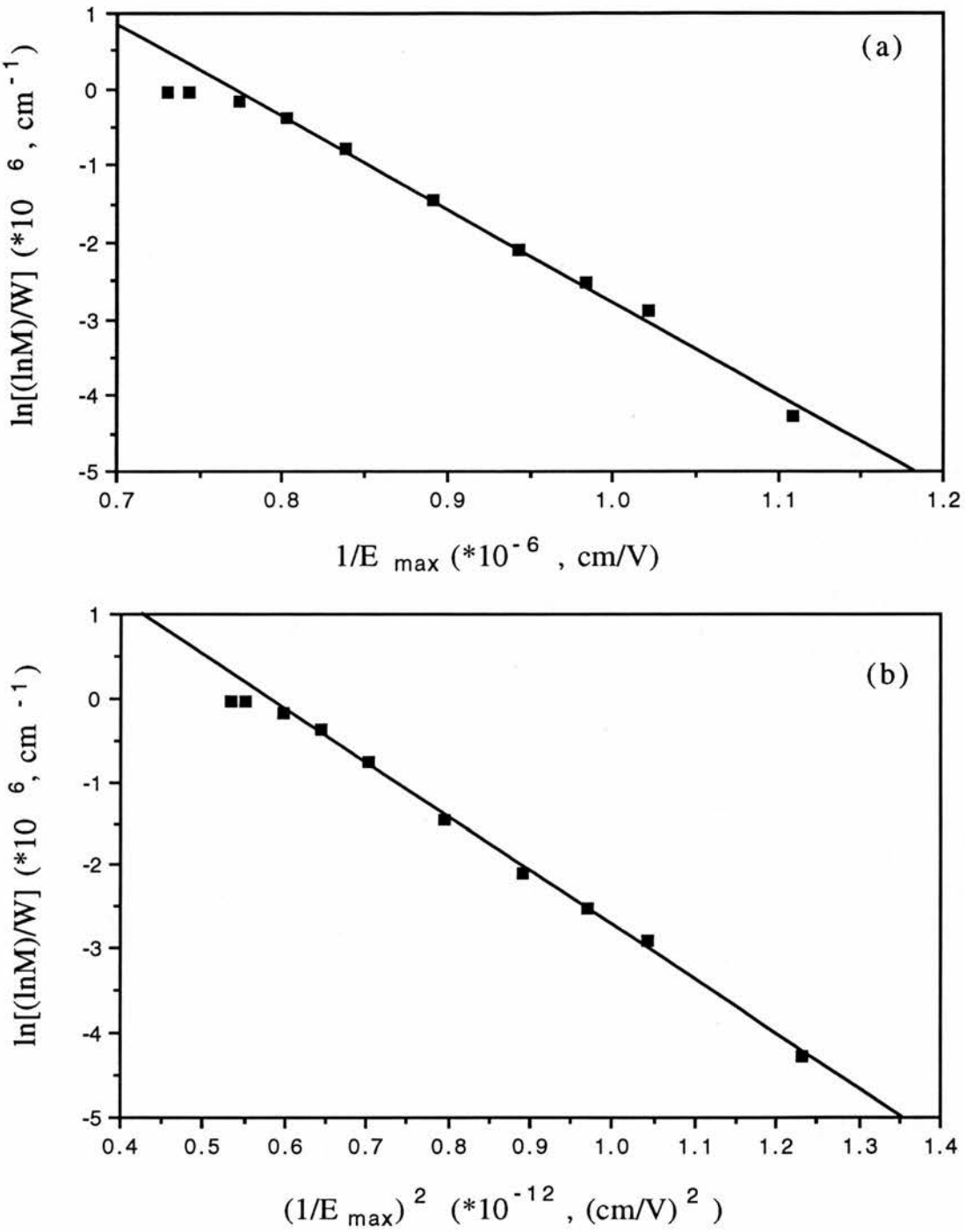

Fig.2.20: The theoretical fit to the equation of $M=\exp(\alpha W)$ for the sample H7002. (a) is based on $\alpha=\alpha_0\exp(-b/E)$ and $b=12.5*10^6$ V/cm, (b) is based on $\alpha=\alpha_0\exp(-E_0^2/E^2)$ and $E_0=2.6*10^6$ V/cm.

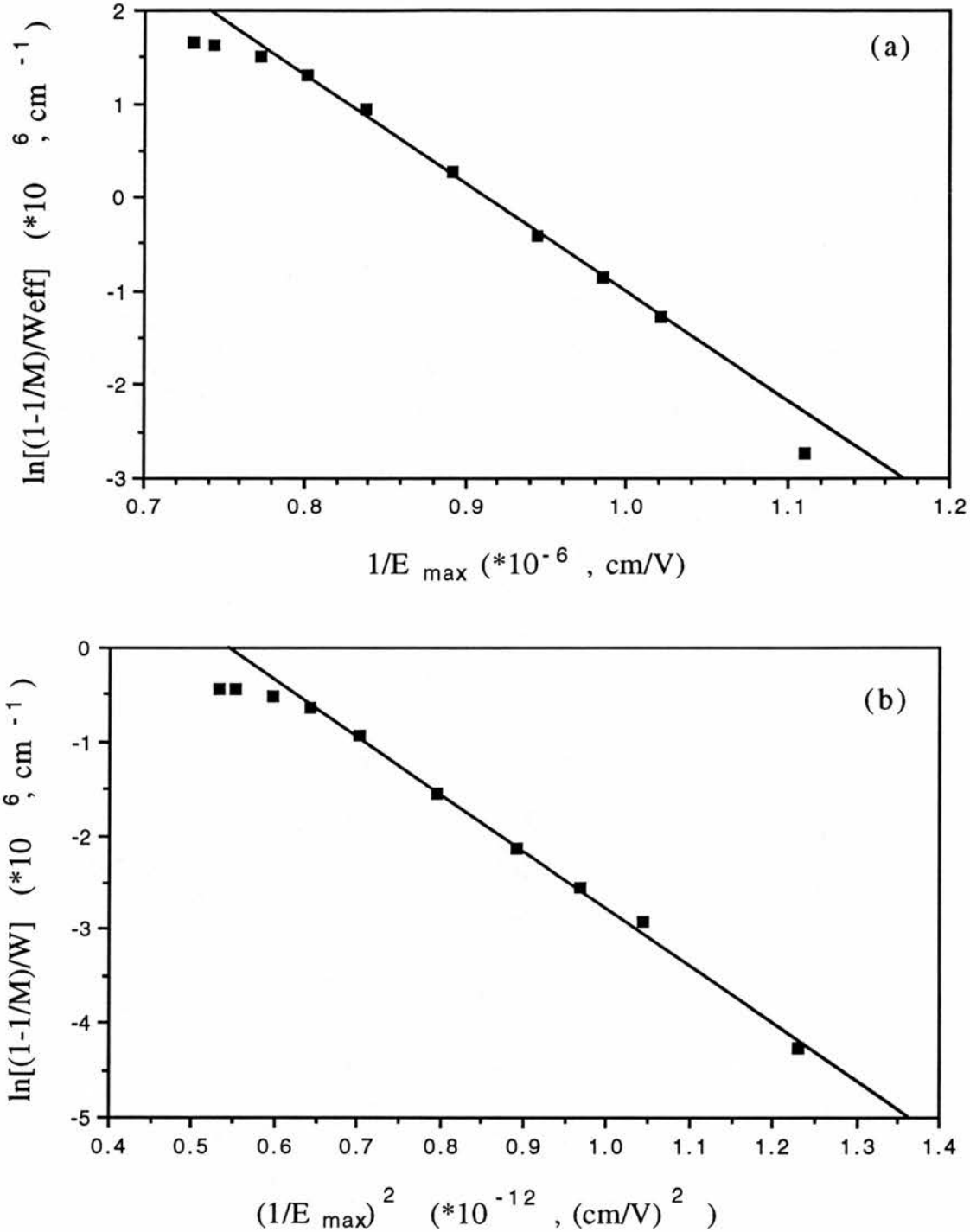

Fig.2.21: The theoretical fit to the equation of $1-\frac{1}{M}=\alpha_m W_{eff}$ for the sample H7002. (a) is based on $\alpha=\alpha_0 exp(-b/E)$ and $b=12.5*10^6$ V/cm, (b) is based on $\alpha=\alpha_0 exp(-E_0^2/E^2)$ and $E_0=2.5*10^6$ V/cm.

value of cross-section chosen for estimate could be big enough. So the deep-level concentration of $1*10^{19}$ cm^{-3} is a necessarily required value for two-stage impact ionization to occur. This raises a question whether there does exist some kind of deep level which has a concentration as high as $1*10^{19}$ cm^{-3}. Many efforts are being made to investigate deep levels in unintentionally-doped ZnSe samples. However, a deep level with a concentration greater than $1*10^{19}$ cm^{-3} has not been reported so far, especially for the samples grown by the advanced technique MOCVD. It indicates, on the one hand, that at least in the samples such as H7002, K001, and Tr1S1 it is quite unlikely to have an observable multiplication process governed by two-stage impact ionization.

In the ZnSe bulk sample E30-1, the nickel concentration was not measured. With reference to Szawelska and Allen's data [28], the nickel concentration might be in the order of 10^{15} cm^{-3}. So in this case the concentration of impurity nickel might be too small to play any observable part in the two-stage impact ionization process.

In general, the growth of wide bandgap II-VI compounds, such as ZnSe and ZnS, is inevitably accompanied by the presence of some kinds of deep centres, even in the case of unintentionally-doping growth. Zheng and Allen [29] have utilized the photoluminescence and junction capacitance measurements to investigate the post-growth annealing effect on ZnSe epilayers with exactly the same sample conditions as in the present study. The carrier concentrations of as-grown ZnSe epilayers were $1.0 \pm 0.3*10^{18}$ cm^{-3}. When the samples were heat-treated in air, the carrier concentration decreased as the annealing temperature increased. This decrease is believed to be due to the increase of some compensating acceptor centres, for example the M-centre, produced by the heat treatment. The compensating acceptor concentration can be of the same order of magnitude as that of the shallow donors, that is, its concentration can be as large as $1*10^{17}$ cm^{-3}. Similar annealing phenomena have been observed in our samples. According to the

theory of two-stage impact ionization, equation (2.19) can be rewritten to $\ln\ln M = \ln N_T W \sigma_0 - \frac{b}{E_{max}}$ combined with equation (2.6). Then we can roughly calculate $N_T\sigma_0$ by taking W at the threshold fields E_{th} of multiplication. The results are listed in Table 2.1. It should be noted that the values of $N_T\sigma_0$ do not show an increasing tendency after annealing. In contrast, it decreases, even in the ZnSe bulk samples. So if the multiplication is due to a two-stage impact ionization process, this result raises another question whether the centres produced by annealing are the same centres performing the multiplication. So far no other deep levels with very high concentration have been found in unintentionally-doped ZnSe samples except the ubiquitous M-centre. Therefore, the results in Table 2.1 are, on the other hand, not in agreement with the conclusion that the multiplication process observed is due to a two-stage impact ionization via deep centres.

Table 2.1: The comparison of the products of N_T and σ_0 for the samples in this work. The calculation of $N_T\sigma_0$ is based on the theory of two-stage impact ionization.

Sample	Growth	Annealing	$N_T\sigma_0$ ($*10^6$ cm^{-1})
K001	epilayer	none	17
H7002	epilayer	none	6.7
HL2-007	epilayer	380°C	1.0
H7001	epilayer	390°C	1.2
H7003	epilayer	400°C	4.5
E30-1	bulk	none	1.4
Tr1 S1	bulk	none	4.1

According to the analysis above, the multiplication processes observed in the present study are more likely to be due to the band-to-band impact ionization processes. The theoretical fits to both equations of $M=\exp(\alpha W)$ and $1-\frac{1}{M} = \alpha_m W_{eff}$, i.e. equations (2.3) and (2.8), are respectively shown in Fig.2.20 and Fig.2.21, and two ionization rate functions of electric field, i.e. equations (2.5) and (2.6) of $\alpha=\alpha_0\exp(-E_0^2/E^2)$ and $\alpha=\alpha_0\exp(-b/E)$, are both applied. It can be seen that there is no obvious difference between the two plots of equations (2.3) and (2.8) when the ionization rate function is certain, as shown in Fig.2.20 (a) and Fig.2.21 (a) or Fig.2.20 (b) and Fig.2.21 (b). Neither is there between the two plots of equations (2.5) and (2.6) when the multiplication equation is certain, as shown in Fig.2.20 (a) and (b) or Fig.2.21 (a) and (b). At lower fields, the fittings are fairly good, in another word, they are good straight lines. Then the ionization parameters b or E_0 can be obtained from the gradients of those straight lines. It is interesting to note that the ionization parameter, either b or E_0, varies over a wide range, about an order of magnitude. The variation is by no means random experimental error. Instead it is found that they are in clear relationships with the carrier concentration n and the threshold field E_{th} of band-to-band impact ionization. They are shown in Fig.2.22 and Fig.2.23. For comparison, the data obtained from the two-stage impact ionization and the band-to-band impact ionization by Livingstone and Allen [12] and obtained from the impact excitation process by Gordon [30] is also included in Fig.2.22 and Fig.2.23. For simplicity, the ionization parameters in Fig.2.22 and Fig.2.23 are obtained by fitting to $1-\frac{1}{M} = \alpha_m W_{eff}$. Actually, the ionization parameters, b or E_0, obtained by fitting to $1-\frac{1}{M} = \alpha_m W_{eff}$ and $M=\exp(\alpha W)$, are quite similar to each other as seen in Fig.2.20 and Fig.2.21 as one example. So the same tendency can be obtained by fitting to $M=\exp(\alpha W)$ as well. It seems that the ionization parameter increases

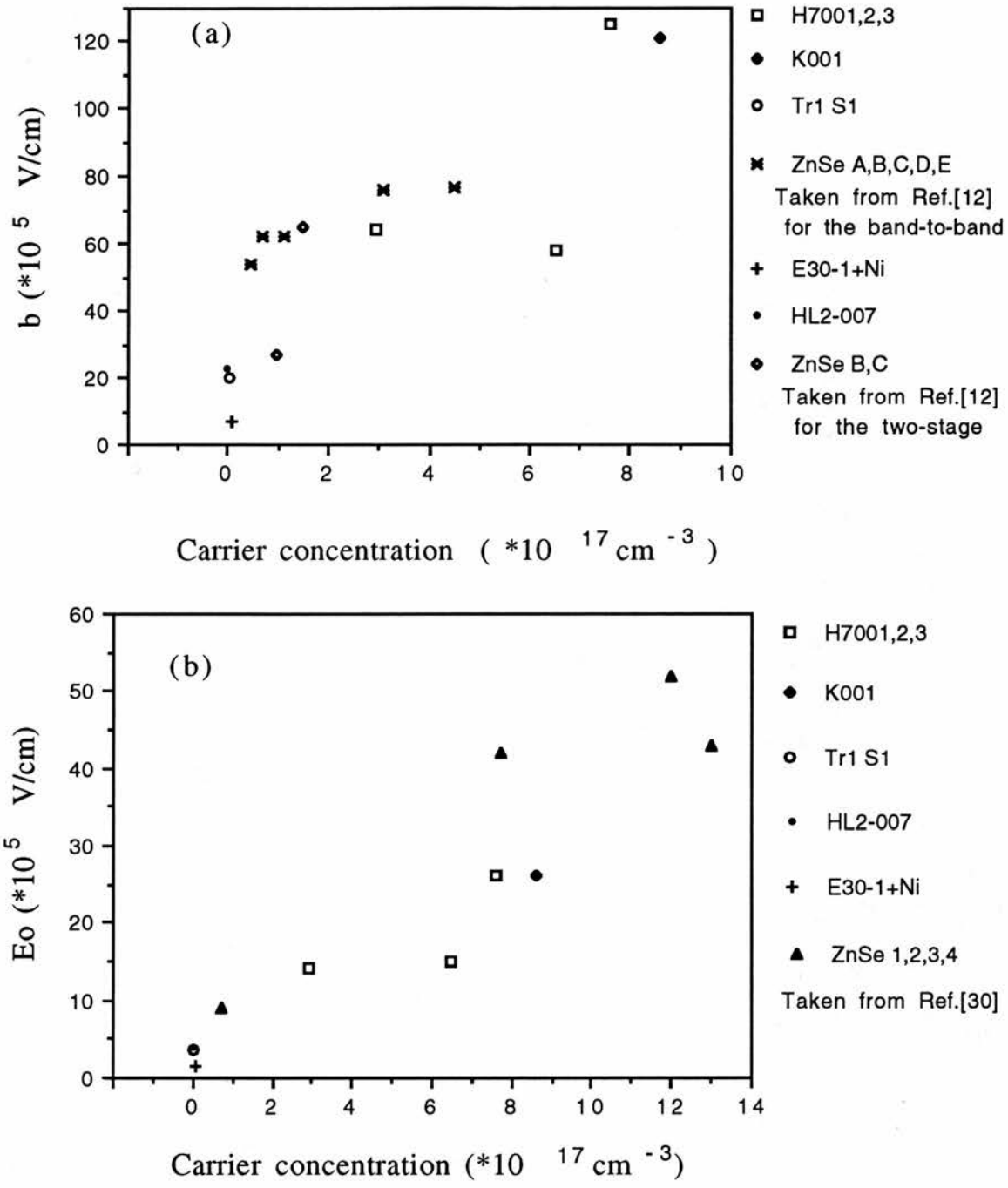

Fig.2.22: The plots of b or E_0, obtained by fitting to $1-\frac{1}{M} = \alpha_m W_{eff}$, against carrier concentration for the various samples.

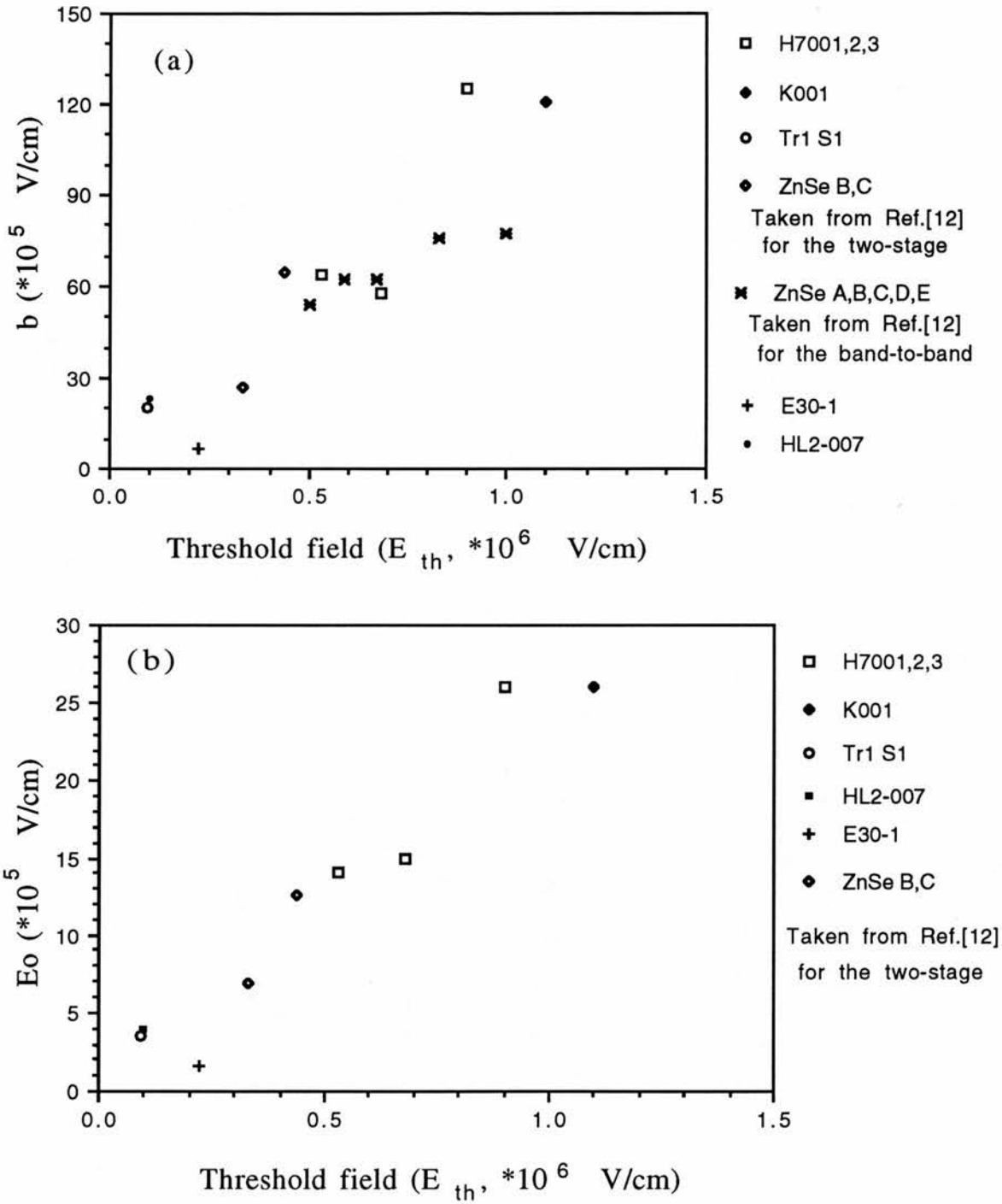

Fig.2.23: The plots of b or E_0, obtained by fitting to $1-\frac{1}{M} = \alpha_m W_{eff}$, against threshold field for the various samples.

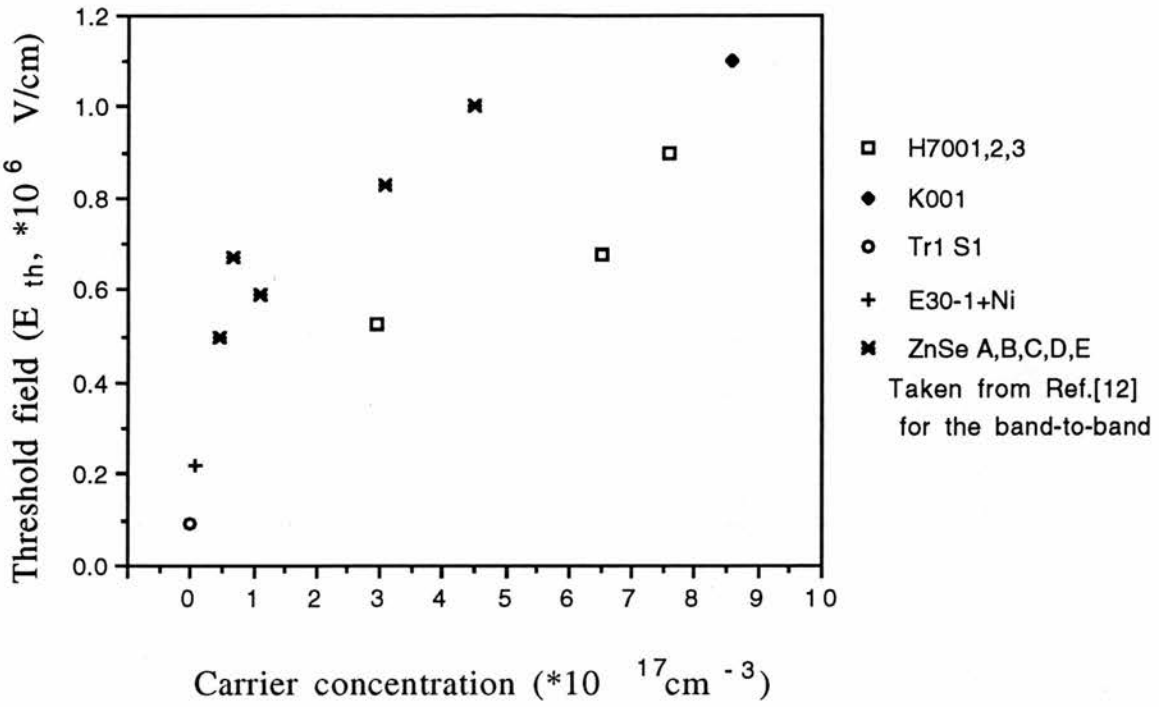

Fig.2.24: The variation of the threshold field with the carrier concentration for the band-to-band impact ionization process.

as the carrier concentration increases. Fig.2.24 shows the variation of the threshold field with the carrier concentration, showing that the threshold field increases with the increase in the carrier concentration. Allen explained this in terms of the band structure of ZnSe shown in Fig.2.25. At high fields electrons are transferred to various higher energy valleys, such as the valley L_1, the valley X_1 or the valley X_3, where the electrons have low velocity and a higher effective mass than at the bottom of the conduction band. Therefore, Rutherford scattering by ionized impurities cannot be neglected. In this case, for different samples with different carrier concentrations, the energy-acceleration rates of the carriers at high fields can be different. The scattering by ionized impurities is stronger in the sample with a larger carrier concentration, so the threshold field at which the carriers reach a certain energy and start the multiplication would be required to be higher. To be clear, we list the various conditions and coefficients of samples, obtained in

Table 2.2: The relevant impact ionization parameters for the samples in the present work and in the literature. They are, respectively, sample, growth condition, annealing temperature, impact ionization parameters b and E_0, carrier concentration and threshold electric field.

Sample	Growth	Annealing	b(10^5V/cm)	E_0(10^5V/cm)	n (10^{17}cm^{-3})	E_{th}(10^6V/cm)
The data obtained in the present work:						
H7002	epilayer	-----	125	25	7.6	0.9
H7001	epilayer	390°C	58	16	6.5	0.68
H7003	epilayer	400°C	64	15	2.9	0.53
Tr1 S1	bulk	-----	20	3.3	0.008	0.094
K001	epilayer	-----	121	27	8.6	1.1
E30-1	bulk+Ni	-----	6.7	1.7	0.06	0.22
HL2-007	epilayer	381°C	23	4.0	0.00	0.1
The data taken from Ref.[12] for the band-to-band impact ionization:						
ZnSe A	bulk	-----	77		4.5	1.0
ZnSe B	bulk	-----	76		3.1	0.83
ZnSe C	bulk	-----	62		0.67	0.67
ZnSe D	bulk	-----	62		1.1	0.59
ZnSe E	bulk	-----	54		0.47	0.5
The data taken from Ref.[30] for the impact excitation process:						
ZnSe 1	bulk+Mn	-----		9.0	0.7	
ZnSe 2	bulk+Mn	-----		42	7.7	
ZnSe 3	bulk+Mn	-----		43	13	
ZnSe 4	bulk+Mn	-----		52	12	
The data taken from Ref.[12] for the two-stage impact ionization:						
ZnSe B	bulk+Mn	-----	27	6.8	1.5	0.33
ZnSe C	bulk+Mn	-----	65	13	3.6	0.44

the present study and in Ref.[12] and Ref.[30], in Table 2.2.

In Ref.[12], Livingstone and Allen investigated the photocurrent in bulk ZnSe: Mn and ZnSe: Cu using the same method as in the present study. In ZnSe: Mn, after the plateau region, one less sharp rise in photocurrent with a saturation region followed by a sharp multiplication process was observed. Obviously, these two rises belong to different processes. Because very high concentration of manganese, for example 1% of Mn in Ref.[12], can be incorporated into ZnSe, it is likely one can observe the multiplication process due to a two-stage impact ionization. In Ref.[12] the less sharp rise was attributed to a two-stage impact ionization, and the sharp rise to a band-to-band impact ionization. In ZnSe: Cu, only one sharp rise in photocurrent was observed and it was attributed to the band-to-band impact ionization. It was explained that the copper impurity solubility in n-type ZnSe is limited by the donor concentration. It should be noted that the behaviour of the rise in photocurrent due to two-stage impact ionization tends to a saturation. This feature cannot be deduced from the simplified theory of two-stage impact ionization. However, it could be interpreted (discussed below) from the band-structure point of view. This is also the reason why the photocurrent behaviours are expected to look like the one shown in Fig.2.8.

In fact, the band structure of ZnSe, especially at high energies, is not simple parabolic which was used in theoretical impact ionization calculations. Quite a lot of ZnSe band structure calculations have been done previously [31,32]. The most detailed one was calculated with the empirical pseudopotential method by Chelikowsky, Wagener, et al. [32] in 1989. According to their results, the relevant conduction band structure and density of states of ZnSe are schematically drawn in Fig.2.25. From Fig.2.25, we can see that there are two satellite valleys X_1 and L_1 in the first conduction band. They lie about 1.71 eV and 1.13 eV above the bottom of the conduction band respectively. Another valley X_3, which belongs to the second conduction

band, lies about 0.25 eV higher than the valley X_1. The corresponding density of states has a very big peak at energy 2.4 eV with respect to the bottom of the conduction band. Although all values here are somewhat rough because of the approximations used, we can still use them to interpret experimental phenomena qualitatively.

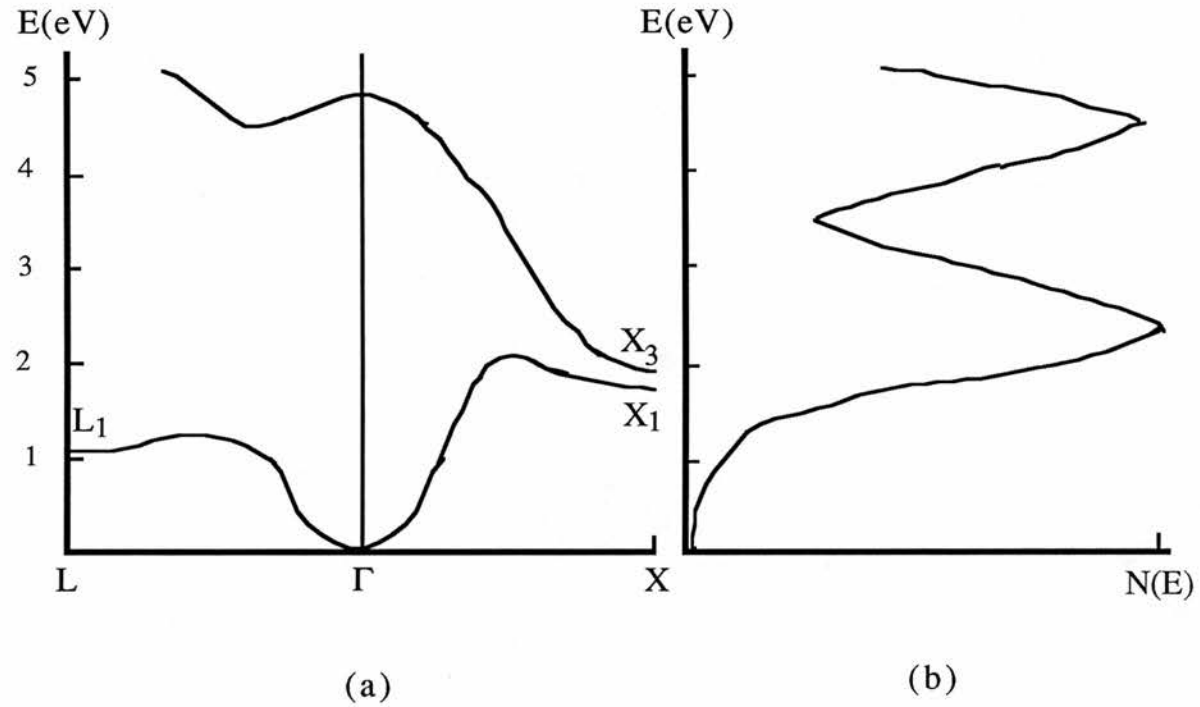

Fig.2.25: Conduction band features of ZnSe. (a) Energy-crystal momentum. (b) Energy-density of states.

At low fields the electron distribution is Maxwellian. At higher fields it departs from the Maxwellian distribution and has a tail at higher energy. As the field increases the tail extends to higher energy and contains more electrons. When the energies of the electrons in this tail are greater than the threshold energy for two-stage impact ionization, the multiplication process starts. Equations (2.5) and (2.6) for the variations of average ionization rate with the field correspond to this situation in which the number of electrons in the tail is increasing. There is a peak in the density of states at about 2.4 eV

above the bottom of the first conduction band in ZnSe (see Fig.2.25). In ZnSe: Mn, the first excited state is located at about 2.2 eV above the ground state of d^5 manganese. At high enough fields, most of the electrons which can involve into a multiplication process can be transferred to energies where the density of states is large. After this transfer, the multiplication has nearly reached a saturation because the electron distribution does not change strongly. This is expected to be a very special feature which could be applied to some special purpose, for instance, the application of two-stage impact ionization.

2.6 Conclusions

In this chapter, we have presented the behaviour of the photocurrent in a wide range of electric fields. The photoconductivity process with recombination at lower fields has been identified by calculating more accurately the electric field in good Schottky diodes. The multiplication process at higher fields fairly fits to the theory of band-to-band impact ionization. The variations of the ionization parameter, b or E_0, with carrier concentration are obtained for band-to-band impact ionization. The reason for these variations is still not very clear. The difficulty of interpretation and prediction of the electrical behaviours at high fields is the lack of the knowledge of the precise band structure of the semiconductors.

It is found that the required deep level concentration for two-stage impact ionization is very high, at least greater than $1*10^{19}$ cm^{-3} when the thickness of the active layer is of order of 1 μm. This requirement is difficult to be met generally by doping impurities, for instance, the transition-metal impurities such as Cu, Co, Ni, because the impurity solubility could be limited by donor concentrations in n-type ZnSe or ZnS. For the manganese impurity, the very high concentration (eg. 1% Mn) of neutral Mn can be substituted in zinc site in n-type ZnSe or ZnS because of its half-complete 3d-shell structure. For the

native deep-level defects, for example, zinc vacancy or selenium vacancy or their complexes with some impurity, the relative information is less known and the control of magnitude of its concentration must be difficult. So the application of two-stage impact ionization mainly depends on the further understanding of impurity deep levels in semiconductors and the techniques of doping impurities.

Chapter 3

Photocapacitance measurements of Co-doped ZnSe

3.1 Introduction

In a pure and perfect crystal, a very small amount of impurity can greatly change the optical and electrical properties of the material. This phenomenon led to the development of n-type and p-type semiconductors which became the basis of a variety of devices. Imperfect lattice defects as well as impurities can introduce some localized energy levels within the band-gap of their host. According to the position of energy level within the gap, the energy levels are divided into two categories, i.e. shallow levels and deep levels. Shallow levels, in general, are well understood and are characterized by a hydrogen-like potential approximation. The shallow levels lie typically within 0.1 eV of the relevant band edge. Deep levels, as their name suggests, lie deeper in the gap than 0.1 eV. There is no general theory to predict deep energy levels successfully. Technologically, deep centres can play an important role in the development of devices.

ZnSe, with a band-gap 2.7 eV at room temperature, is a potential semiconductor for optoelectronic devices, for example blue LED's and blue semiconductor lasers. However, the production of those optoelectronic devices is restricted by some difficulties which are mainly caused by the presence of unintentionally-doped deep centres. For example, deep levels can produce non-radiative recombination, which makes the blue emission very inefficient. Self-compensation, either by the native deep donors for p-type ZnSe or by the native deep acceptors for n-type ZnSe, could make the precise control of carrier concentration difficult. A lot of effort has been made in the investigation of deep levels in ZnSe grown by different techniques, such as

vapour-phase epitaxy (VPE), liquid-phase epitaxy (LPE), metalorganic chemical vapour deposition (MOCVD) and molecular beam epitaxy (MBE).

Junction capacitance and current techniques have been widely used in the investigation of deep centres. Several deep levels have been found in the upper half of the gap in ZnSe by DLTS measurements [33,34,35]. In the lower half of the gap, three levels, lying in the range 0.5 to 0.9 eV above the valence band and labelled L1, M and L2, were observed in undoped ZnSe by junction photocapacitance and photocurrent measurements [36,37,38,39]. The so-called undoped ZnSe in this work means a sample which is not deliberately doped with any deep impurity. When more than one deep level exists, the precise photoionization cross-section spectrum for each deep level cannot be easily obtained because of the superposition of the photoionization cross-section spectra arising from different centres, whose energy levels are close. For instance, it had been said for many years that the typical hole photoionization cross-section spectrum of the M-centre was a sharp peak at about 0.85 eV, with a threshold at 0.68 eV, followed by another broad peak at higher energy. However a clearer spectrum of the M-centre was recently discovered in ZnSe epilayers, grown by MOCVD, by Zheng and Allen [40,41]. It is characterized by a very narrow strong peak at 0.83 eV, with a threshold at 0.68 eV, followed by a much weaker and broader peak at higher energy. Apparently, the spectra of the M-centre presented in the earlier works were affected by some other centre. That is why in practice the observed spectra are slightly different from sample to sample, especially at higher energy. Fig.3.1 shows a previous typical and the newly-observed hole photoionization cross-section spectra of the M-centre. Fig.3.2 shows the spectra of the hole photoionization cross-section of the L1-centre and the L2-centre.

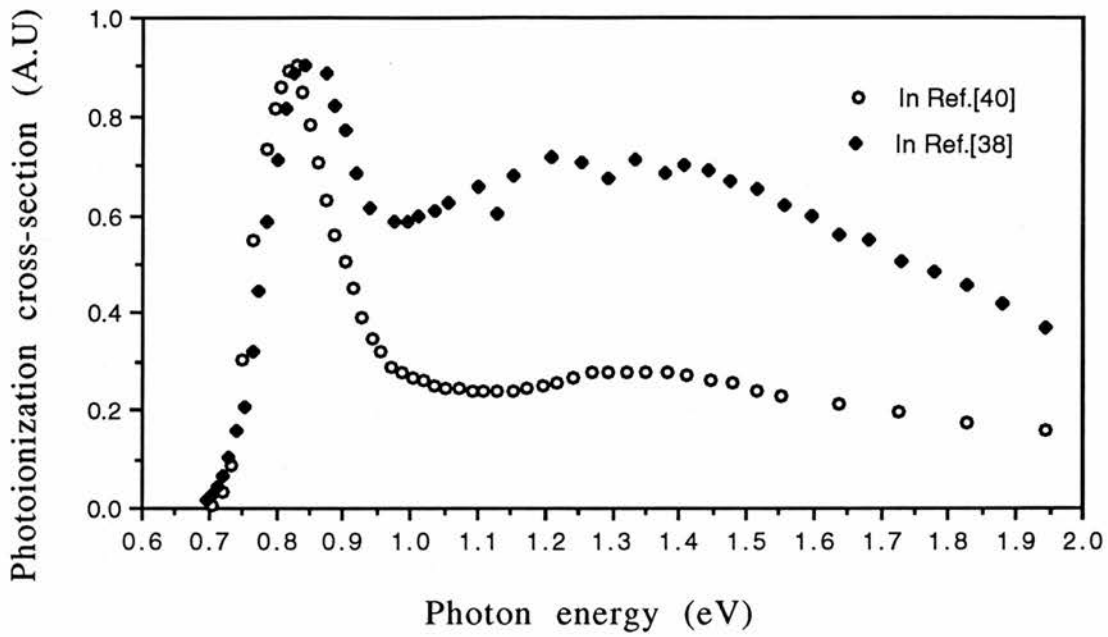

Fig.3.1: The hole photoionization cross-section spectra of the M-centre. (♦) is the typical spectrum of the M-centre obtained in undoped or Cu-doped ZnSe samples in the early days [38]. (○) the spectrum of the M-centre measured in ZnSe epilayers in Ref.[40]. They are plotted on a linear scale.

The origins of these three deep levels are still unknown. The chemical nature of deep levels cannot be identified by junction capacitance and current techniques. Actually, the L1-centre and the M-centre were observed in both undoped and Cu-doped ZnSe samples [36,37,38] and it is found by other techniques [37,42], such as photoluminescence [42], that ZnSe is easily contaminated by copper impurity from the environment. In a word, the presence of native lattice defects and unintentionally-doped impurities could make the analysis of intentionally-doped impurities difficult.

Noras, Szawelska and Allen [43] have investigated the deep levels in Co-doped ZnSe by the transient photocapacitance measurements. However, they did not consider the case of many deep levels in the analysis of the electron and hole photoionization cross-section spectra. They interpreted those spectra in terms of cobalt impurity, which is not completely correct.

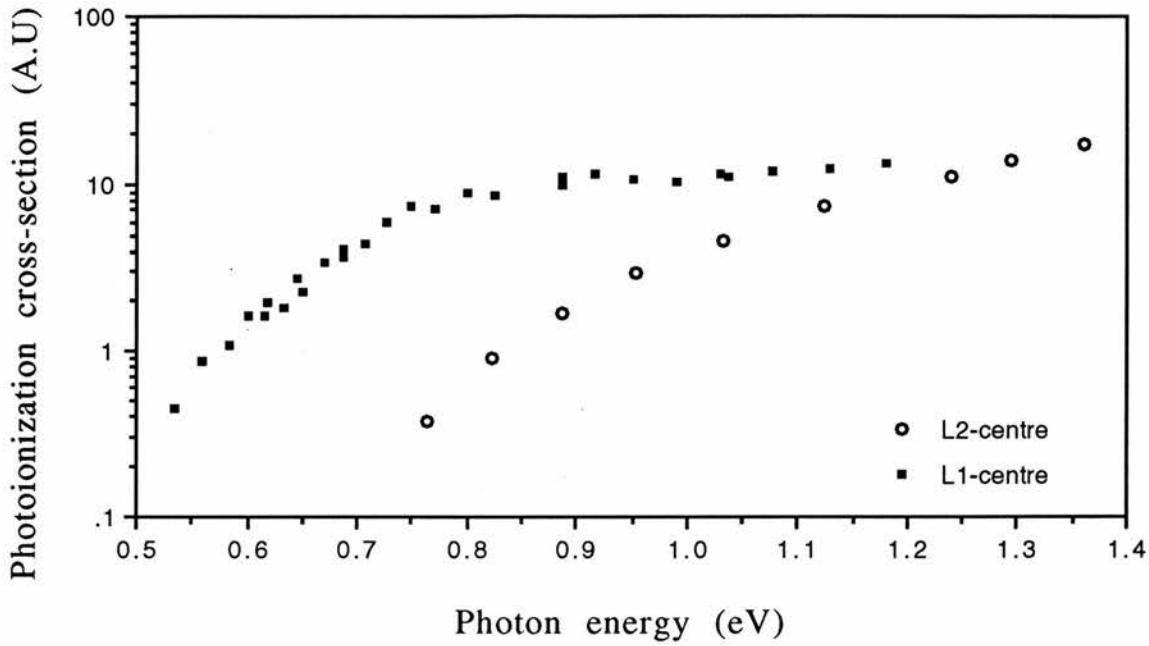

Fig.3.2: The spectra of the hole photoionization cross-section of two deep levels in undoped ZnSe measured by photocapacitance measurements. (o) obtained in Ref.[36]; (▪) obtained in Ref.[37]. They are roughly normalized at high energy 1.2 eV. These two deep centres are labelled as L1 and L2 in Ref.[39].

In this chapter, as an example, the deep levels in a Co-doped bulk ZnSe sample were investigated by dual-light steady state (DLSS) photocapacitance measurements. Three deep centres were observed in the range 0.5 to 0.9 eV above the valence band. The photoionization cross-section spectra of different centres were separated by choosing different pump photon energies. Two of these three deep centres are identified to be the L1-centre and the M-centre. Another deep level is a new centre which has not previously been observed in undoped ZnSe. Its origin is unknown. The very steep electron photoionization cross-section spectrum observed in several Co-doped bulk samples by Noras, Szawelska and Allen [43] was not seen in this work again. From the experimental point of view, it can be seen from this work that the DLSS photocapacitance method has its peculiar advantages over the transient

technique, which was widely used in the early days, to study deep levels in semiconductors when several deep levels exist in the same sample.

3.2 Principles of photocapacitance measurements

The theories of junction measurements in the study of deep energy levels in semiconductors were reviewed in the article by Grimmeiss and Ovrén [44]. Further theoretical treatments of photocapacitance measurements can be found in Zheng's thesis [39]. In this chapter, a relevant theoretical outline will be presented below. The emphasis will be on the optical cross-section spectrum involving more than one deep level.

3.2.1 Depletion region capacitance

For simplicity, the treatment here is only for an ideal Schottky diode on n-type semiconductors. Suppose that the shallow donor concentration is N_D, and a deep level concentration is N_T. Within the depletion region, the free electrons in the conduction band are swept out by an electric field, so a space-charge region is left behind. The schematic diagram of a Schottky barrier is shown in Fig.2.6. According to Poisson's equation, the electric field E(x) in the space-charge region can be written as

$$\frac{dE(x)}{dx} = \frac{\rho(x)}{\varepsilon_0 \varepsilon_s} \tag{3.1}$$

where $\rho(x)$ is the charge density, ε_0, ε_s are dielectric constants of vacuum and semiconductor respectively. Consider a simple case, i.e. the thermal filling effect at the edge of the depletion region near the bulk can be neglected, $N_D >> N_T$ and there is no carrier left in the conduction band in the space-charge region. Then the charge density is constant, and can be expressed as

$$\rho(x) = \rho = q(N_D - sn_T), \qquad 0<x<W \tag{3.2}$$

where s is the number of electrons trapped at a deep centre, n_T is the deep level concentration occupied by electrons. Integration of equation (3.1) gives

$$\int dE(x) = \int \frac{\rho}{\varepsilon_0 \varepsilon_s} dx \qquad (3.3)$$

and

$$E(x')-E(0)= \frac{\rho}{\varepsilon_0 \varepsilon_s} x'.$$

When x=0, $E(0)=- E_{max} =- \frac{\rho}{\varepsilon_0 \varepsilon_s} W$, so

$$E(x)= \frac{\rho}{\varepsilon_0 \varepsilon_s} (x-W) .$$

Since $E(x)=-\frac{dV(x)}{dx}$, the total voltage across the depletion region can be integrated as

$$\int dV(x) = \int - \frac{\rho}{\varepsilon_0 \varepsilon_s} (x-W) dx , \qquad (3.4)$$

so

$$V(W)-V(0)= \frac{1}{2} \frac{\rho}{\varepsilon_0 \varepsilon_s} W^2 \qquad (3.5)$$

and

$$V_d + V_R = \frac{1}{2} \frac{q}{\varepsilon_0 \varepsilon_s} (N_D - s n_T) W^2 \qquad (3.6)$$

where V_d is the built-in barrier potential, V_R is the applied reverse bias. The width of the depletion region is

$$W=\left(\frac{2\varepsilon_0 \varepsilon_s (V_d + V_R)}{q(N_D - s n_T)}\right)^{1/2} . \qquad (3.7)$$

When the test signal frequency is high enough for the change of occupancy of the deep centres not to respond, the change of the voltage across the depletion region under the perturbation of the small high frequency signal can be derived from equation (3.6), that is

$$(dV)_{HF}= \frac{q}{\varepsilon_o\varepsilon_s}(N_D\text{-}sn_T)W(dW)_{HF}\,. \tag{3.8}$$

So the capacitance of the depletion layer, under the small signal condition, is

$$C=(\frac{dQ}{dV})_{HF}=(\frac{dQ}{dW})_{HF}(\frac{dW}{dV})_{HF} \tag{3.9}$$

where

$$(\frac{dQ}{dW})_{HF} = qA(N_D\text{-}sn_T)$$

and A is the area of the Schottky contact. Then one has

$$C = \frac{A\varepsilon_o\varepsilon_s}{W} = (\frac{A^2q\varepsilon_o\varepsilon_s}{2(V_d+V_R)}(N_D\text{-}sn_T))^{1/2}\,. \tag{3.10}$$

In the dark, the carrier concentration of the bulk equals to N_D-sn_T. In practice, this is one conventional method to get the carrier concentration of semiconductors. Under illumination, the capacitance of the depletion region can be changed by the change of the electron occupancy of deep levels within the depletion region. If this capacitance change is small and $N_T<<N_D$, then the change in the electron occupancy of deep levels, Δn_T, is proportional to the change in capacitance, ΔC. The derived formula for the fractional change of capacitance is

$$\frac{\Delta C}{C} = -\frac{\Delta n_T}{2N_D}\,. \tag{3.11}$$

This is the basis of photocapacitance measurements. The sign of the capacitance change can further offer information about the band involved.

An increase in the capacitance is the result of the electron ionization process from the deep centre to the conduction band and a decrease in the capacitance is the result of the hole ionization process from the deep centre to the valence band (i.e. an electron transition from the valence band to the deep centre).

3.2.2 The rate equation

First of all, the case of a single deep level within the band gap is considered. The possible transitions through this deep level are shown in Fig.3.3. The optical and thermal emission rates of a bound electron to the conduction band and of a bound hole to the valence band are denoted as e_n^o, e_n^t and e_p^o, e_p^t respectively. The capture constants from the conduction band into a deep level and from the valence band into a deep level are denoted as c_n and c_p. The change in the electron occupancy of deep energy levels can be expressed by the following rate equation

$$\frac{dn_T}{dt} = \frac{dp}{dt} - \frac{dn}{dt} = e_p p_T - c_p p n_T - e_n n_T + c_n n p_T \qquad (3.12)$$

where $e_{n,p}=e_{n,p}^o+e_{n,p}^t$, n and p are the free electron and hole concentrations in the conduction band and the valence band.

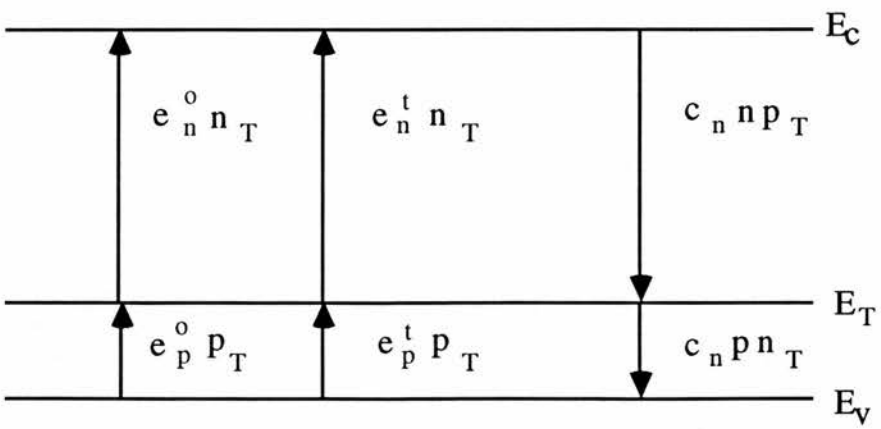

Fig.3.3: The schematic diagram of possible emission and recombination transitions through a deep level in a semiconductor.

Within the depletion region, if the thermal filling effect at the edge of the depletion layer near the bulk is neglected, then n=p=0. Equation (3.12) reduces to

$$\frac{dn_T}{dt} = (e_p^o+e_p^t)(N_T-n_T) - (e_n^o+e_n^t)\, n_T. \tag{3.13}$$

Integration of equation (3.13) gives

$$n_T(t) = \frac{e_p^o+e_p^t}{e_p^o+e_p^t+e_n^o+e_n^t}\, N_T +$$

$$(n_T(0) - \frac{e_p^o+e_p^t}{e_p^o+e_p^t+e_n^o+e_n^t} N_T) \exp[-(e_p^o+e_p^t+e_n^o+e_n^t)\, t] \tag{3.14}$$

It is readily seen that the electron occupancy of the deep level varies exponentially with time, whatever the initial conditions are, and the time constant is given by

$$\tau = \frac{1}{e_p^o+e_p^t+e_n^o+e_n^t}. \tag{3.15}$$

Under the steady-state conditions, equation (3.14) gives the expression for the electron occupancy by

$$\frac{n_T}{N_T} = \frac{e_p^o+e_p^t}{e_p^o+e_p^t+e_n^o+e_n^t}. \tag{3.16}$$

3.2.3 Transient photocapacitance

If the temperature is low enough, e_p^t and e_n^t can be neglected. Equation (3.15) reduces to

$$\tau = \frac{1}{e_p^o+e_n^o}. \tag{3.17}$$

For a single deep level in the upper half of the gap, if the photon energy of the monochromatic illumination is restricted to $E_T<h\nu<E_g-E_T$, then the

electron optical emission coefficient e_n^o could be much bigger than the hole optical emission coefficient e_p^o. Thus the time constant is expressed by

$$\tau = \frac{1}{e_n^o}. \tag{3.18}$$

Since the optical emission coefficient is related to the photoionization cross-section σ^o by $\sigma_{n,p}^o = e_{n,p}^o/\phi$, where ϕ is the photon flux, the absolute electron photoionization cross-section can be obtained by

$$\sigma_n^o = 1/\tau\phi. \tag{3.19}$$

For a single deep level in the middle or lower half of the gap, illumination in the energy range $E_T < h\nu < E_g$ will cause two electron transitions, i.e. from the valence band to the deep level and from the deep level to the conduction band, to occur simultaneously. In this case, e_n^o cannot be easily found by equation (3.17) unless more parameters of deep centres are known.

If the level is first completely filled in the dark, for example by applying a forward bias, and then emptied under illumination, the capacitance change, $C_\infty - C_d$, is obtained from equation (3.11), i.e.

$$\frac{C_\infty - C_d}{C_d} = -\frac{n_\infty - n_d}{2N_D} \tag{3.20}$$

where the subscripts d and ∞ stand for the dark and the steady-state conditions respectively, and $n_d = N_T$. n_∞ can be derived from equation (3.16), i.e. $n_\infty = n_T = \frac{e_p^o}{e_p^o + e_n^o} N_T$. So equation (3.20) becomes

$$\frac{C_\infty - C_d}{C_d} = \frac{N_T}{2N_D} \frac{e_n^o}{e_p^o + e_n^o}. \tag{3.21}$$

Substituting equation (3.17) into the above equation, one has

$$e_n^o = \frac{(C_\infty - C_d)}{\tau} * \frac{2N_D}{C_d N_T}, \tag{3.22}$$

and the relative electron photoionization cross-section is given by

$$\sigma_n^o \propto (\tau \phi)^{-1}(C_\infty - C_d). \tag{3.23}$$

The absolute electron photoionization cross-section can only be obtained when N_D and N_T are known.

Suppose the level is first emptied by illumination with a photon energy greater than E_T, and then illuminated with the light in the energy range $E_g - E_T < h\nu < E_T$. In this case, $e_n^o << e_p^o$, and the absolute hole photoionization cross-section is given by

$$\sigma_p^o = (\tau \phi)^{-1}. \tag{3.24}$$

3.2.4 Dual-light source steady-state photocapacitance

In the DLSS photocapacitance measurements, two beams of light are employed. A pump light with much stronger intensity is used to establish the initial electron occupancy of the deep level and a probe light with weaker intensity is used to perturb the occupancy of the deep level. The theoretical derivations are presented below.

Within the depletion region, when the thermal filling effect near the depletion region edge can be neglected, the possible optical and thermal transitions through the deep level in the lower half of the band gap are shown in Fig.3.4. The capture rates are omitted because the carrier concentrations n and p are small.

When the steady state is established under illumination with the pump light, the electron occupancy of the deep level is given by

$$\frac{n_T}{N_T} = \frac{e_{ps}^o + e_p^t}{e_{ps}^o + e_p^t + e_{ns}^o + e_n^t} \tag{3.25}$$

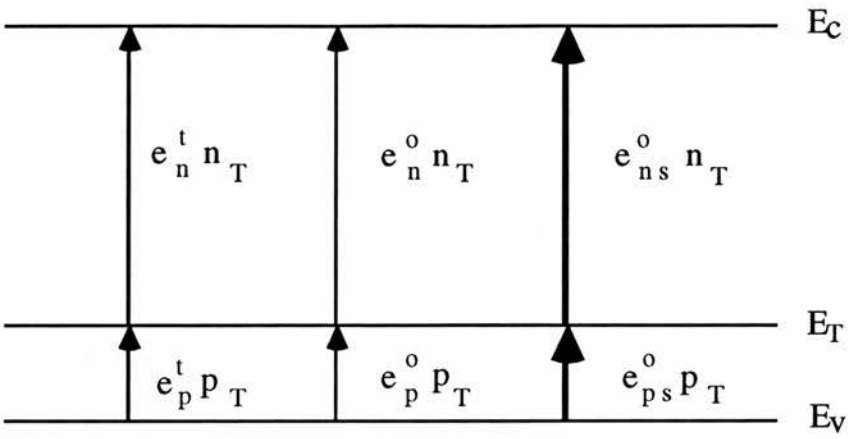

Fig.3.4: The schematic diagram of possible transitions within the depletion region of a Schottky diode under illumination with the pump light and the probe light.

where e_{ps}^o and e_{ns}^o are the hole and electron emission rates of the pump light, e_p^o and e_n^o are the hole and electron emission rates of the probe light. When the sample is illuminated with both the pump light and probe light, the steady-state electron occupancy of the deep level is

$$\frac{n_T'}{N_T} = \frac{e_{ps}^o+e_p^o+e_p^t}{e_{ps}^o+e_p^o+e_p^t+e_{ns}^o+e_n^o+e_n^t}. \qquad (3.26)$$

When the pump light is much stronger than the probe light, $e_{ps}^o+e_{ns}^o >> e_p^o+e_n^o$. The change of the electron occupancy Δn_T, produced by the probe light, is

$$\frac{\Delta n_T}{N_T} = \frac{(e_{ns}^o+e_n^t)e_p^o-(e_{ps}^o+e_p^t)e_n^o}{(e_{ps}^o+e_p^t+e_{ns}^o+e_n^t)^2} = \frac{Ae_p^o-Be_n^o}{(A+B)^2} \qquad (3.27)$$

where $A=e_{ns}^o+e_n^t$ and $B=e_{ps}^o+e_p^t$. The quantities A and B are constant at a given temperature when the photon energy of the pump light is not changed. By choosing the photon energy of the pump light, $h\nu_s$, and the scanning energy range of the probe light, $h\nu$, the change of the electron occupancy Δn_T

can be simply proportional to either e_n^o or e_p^o. For example, consider the case shown in Fig.3.4, when $E_g-E_T<h\nu_s<E_T$ and $E_T<h\nu<E_g$, $A<<B$. Thus one has

$$\frac{\Delta n_T}{N_T}=\frac{-Be_n^o}{(A+B)^2} \tag{3.28}$$

and

$$\sigma_n^o= e_n^o/\phi \propto \Delta n_T/\phi \propto \Delta C/\phi. \tag{3.29}$$

When $E_T<h\nu_s<E_g$ and $E_g-E_T<h\nu<E_T$, $e_n^o<<e_p^o$, thus one has

$$\frac{\Delta n_T}{N_T}=\frac{Ae_p^o}{(A+B)^2} \tag{3.30}$$

and

$$\sigma_p^o= e_p^o/\phi \propto \Delta n_T/\phi \propto \Delta C/\phi. \tag{3.31}$$

where ϕ is the photon flux of the probe light. Therefore, the relative electron and hole photoionization cross-section spectra can be obtained by measuring the photocapacitance change produced by the probe light.

3.2.5 Consideration of many deep levels within the band-gap

The case of a single deep level is quite rare in a wide-gap semiconductor, e.g. ZnSe and ZnS. When more than one deep level exists the total capacitance change is obtained by the sum of the changes of the electron occupancy for each level. Equation (3.11) is replaced by

$$\frac{\Delta C}{C}=-\frac{\Sigma \Delta n_{T_i}}{2N_D} \tag{3.32}$$

where the summation is over all deep levels within the gap, the suffix 'i' stands for the ith deep level. Similarly, when the thermal filling effect is neglected, the rate equation (3.12) for each deep level is still valid, that is

$$\frac{dn_{T_i}}{dt} = (e_{p_i}{}^{o}+e_{p_i}{}^{t})(N_{T_i}-n_{T_i}) - (e_{n_i}{}^{o}+e_{n_i}{}^{t})\, n_{T_i}. \tag{3.33}$$

Integration of the above equation gives the time dependence of the electron occupancy for each deep level, which is an exponential process and the time constant for the ith deep level is given by

$$\tau_i = \frac{1}{e_{p_i}{}^{o}+e_{p_i}{}^{t}+e_{n_i}{}^{o}+e_{n_i}{}^{t}}. \tag{3.34}$$

For different deep levels, the time constants could be different because of different emission rates. The transient process involving many deep levels is the sum of all transient processes due to each deep level. It is not a simple exponential process. This is the case which is often observed in practice. Even in the case when the fastest and slowest time constants can be resolved they could be due to levels in relatively small concentration. Generally, the transient photocapacitance measurement is less useful in this case.

In the steady state, the electron occupancy for each deep level is still given by equation (3.16), that is

$$\frac{n_{T_i}}{N_{T_i}} = \frac{e_{p_i}{}^{o}+e_{p_i}{}^{t}}{e_{p_i}{}^{o}+e_{p_i}{}^{t}+e_{n_i}{}^{o}+e_{n_i}{}^{t}}. \tag{3.35}$$

In the DLSS measurement, the change of the electron occupancy for each deep level, Δn_{T_i}, produced by the probe light, is

$$\frac{\Delta n_{T_i}}{N_{T_i}} = \frac{A_i e_{p_i}{}^{o}-B_i e_{n_i}{}^{o}}{(A_i+B_i)^2} \tag{3.36}$$

where $A_i=e_{ns_i}{}^{o}+e_{n_i}{}^{t}$ and $B_i=e_{ps_i}{}^{o}+e_{p_i}{}^{t}$ for the ith deep level. In some certain conditions as discussed in the case of a single deep level, the above equation can be further simplified as either $\Delta n_{T_i} \propto e_{p_i}{}^{o}$ or $\Delta n_{T_i} \propto e_{n_i}{}^{o}$. Therefore, the sum of the changes of the electron occupancy for each level can be proportional to

either $\Sigma A_i e_{p_i}^{o}$ (i.e. $\phi\Sigma A_i \sigma_{p_i}^{o}$) or $\Sigma B_i e_{n_i}^{o}$ (i.e. $\phi\Sigma B_i \sigma_{n_i}^{o}$). In principle, the total change of the electron occupancy of many deep levels can be dominated by that of a single deep level. In the DLSS photocapacitance measurements, one can preferentially fill or empty a particular level by choosing an appropriate pump photon energy and the probe light can be used to study this particular level. Therefore the photoionization cross-section spectra of different deep levels can be separated.

3.3. Experiments

3.3.1 Sample preparation

There are several ways to introduce impurities into a crystal. One way is by diffusion. For example, cobalt can be introduced into ZnSe either by evaporating a thin layer of cobalt onto one face of a ZnSe slice and then heating in vacuum, or by heating the ZnSe in a liquid zinc-cobalt bath. Using these two methods, the maximum cobalt concentration is limited by the diffusion temperature, and the cobalt distribution may not be uniform. For example, a cobalt concentration of 10^{18} cm^{-3} was obtained in Ref.[45] by the former method. The samples treated in the former method are high resistivity, which are suitable for absorption measurements, photoluminescence measurements and so on. The samples treated in the latter method are usually low resistivity, which is required for a Schottky diode.

Cobalt can also be introduced when the ZnSe crystal is being grown. Using this way, very high cobalt concentrations, for example ZnSe: Co 0.5%, can be achieved. However the resulting ZnSe samples are high resistivity. It has been found that treatment in a molten zinc bath can make other ZnSe samples conducting. Several zinc-treatments were tried on ZnSe: Co 0.3% and ZnSe: Co 0.5% with different recipes, i.e. different time periods and different

temperatures and in horizontal and vertical furnace, in this laboratory. However, severe cobalt precipitation on the sample surface was seen in all of the zinc-treated ZnSe: Co 0.3% and ZnSe: Co 0.5% samples. After the cobalt precipitation was removed by the etching in acid and gentle polish, the indium dots as the ohmic contacts were heated on the surface. The procedure of making the ohmic contacts will be described below. The I-V measurements between those indium dots showed that some samples were conducting at the beginning. However after being polished gently or being etched in Br-methanol, the samples became insulating again. This phenomenon indicated that the samples were only conducting on the sample surface. It is possible that the high cobalt concentration or the cobalt precipitation may produce some other centre within the gap of ZnSe so as to make the samples very insulating. Therefore the zinc-treatment on heavy Co-doped ZnSe cannot make the samples conducting successfully.

In this work, in order to get a conducting Co-doped ZnSe sample, the cobalt was introduced by heating the sample in a molten zinc-cobalt bath at about 960°C for 160 hours. After the treatment, the sample was soaked in acid until metals zinc and cobalt had been removed from the sample surface. The sample is labelled as E32-5.

3.3.2 Making a Schottky diode

Before making the ohmic contacts, the sample E32-5, doped with cobalt, was etched in 1% Br-methanol for two and half minutes, then left in carbon disulphide for about 30 minutes followed by another etching in 50% caustic soda solution at 50°C for 20 minutes and rinsing with deionized water several times. Ohmic contacts were then made on one side with indium dots by heating at 310°C in $90\%N_2/10\%H_2$ for 30 seconds. The I-V characteristics between two indium dots were measured in both directions of current. They showed straight lines which indicated that the contacts were ohmic. After the

same etching and rinsing procedures were performed on the sample again aluminium was evaporated on the other side in vacuum (about $2*10^{-6}$ torr) to form a semi-transparent metal Schottky contact.

The quality of the Schottky diode was checked in the dark by the conventional I-V and C-V measurements. The I-V characteristics showed the rectification property of a Schottky diode, which means the forward-biassed current is large and the reverse-biassed current is smaller. However, the leakage current in reverse bias was fairly high. This could be due to an extra layer between the aluminium and the ZnSe. The capacitance of the diode at zero voltage was about 1045 pF. The C^{-2}-V capacitance characteristic could not be obtained because of this high leakage current, therefore the carrier concentration of this sample was not known. Although the quality of the diode was not very good, it could still be used for the photocapacitance measurements since a true resistance-capacitance bridge is used.

3.3.3 Apparatus for photocapacitance measurements

The photocapacitance measurements were carried out in a dark room. The sample was mounted on a metal finger by two spring contacts, and placed inside a gas-flow cryostat where the temperature was accurately controlled at liquid nitrogen temperature (LNiT) of 77°K during the measurements.

The optical path and the measuring system are schematically shown in Fig.3.5. The pump light came from a 250 W tungsten-halogen lamp, went through a monochromator with wide slits, then appropriate filters and lenses, finally was focused on the Schottky contact. The probe light came from a 100 W tungsten-halogen lamp, went through another monochromator with much narrower slits and then appropriate filters and lenses to be shone on the diode. The wavelength of the probe light was remotely controlled by a stepper-motor drive controlled by an IBM PC computer. A remotely

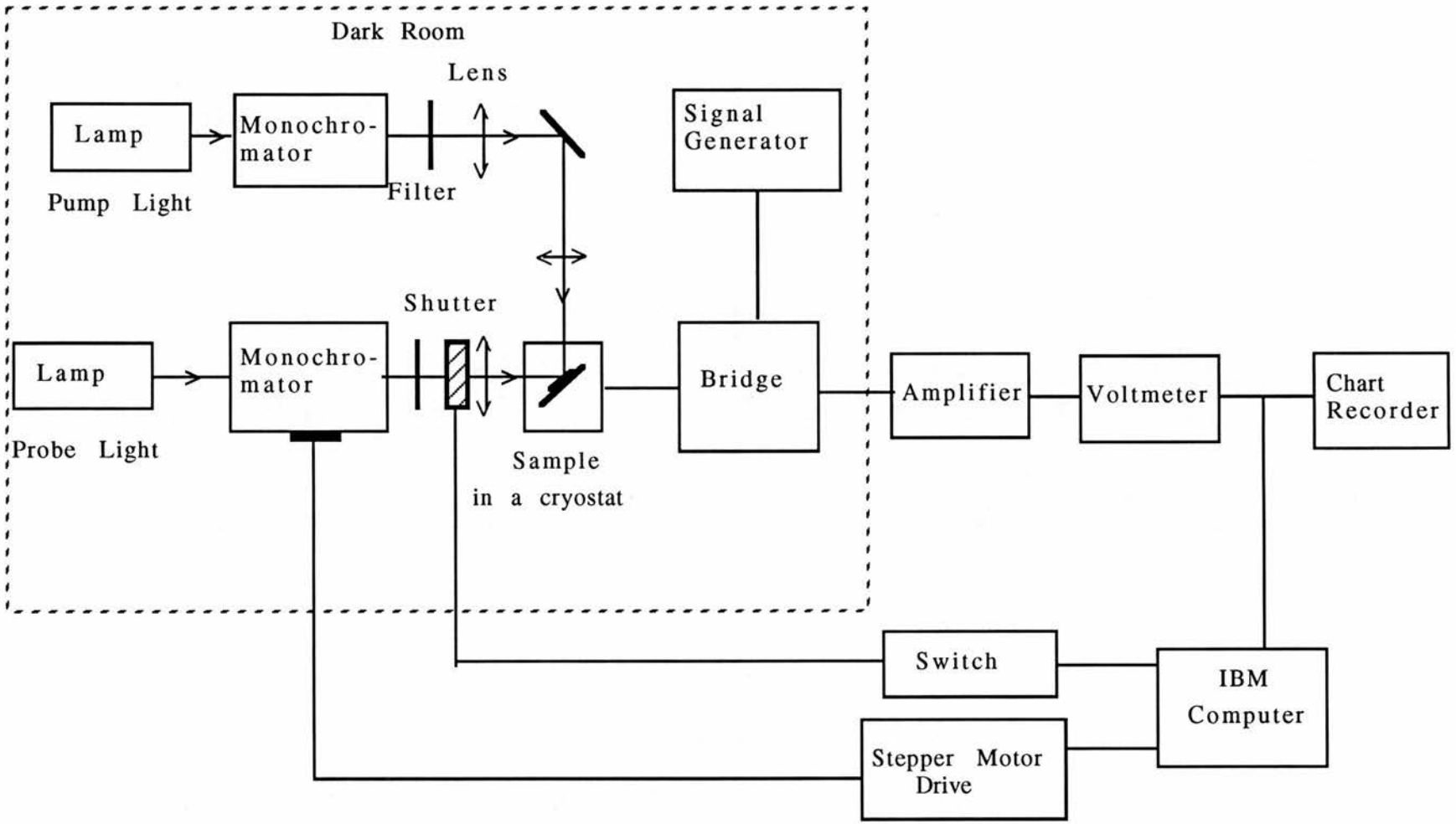

Fig.3.5: Schematic diagram of the optical path and the measuring system of photocapacitance measurements

controlled shutter was placed in the optical path of the probe light in order to measure the capacitance change produced by the probe light.

The capacitance measurements were made with a specially constructed ratio-arm bridge. The off-balance voltage signal is proportional to the capacitance change in the sample. The AC voltage on the diode was 30 mV peak-to-peak at 400 kHz. No DC reverse bias was applied to the diode. Photon fluxes were measured by a thermopile at room temperature in the same optical conditions as those in which the sample was measured.

3.4 Results

All photocapacitance measurements were made at liquid nitrogen temperature. A single beam photocapacitance measurement was first carried out on the diode in order to get rough information about the deep level positions within the band gap. Initially, all levels were filled by applying a forward bias in the dark, then the light was shone on the sample. A positive capacitance change, produced by the light, was observed in the wide energy range 0.7 to 2.7 eV. The sign of the capacitance change shows that the involved electron transition is from the centre to the conduction band. The spectrum shown in Fig.3.6 is the relative capacitance change, calibrated by the photon flux, at different photon energies. The observed capacitance change at 0.78 eV, which was the energy where the spectrum started to be scanned in the experiment, and the increase at about 2.0 eV in the spectrum indicate that there are some levels in both the lower half and the upper half of the band gap.

To investigate the deep levels in the lower half of the band gap, DLSS photocapacitance measurements were carried out. For the hole photoionization cross-section, the sample was initially illuminated with the

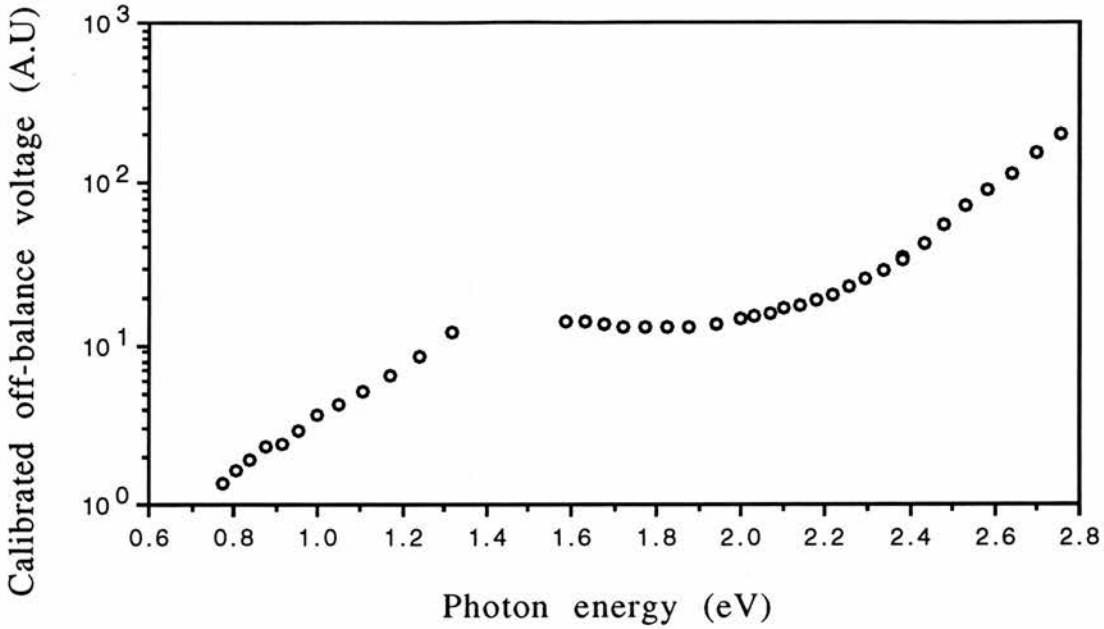

Fig.3.6: The spectrum of the calibrated off-balance voltage as a function of photon energy obtained in ZnSe E32-5 by the single-beam photocapacitance measurement.

pump light of photon energy $h\nu_s$ ($E_T<h\nu_s<E_g$), where E_T is the deep level position within the gap with respect to the conduction band. At this photon energy the deep level was only partially emptied because the two electron transitions, i.e. from the deep level to the conduction band and from the valence band to the deep level, took place simultaneously. The capacitance bridge was balanced in this initial condition. Then the probe light of photon energy $h\nu$ ($E_g-E_T<h\nu<E_T$) was switched on and the off-balance signal was recorded at different photon energies. The capacitance change was negative, showing that the probe light induced the electron transition from the valence band to the deep level (i.e. the hole photoionization process from the deep level to the valence band). Therefore the corresponding hole photoionization cross-section spectrum was obtained in accordance with equation (3.31).

Fig.3.7 shows the relative hole photoionization cross-section spectra, in the range 0.7 to 1.4 eV, pumped at different photon energies. The spectra are

normalized at 1.22 eV. The spectrum with the pump light of 490 nm (2.53 eV) has a strong peak at 0.86 eV followed by a rise at higher energy. As the pump photon wavelength increases the intensity of the peak at 0.86 eV decreases compared with the rise at higher energy. When the pump wavelength is 550 nm (2.25 eV) this peak nearly disappears in the background of the rise. The spectra at high energy are in excellent agreement. This phenomenon indicates that the peak at 0.86 eV and the rise at higher energy originate from different deep levels. The spectrum in Fig.3.7, pumped at a given photon energy, is the linear sum of hole photoionization cross-sections of different levels, as discussed in section 3.2.5. Since different deep levels have different photon energy dependences of emission rates, the electron occupancy of different deep levels could be very different at different pump photon energies. The spectrum with the pump wavelength 490 nm has a dominant component of the peak at 0.86 eV due to one centre. The spectrum with the pump

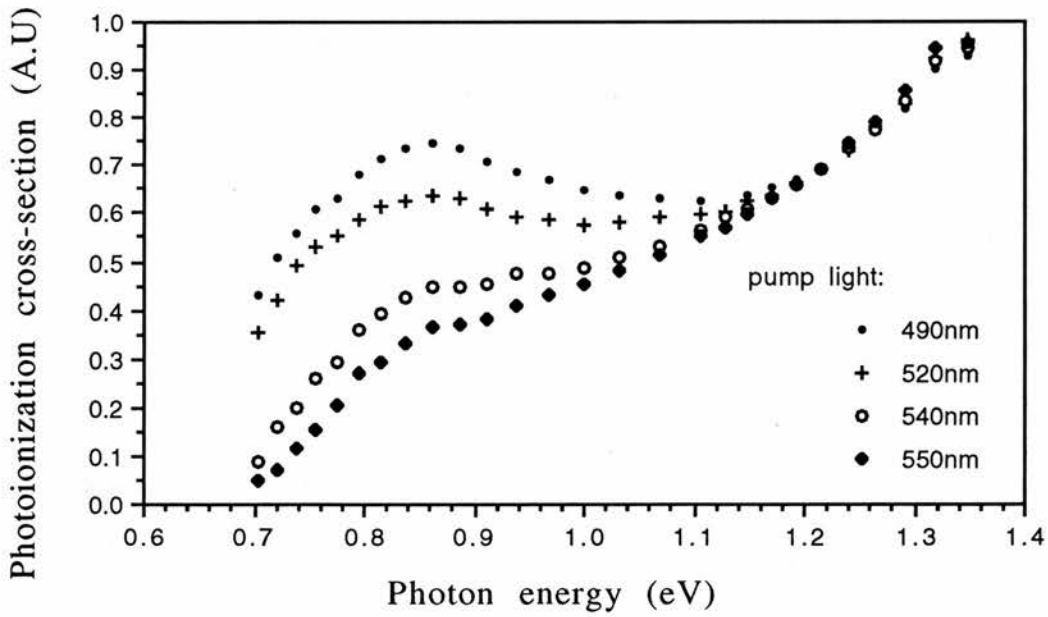

Fig.3.7: The hole photoionization cross-section spectra obtained in ZnSe E32-5 by DLSS photocapacitance measurements. The pump wavelengths are 490 nm (2.53 eV), 520 nm (2.38 eV), 540 nm (2.30 eV) and 550 nm (2.25 eV) respectively. The spectra are normalized at 1.22 eV.

wavelength 550 nm has a dominant component of the rise at higher energy due to another centre. As the pump wavelength increased the observed signal decreased. 550 nm was the highest photon wavelength for the pump light to get an observable spectrum. Therefore the hole photoionization cross-sections of these two levels could not be completely separated by choosing a pump photon wavelength, for example 610 nm (2.03 eV), which could only pump the level corresponding to the rise at higher energy but not the other level. So the threshold photon energy corresponding to the feature at high energy cannot be obtained. However, this level position could be estimated to be at about 0.9 eV above the valence band by extrapolation. This deep level is labelled L3. The hole photoionization cross-section spectra in the extended energy range up to 2.0 eV are shown in Fig.3.8. The more complete optical cross-section spectrum of the L3-centre is a broader feature peaked at about 1.5 eV.

Comparing the shape and the peak position of the feature peaked at 0.86 eV in Fig.3.7, especially in the spectrum with the pump light of 490 nm, with those of the characteristic peak of the M-centre shown in Fig.3.1 after Allen and Zheng [40], it can be seen that they are very similar. In Fig.3.7, the small shift of the peak position to higher energy could be due to superposition of the optical cross-section of the L3-centre, and the less sharp rise in the range 0.70 to o.86 eV could be due to another feature at even lower energy, which will be discussed below. Moreover, it has been found that the M-centre occurs in many samples of ZnSe, whatever the growth method is. Therefore it can be concluded that the peak at 0.86 eV in Fig.3.7 arises from the M-centre, which is located at 0.68 eV above the valence band.

It has been suggested in Ref.[40] that there must be another centre which lies close to the level position of the M-centre within the band gap and its hole photoionization cross-section spectrum superposes on that of the M-centre at photon energies higher than 0.83 eV. The origin of this centre is

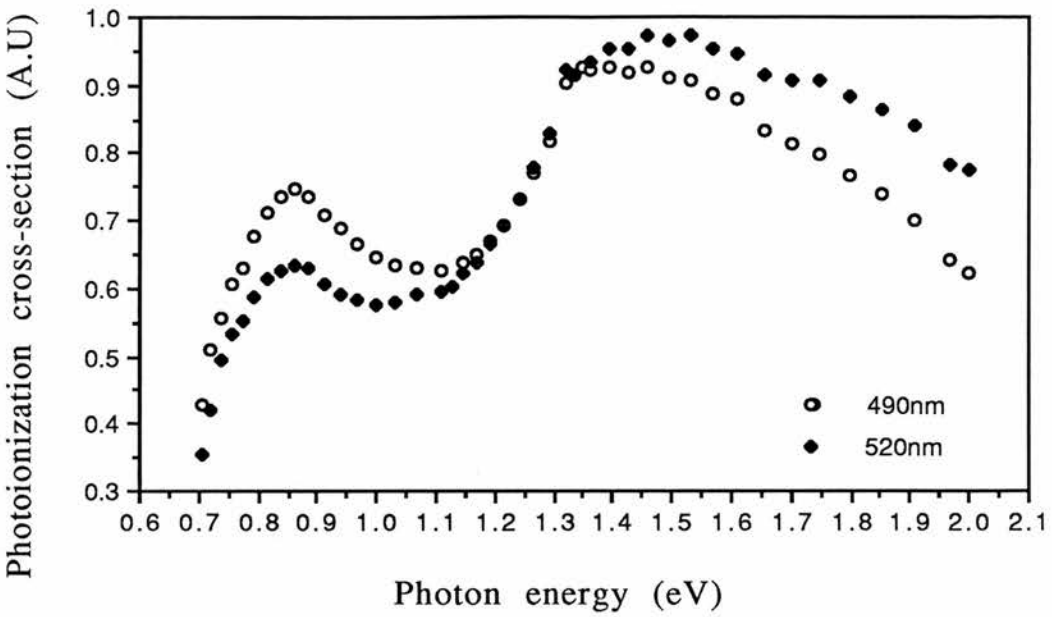

Fig.3.8: The hole photoionization cross-section spectra of ZnSe E32-5 in the wider energy range obtained by DLSS photocapacitance measurements. The pump wavelengths are 490 nm (2.53 eV) and 520 nm (2.38 eV) respectively.

unknown. It has been found in many undoped and Cu-doped ZnSe samples. Its typical spectrum, as observed in Cu-doped ZnSe samples in Ref.[38], is a broad feature peaked at 1.3 eV. Comparing the spectrum in Ref.[38] with that of the L3-centre, shown in Fig.3.9, it can be seen that they are not in agreement. So the L3-centre is a different centre from the one (labelled L4) with peak at 1.3eV observed previously in undoped and Cu-doped ZnSe samples. It is also noted from Fig.3.9 that the M-centre appears in all samples and the L3-centre is only important in Co-doped ZnSe E32-5, but in the spectra obtained by Zheng and Grimmeiss at el the L3-centre is not obvious but the L4-centre is.

We have also compared the hole photoionization cross-section spectrum of the L3-centre with that of the L2-centre shown in Fig.3.2. They are not in agreement, showing that they are not the same centre.

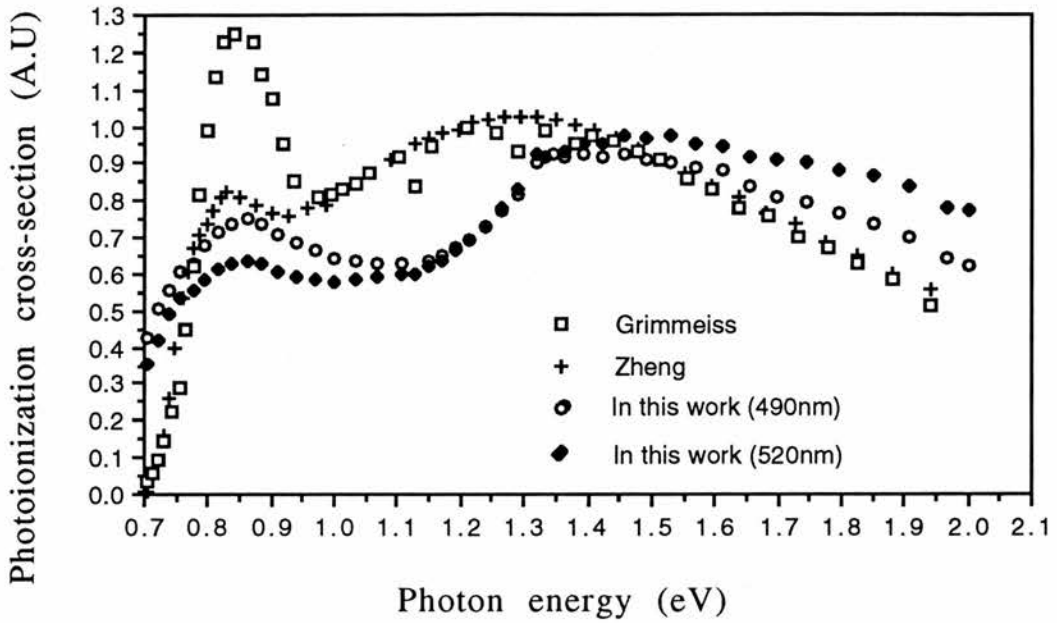

Fig.3.9: The comparison of the hole photoionization cross-section spectra obtained in different ZnSe samples by photocapacitance measurements. (♦) and (○) for Co-doped ZnSe E32-5 in this work with the pump light of 520 nm (2.38 eV) and 490 nm (2.53 eV) respectively; (+) for an undoped ZnSe epilayer sample H814 measured by Zheng (This data has not been published); (□) for Cu-doped ZnSe after Grimmeiss et al [38].

When the pump light of 460 nm (2.70 eV) was used, the hole photoionization cross-section spectrum at even lower energies was revealed. It is plotted in Fig.3.10. For comparison, the spectrum of the L1-centre shown in Fig.3.2 is also plotted in Fig.3.10. They are normalized at about 0.62 eV. It can be seen that they are in very good agreement. Therefore they have the same origin. Using the data obtained in this work, a plot of $(\sigma h\nu)^{2/3}$ against $h\nu$ (see Fig.3.11) gives a straight line, near the threshold, with the intercept of 0.500 eV±0.008 eV on the photon energy scale. It indicates that the phonon coupling is weak in the optical transition, and the photoionization threshold energy is 0.500 eV±0.008 eV for the L1-centre [46]. This is the first time for the L1-centre to be reported with the accurate level position. The same plot could

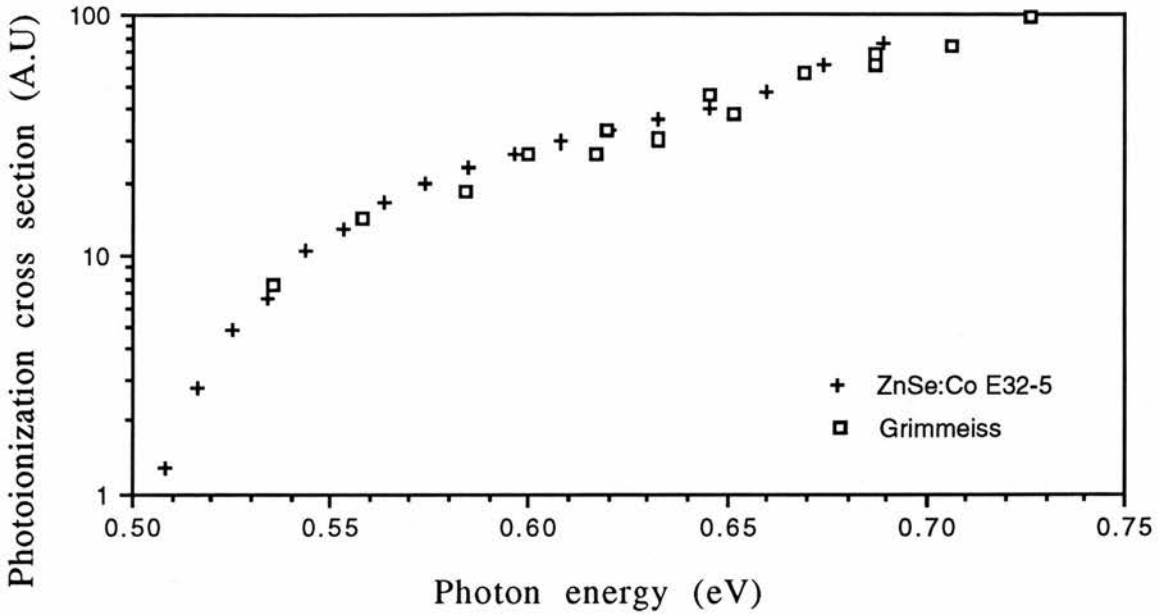

Fig.3.10: The comparison of the hole photoionization cross-section spectra in the lower energy range. (+) for ZnSe E32-5 in this work; (□) for undoped ZnSe after Grimmeiss et al [37]. The spectra are normalized at about 0.62 eV.

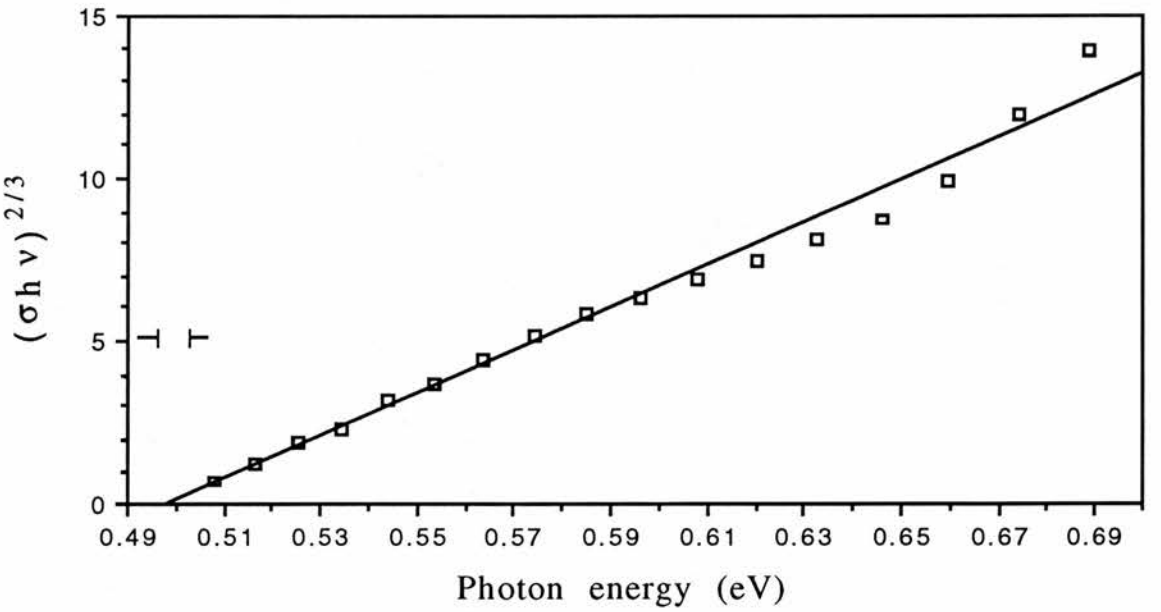

Fig.3.11: A plot of $(\sigma h\nu)^{2/3}$ against photon energy for the spectrum (+) shown in Fig.3.10. The energy resolution of the monochromator at 0.500 eV is 0.008 eV, which is greater than the random error. So the intercept of the straight line on the horizontal scale is 0.500 eV ± 0.008 eV.

not be obtained by using the data after Grimmeiss et al [37] because of the less data. The departure from the straight line at higher energies could be due to the presence of the M-centre.

From the investigation of hole photoionization cross-section, three deep levels in the lower half of the band gap were found in the sample ZnSe E32-5. Their level positions are at 0.500 eV, 0.68 eV and about 0.9 eV above the valence band respectively. In order to get the electron photoionization cross-section spectra of these deep levels, different pump photon energies (E_g-E_T<$h\nu_s$<E_T) were chosen. The probe light (E_T<$h\nu$<E_g) was scanned in the wide energy range 1.60 to 2.75 eV. The electron photoionization cross-section spectra pumped at different photon energies are shown in Fig.3.12. The spectra observed at lower energies than the substraction of the pump light photon energy from the band-gap 2.8 eV could be due to some other deep level.

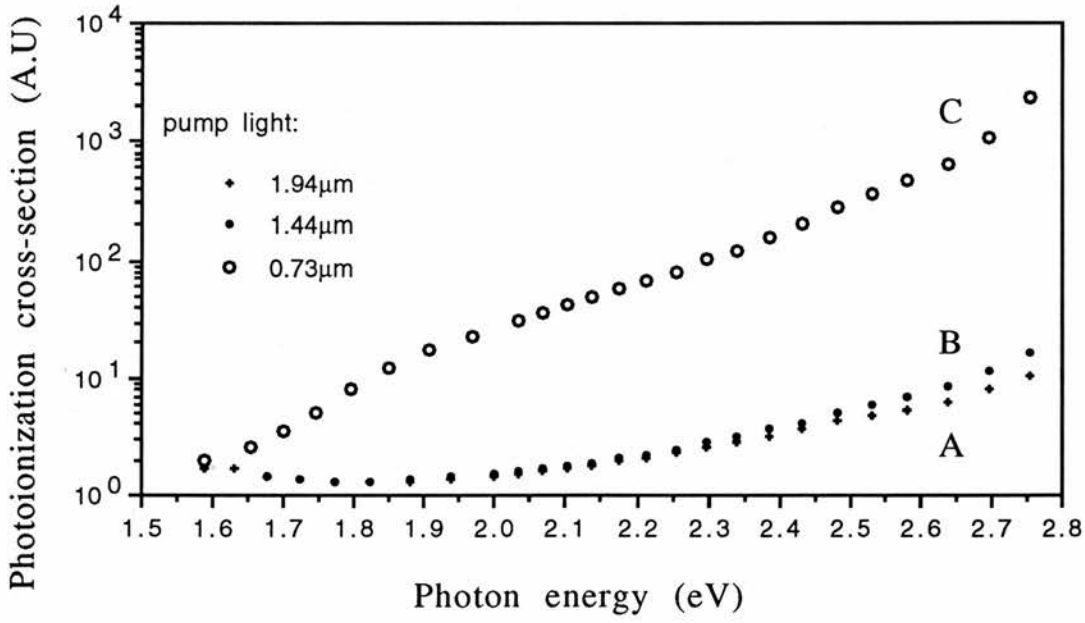

Fig.3.12: The electron photoionization cross-section spectra obtained in ZnSe E32-5 by DLSS photocapacitance measurements. The pump wavelengths are 1.94 μm (0.64 eV), 1.44 μm (0.86 eV) and 0.73 μm (1.70 eV) respectively.

Suppose that there are no other deep levels within the band gap except for the L1-centre, the M-centre and the L3-centre. When the pump light is 1.94 μm (0.64 eV), only the L1-centre can be filled by the electron transition from the valence band to the centre. So the spectrum (labelled A) in Fig.3.12 is mainly attributed to the change of the electron occupancy of the L1-centre, produced by the probe light. When the pump light is 1.44 μm (0.86 eV), both the L1-centre and the M-centre can be filled by the pump light. So the spectrum (labelled B) is the linear sum of the changes of the electron occupancy of these two centres, as discussed in section 3.2.5. The electron optical cross-section of the M-centre can be obtained approximately by subtracting A from B. When the pump light is 0.73 μm (1.70 eV), all three of the L1-centre, the M-centre and the L3-centre can be filled by the pump light. So the spectrum (labelled C) is the linear sum of the changes of the electron occupancy of three centres. The electron optical cross-section of the L3-centre can be obtained approximately by subtracting B from C. Therefore, the electron photoionization cross-section spectra of each deep centre can be found. They are shown in Fig.3.13. Actually, the spectra in Fig.3.12 could include the contribution of other deep centres in the upper half or the middle of the band gap. So the electron photoionization cross-section spectra of each deep centre in Fig.3.13 are less reliable than those of the hole photoionization cross-section.

In Fig.3.13, the spectrum of the L1-centre is the one with the pump photon wavelength of 1.94 μm in Fig.3.12; the spectrum of the M-centre, obtained by subtracting A from B in Fig.3.12, is only shown in the high photon energy range because the obvious difference between the spectra A and B is mainly at photon energies greater than 2.3 eV. The L3-centre is estimated above to be at about 1.9 eV below the conduction band (the band gap of ZnSe is 2.8 eV at LNiT). However, there is a rise in the range 1.6 to 1.9 eV in the spectrum C in Fig.3.12. This feature is not expected. It could be due to some other deep level

located near the middle of the gap. The spectrum of the L3-centre in the range 2.0 to 2.8 eV, shown in Fig.3.13, is then tentatively obtained by normalizing the spectra C and B at about 1.96 eV followed by the subtraction.

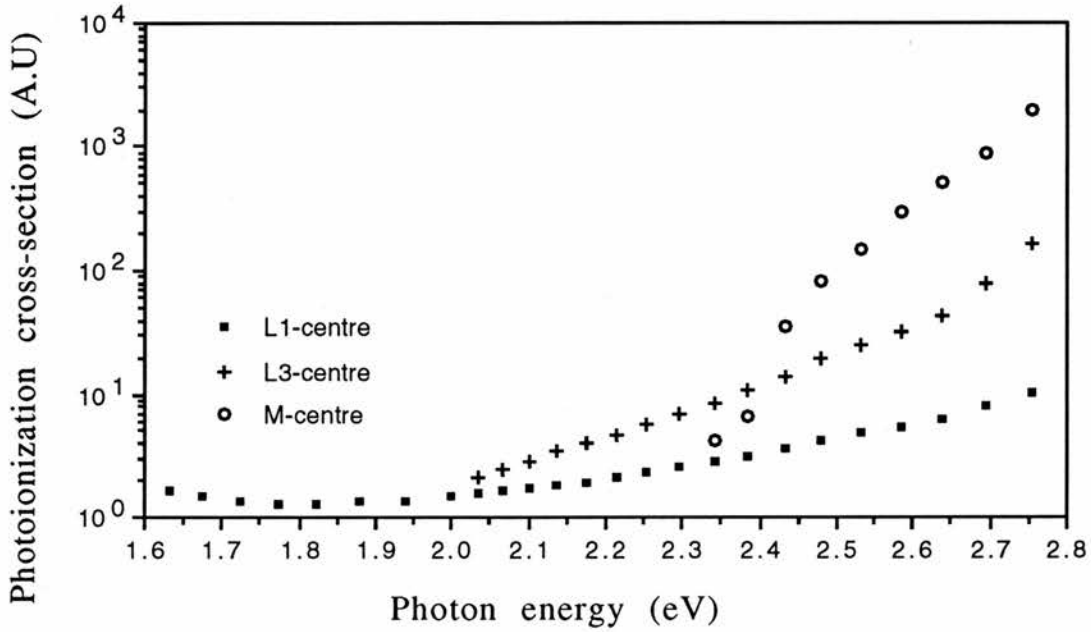

Fig.3.13: The electron photoionization cross-section spectra of three different deep levels observed in ZnSe E32-5.

Fig.3.14 shows the comparison of the spectrum of the electron photoionization cross-section of the M-centre, shown in Fig.3.13, with that of the M-centre obtained in Ref.[41]. They are in fairly good agreement, especially at higher energies. It confirms the attribution to the M-centre, in the sample ZnSe E32-5, proposed above according to the spectra of hole photoionization cross-section.

It can be seen from the result, shown in Fig.3.6, obtained by the single-beam photocapacitance measurement that there must be at least one level in the upper half of the band gap. However, it is difficult to get the separate spectrum of the level in the upper half of the band gap by using DLSS photocapacitance measurements since there are at least three deep levels in

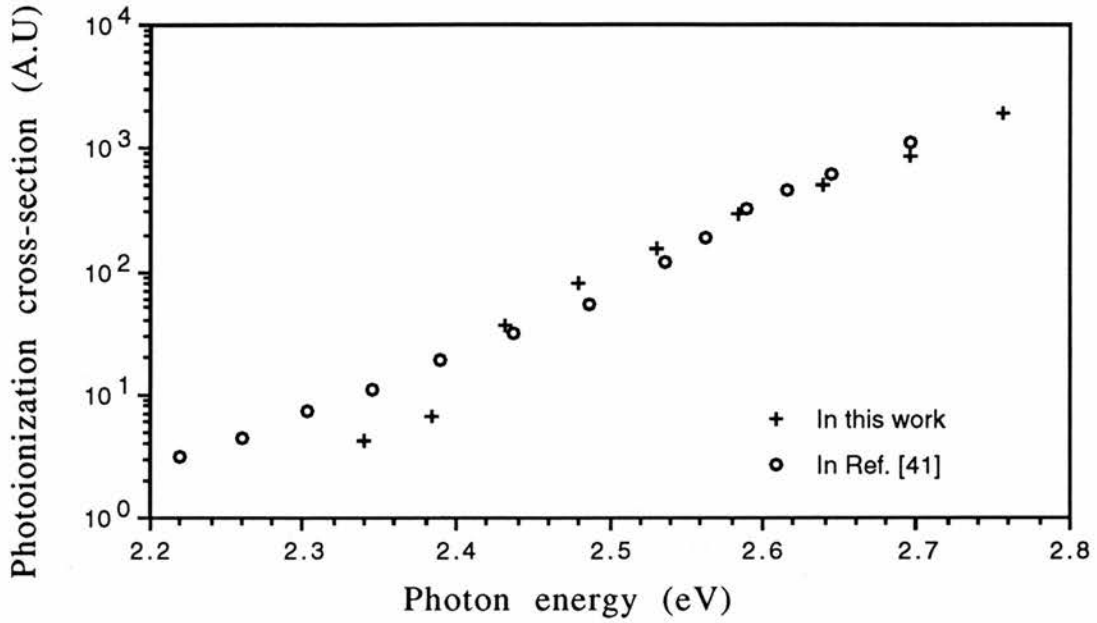

Fig.3.14: The comparison of the electron photoionization cross-section spectra of the M-centre. (+) for ZnSe E32-5 in this work; (o) for the sample H8 in Ref.[41].

the lower half of the band gap. The transient photocapacitance measurement was employed to measure the spectrum of electron photoionization cross-section of the level in the upper half of the band gap. The method was described in detail in Ref.[43]. All levels were first filled by applying a forward bias in the dark. Then, for each monochromatic light the off-balance voltage was recorded as a function of time. The observed positive capacitance change indicated that electrons were emptied from the centres to the conduction band. The time variation was not a good exponential process. A tail with time constants of a few hours could be resolved in the time variation. The proper spectrum against photon energy could not be achieved. However, when the photon energy was 0.58 eV, the positive capacitance change could be still observed. So one level could lie shallower than 0.58 eV below the conduction band.

3.5 Discussion

Three deep levels in the lower half of the band gap have been found in the sample ZnSe E32-5 by the DLSS photocapacitance measurements. They are the L1-centre, the M-centre and the L3-centre. The L1-centre and the M-centre have been observed previously in undoped ZnSe semiconductors. So they could be some kinds of native defects, but not related with the doped cobalt impurity. The L3-centre is a new centre, which has not been reported in undoped ZnSe semiconductors.

Noras, Szawelska and Allen [43] investigated the deep levels in Co-doped ZnSe by the transient photocapacitance measurements. Two exponential processes, i.e. a faster component and a slower component, were resolved in the time variation, where the faster component had a time constant from a few seconds to a few minutes depending on the wavelength. The hole and electron photoionization cross-section spectra were obtained by the time constants of the faster component. The hole photoionization cross-section spectra obtained from three samples are in good agreement in the range 0.9 to 1.4 eV, then deviate from each other at higher energies up to 1.6 eV. The reason of the deviation was not explained in Ref.[43]. The electron photoionization cross-section spectra obtained from two samples are in good agreement in the investigated energy range 2.2 to 2.8 eV. The electron spectra have a less steep increase, starting at 2.2 eV, followed by a very steep rise at photon energies greater than 2.52 eV. The identification of these spectra was not obtained in Ref.[43].

Fig.3.15 shows the comparison of the hole photoionization cross-section spectra, mainly in the range 0.9 to 1.4 eV, obtained in Ref.[43] and in this work. The spectra obtained by the DLSS photocapacitance measurement are the sum of the optical cross-sections of the M-centre and the L3-centre. The spectrum of the M-centre in the range 0.9 to 2.0 eV is fairly weak and flat [40].

The spectra obtained by the transient photocapacitance method should be mainly due to one centre because the resolved time constants are mainly the features of one deep level. So the spectra in Fig.3.15 have been shifted and normalized at about 1.3 eV for comparison. It can be seen that they are in good agreement. Therefore, they probably have the same origin, say, the L3-centre.

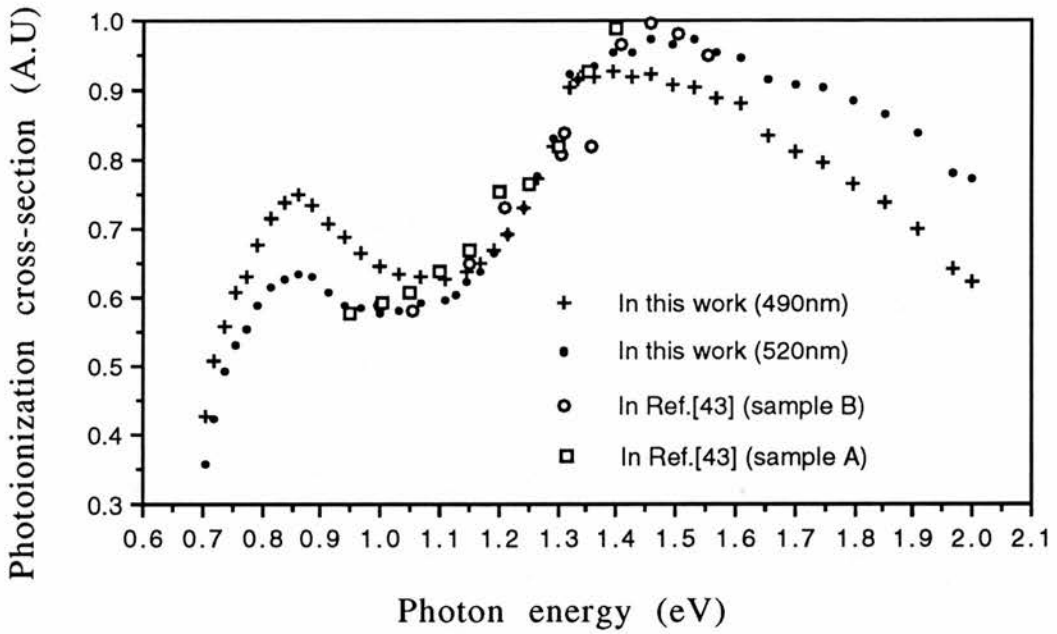

Fig.3.15: The comparison of the hole photoionization cross-section spectra obtained in this work and in Ref.[43]. (+) and (•) for ZnSe E32-5 in this work with the pump light of 490 nm (2.53 eV) and 520 nm (2.38 eV) respectively; (o) and (□) for the samples B and A in Ref.[43] respectively. The spectra have been shifted and normalized at about 1.30 eV.

Fig.3.16 and Fig.3.17 show the comparison of the electron photoionization cross-section spectra obtained in Ref.[43] and in this work. The electron photoionization cross-section spectra of each deep level have been separated tentatively in this work, as shown in Fig.3.13. So the spectra obtained in Ref.[43] are compared with those of each deep level, obtained in ZnSe E32-5,

respectively. Fig.3.16 shows the comparison of the electron photoionization cross-section spectrum, obtained in Ref.[43], with the one of the L3-centre, obtained in ZnSe E32-5. They are normalized at a lower photon energy of 2.30 eV. It can be seen that they are in fairly good agreement in the energy range 2.2 to 2.5 eV, showing that the spectrum obtained in Ref.[43] consists of two parts due to different deep centres and where the less steep rise could be due to the L3-centre. Fig.3.17 shows the comparison of the electron photoionization cross-section spectrum, obtained in Ref.[43], with the ones of the M-centre, obtained in this work and Ref.[41]. They are normalized at a higher energy of about 2.56 eV. The spectrum obtained in Co-doped ZnSe samples in Ref.[43] has the much steeper rise at higher photon energies than the ones of the M-centre, obtained in Co-doped ZnSe E32-5 and in Ref.[41].

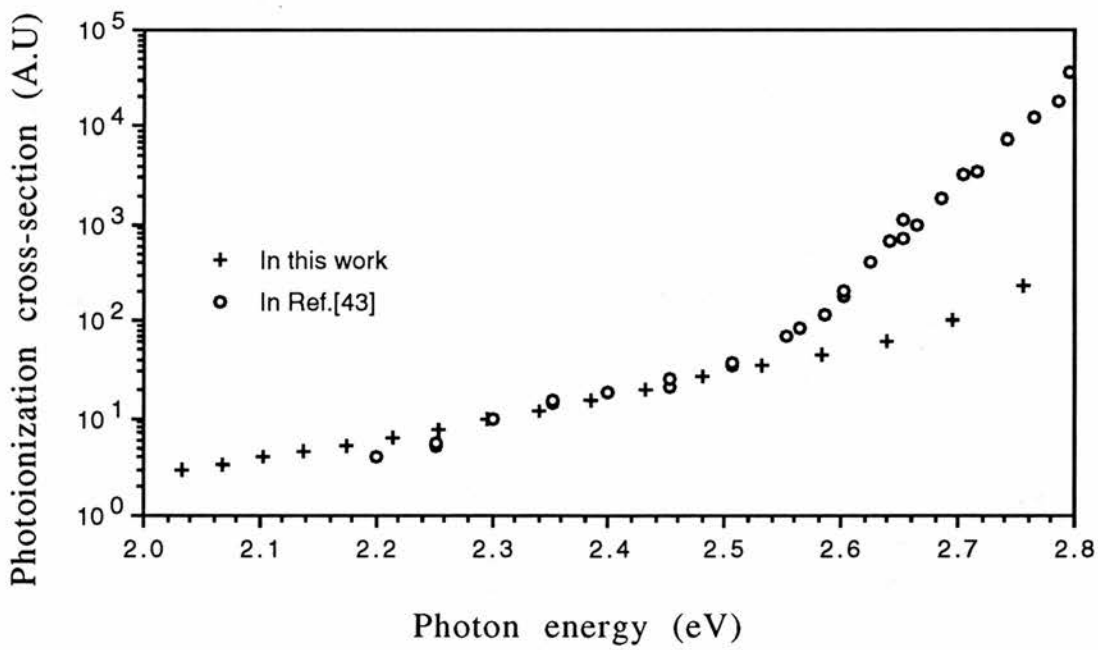

Fig.3.16: The comparison of the electron photoionization cross-section spectra normalized at lower energy of 2.30 eV. (+) is the spectrum of the L3-centre obtained in ZnSe E32-5 in this work; (o) for Co-doped ZnSe samples in Ref.[43].

Therefore, there must be some other centre responsible for this very steep rise in the spectrum obtained in Ref.[43]. Although the threshold energy corresponding to this steep rise cannot be obtained from the spectrum, estimating by extrapolation, it could be close to 2.4 eV below the conduction band, which is consistent with the prediction of the level position of the Co d^7 ground level in ZnSe semiconductors [47]. So it is very likely that the spectrum of the electron photoionization cross-section in Ref.[43] comes from two centres, i.e. the Co d^7 ground level and the L3-centre. The level position of the L3-centre has been estimated to be at about 1.9 eV below the conduction band. So the Co d^7 level, lying at about 2.4 eV below the conduction band, is different from the L3-centre.

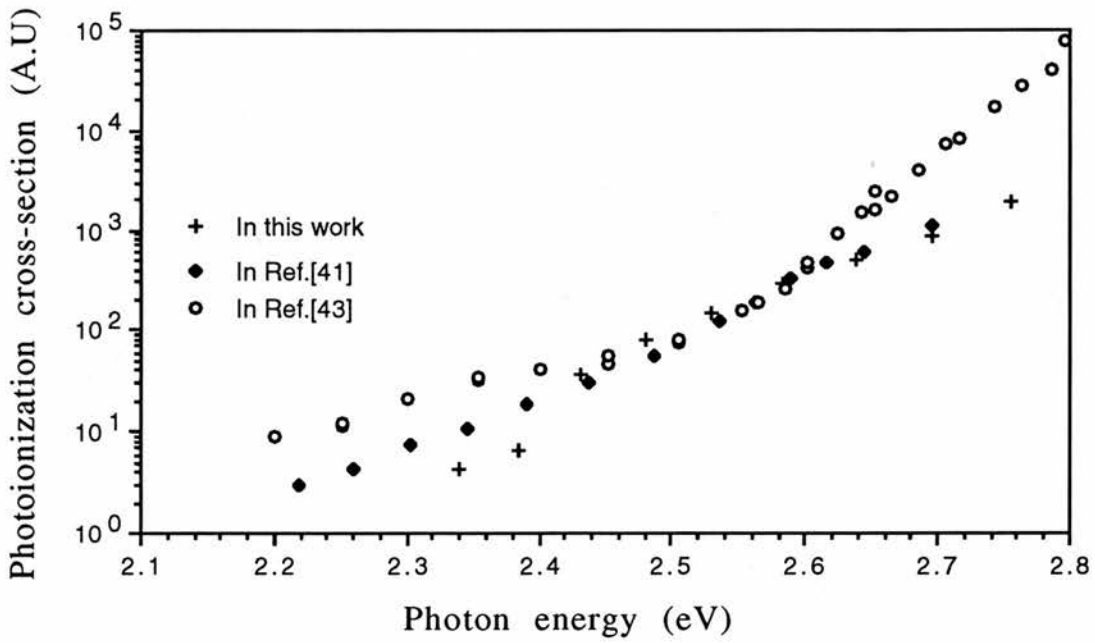

Fig.3.17: The comparison of the electron photoionization cross-section spectra normalized at higher energy of 2.56 eV. (+) is the spectrum of the M-centre obtained in ZnSe E32-5; (♦) the one of the M-centre obtained in Ref.[41]; (o) the one obtained in Co-doped ZnSe samples in Ref.[43].

In Ref.[43] and this work, the ZnSe samples were all doped with the cobalt impurity in the same way. However, the L3-centre was observed in all Co-doped ZnSe samples, the Co d^7 ground level was only seen in Ref.[43]. For the L3-centre, its chemical nature is unknown. It could be related to the cobalt impurity as a complex. For the Co d^7 level, the cobalt concentration in the Co-doped ZnSe E32-5 sample in this work could be too small to be observed by the DLSS photocapacitance measurements.

3.6 Conclusions

A method to investigate deep levels in semiconductors has been improved in this work. By choosing different pump photon energy, a system with more than one deep level within the gap can be studied thoroughly by the DLSS photocapacitance measurements. Since, in practice, the case of many deep levels is more common in the wide band-gap semiconductors, this method would be more useful. However, since the chemical nature of deep levels cannot be identified directly by the DLSS photocapacitance measurement, the analysis of the spectrum obtained in samples with an intentionally-doped impurity would not be so easy because of the presence of native lattice defects and unintentionally-doped impurities.

In ZnSe, four deep levels, which might be the native defects, have been further distinguished by their characteristic photoionization cross-section spectra in this work. They are the L1-centre, the L2-centre, the M-centre and the L4-centre. Another new centre, i.e. the L3-centre, is only observed in the Co-doped ZnSe samples. Its origin is unknown. It could be related to the cobalt impurity. The Co d^7 ground level in ZnSe semiconductors is estimated to be at about 2.4 eV below the conduction band by the analysis of the previous spectra obtained by photocapacitance measurements.

Chapter 4

Photocurrent studies of deep levels in zinc sulphide grown by MOCVD

4.1 Introduction

Junction space-charge techniques have provided powerful tools for the investigation of deep levels in semiconductors. This can be seen from the example shown in the last chapter. A centre, labelled as the M-centre, has been found in nearly all ZnSe samples by the junction techniques. Recently, its characteristic hole photoionization cross-section spectrum was revealed [40] in ZnSe epilayers, grown by MOCVD. It is a very narrow strong peak at 0.83 eV, with a threshold at 0.68 eV, followed by a much weaker and broader peak at higher energy (see Fig.3.1). The origin of this centre is still unknown.

The application of the junction techniques to ZnS, with a wide band-gap 3.7 eV at room temperature, was once restricted by the absence of good p-n junctions, the difficulty of making good Schottky contacts, and the difficulty of making measurements below room temperature because of carrier freeze-out. It was only recently found that low resistivity n-type ZnS could be made by being heated in high-purity molten zinc containing a small amount of aluminium. The typical shallow donor ionization energies in ZnSe are about 100 mV [48,49]. In unintentionally-doped bulk ZnS, Fornell et al [50] obtained a hole photoionization cross-section spectrum of deep levels in the lower half of the band-gap by the transient photocapacitance measurement, and no other centre was found in the upper half of the band-gap. Zheng and Allen [51] also obtained the hole photoionization cross-section spectra in two ZnS samples, grown by different methods, by the DLSS photocapacitance measurement. Their results are shown in Fig.4.1 with Fornell's result for comparison. They are in fairly good agreement in the energy range of 0.78 eV to 1.1 eV, which

indicates that they might arise from the same centre. The spectral characteristic of this centre is a peak at about 0.9 eV with a sharp rise at lower energy. This feature is then followed by either a plateau or another less sharp rise at higher energy which could be due to the existence of another centre. This phenomenon is similar to that observed in bulk ZnSe, as shown in Fig.3.1 and discussed in the last chapter. Therefore, it is necessary to do similar experiments in ZnS samples with different conditions, such as with samples grown by different methods in order to get more information of deep levels in ZnS.

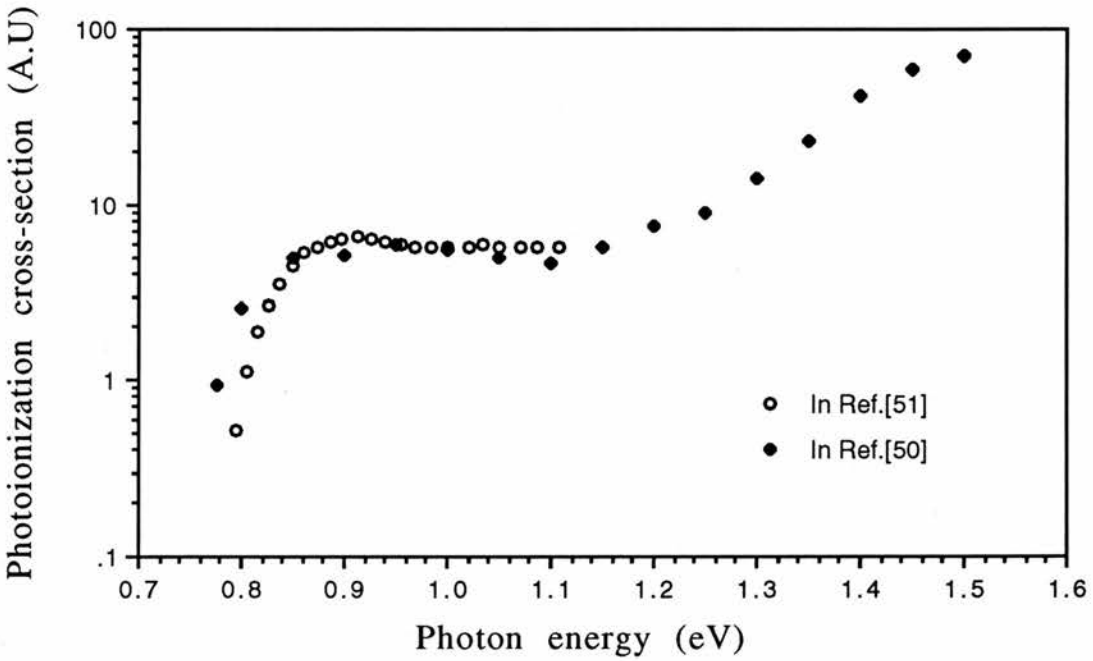

Fig.4.1: The hole photoionization cross-section spectra obtained in unintentionally-doped bulk ZnS samples by Fornell et al [50] and Zheng and Allen [51] respectively. They are plotted on a logarithmic scale.

The metalorganic chemical vapour deposition (MOCVD) growth method can grow crystals under more controlled conditions at low substrate temperature. It has been found that the band-edge emission can be effectively increased in ZnSe epilayers grown by MOCVD compared with those broad

emission bands at lower energies due to the presence of deep levels within the band-gap. So the quality of crystals, such as ZnSe and ZnS, is expected to be improved by MOCVD growth method.

In this chapter, the dual-light source steady-state junction photocurrent measurement was performed at room temperature, for reasons discussed below, to investigate deep levels in a MOCVD grown epilayer ZnS sample. The hole photoionization cross-section spectrum of the centre, which has been found in the previous works, was measured again more clearly in the photon energy range of 0.78 eV to 1.16 eV. Its distinctive spectrum is a narrow strong peak at 0.87 eV, with a threshold at about 0.78 eV. This characteristic is very similar to that of the M-centre found in ZnSe. Therefore, the centres may have the same nature, ie. some kind of native lattice defect. This centre in ZnS is then labelled as the M'-centre.

4.2 Principles of the DLSS junction photocurrent measurement

In the last chapter, the principles of photocapacitance measurements have been discussed in great detail. It can be seen that the DLSS photocapacitance measurement is a more powerful method than the transient photocapacitance measurement and other junction techniques, especially in the case of many deep levels. However, when the resistivity of samples is high, the depletion region capacitance of a diode will be small and the series resistance will be high. In our laboratory, the photocapacitance measurements are performed with a specially constructed ratio-arm bridge which can only be balanced when the series resistance is less than 2000 Ω. Therefore, for a high resistivity sample, the photocurrent measurement performed in a Schottky diode could be preferentially employed to study deep levels in semiconductors. It can be seen from the principles described below that this junction photocurrent method has advantages over the conventional photocurrent measurement performed with ohmic contacts on an insulating

semiconductor, where an applied voltage is required to drive the current and the recombination processes cannot be ignored.

The current produced by illumination has two components. One component is formed by the free electrons or free holes, photoionized from deep levels to the conduction band or from deep levels to the valence band respectively, moving along the electric field within the depletion region. The measurement of the behaviour of this photocurrent can offer information about deep levels. It is called the deep level photocurrent here. However, when the photon energy is above the built-in barrier potential between the metal and the semiconductor, the electrons in the metal can be photoexcited to the conduction band of the semiconductor, then move along the electric field within the depletion region so that a photoemission current is formed [52]. The photoemission current, J_e^o, increases with the increase of photon energy, $h\nu$, approximately obeying the Fowler rule, i.e. $(J_e^o)^{1/2}=C(h\nu-h\nu_o)$, where C is constant and $h\nu_o$ is the barrier height between the metal and the semiconductor. Above the photoemission threshold, i.e. the barrier height, the photoemission current could be much greater than the deep level photocurrent and it is difficult to separate the two contributions in a steady-state measurement. Therefore, the DLSS photocurrent measurement can only be performed in an energy range where the photoemission current is small enough compared with the deep level photocurrent. The principles of the DLSS photocurrent measurement are outlined below.

The case of a single deep level in the lower half of the band-gap is considered here. The possible transitions through this deep level have been shown in Fig.3.4. The notations of all parameters of the deep level here are the same as those given in the last chapter. Under steady-state illumination with a single beam, the expression for the electron occupancy has been derived from the rate equation in the last chapter, which is

$$\frac{n_T}{N_T} = \frac{e_p{}^o + e_p{}^t}{e_p{}^o + e_p{}^t + e_n{}^o + e_n{}^t} \quad , \tag{4.1}$$

where it is assumed that the thermal filling effect taking place at the edge of the depletion region near the bulk is neglected. The general steady-state photocurrent through the junction can be written as [53]

$$J^o(\infty) = qA(W-W_o)N_T \frac{(e_p{}^o + e_p{}^t)(e_n{}^o + e_n{}^t)}{e_p{}^o + e_p{}^t + e_n{}^o + e_n{}^t} \quad , \tag{4.2}$$

where A is the contact area, W is the depletion layer width, and W_o is the width of that part of the depletion layer where the optical process cannot contribute to the net generation current because of recombination processes [54]. The region $W-W_o$ is an effective part in the depletion layer for the current generation and is the part where the recombination processes, i.e. the thermal filling effects, are neglected.

When the sample is illuminated with the pump light, the steady-state photocurrent is then

$$J_{pump}{}^o(\infty) = qA(W-W_o)N_T \frac{(e_{ps}{}^o + e_p{}^t)(e_{ns}{}^o + e_n{}^t)}{e_{ps}{}^o + e_p{}^t + e_{ns}{}^o + e_n{}^t}$$

$$= qA(W-W_o)N_T \frac{AB}{A+B}, \tag{4.3}$$

where $A=e_{ps}{}^o+e_p{}^t$, $B=e_{ns}{}^o+e_n{}^t$. When the sample is illuminated with both the pump light and the probe light, the steady-state photocurrent is

$$J_{pump+probe}{}^o(\infty) = qA(W-W_o)N_T \frac{(e_p{}^o + A)(e_n{}^o + B)}{e_p{}^o + A + e_n{}^o + B} \quad . \tag{4.4}$$

So the change of the photocurrent produced by the probe light is

$$\Delta J_{DLSS}{}^o(\infty) = J_{pump+probe}{}^o(\infty) - J_{pump}{}^o(\infty)$$

$$= qA(W-W_o)N_T \frac{(A+B)e_p{}^o e_n{}^o + A^2 e_p{}^o + B^2 e_n{}^o}{(A+B)(e_p{}^o + A + e_n{}^o + B)} \quad . \tag{4.5}$$

If the intensity of the pump light is much stronger than that of the probe light, $A+B>>e_p^o+e_n^o$. When the photon energy of the pump light, $h\nu_s$, is chosen in the range of $E_T<h\nu_s<E_g$ and the probe light, $h\nu$, is scanned in the photon energy range of $E_g-E_T<h\nu<E_T$, the quantities of A and B are constant and $e_p^o>>e_n^o$. The above equation can be simplified as

$$\Delta J_{DLSS}^{o}(\infty)=qA(W-W_o)N_T \frac{A^2 e_p^o}{(A+B)^2}. \qquad (4.6)$$

So one has

$$\Delta J_{DLSS}^{o}(\infty) \propto e_p^o . \qquad (4.7)$$

Since the optical emission rate e_p^o is related to the photoionization cross-section σ_p^o by $e_p^o=\phi\sigma_p^o$, where ϕ is the photon flux, the relative hole photoionization cross-section can be obtained by measuring the photocurrent change produced by the probe light. However, the band involved in the photoionization process cannot be found from the photocurrent measurements.

When the deep level is in the lower half of the band-gap, the fixed photon energy of the pump light, $h\nu_s$, could be above the photoemission threshold so that the total photocurrent, produced by the pump light, could be the sum of the deep level photocurrent and the photoemission current. However, the photocurrent change produced by the probe light should still follow the equation (4.6) if the photoemission current produced by the probe light can be neglected. It also can be seen from the above derivation that the temperature at which the experiment is performed is not required to be low.

4.3 Experiments

4.3.1 Making a Schottky diode

The epilayer of ZnS was grown on semi-insulating GaAs (100) substrate by MOCVD at 395°C in the laboratories at UMIST. The thickness of the ZnS epilayer is about 5.5 μm.

Before making ohmic contact, the epilayer sample was etched in 50% NaOH solution for at least 10 minutes in order to remove the oxide layer from the surface, followed by rinsing with deionized water several times. Ohmic contacts were then immediately made on the ZnS epilayer surface with indium dots by heating at 420°C in 90% N_2/10% H_2 for 40 seconds. The I-V characteristics of two indium dots were measured in both directions of current. They showed straight lines, which indicated that the contacts were ohmic. After the same etching and rinsing procedures were performed on the sample again, aluminium was evaporated on the same side of the sample.

The I-V and C-V characteristics of this diode were measured in the dark at room temperature. The I-V characteristic showed the typical rectification properties of a Schottky diode, which means the forward-biassed current increased nearly exponentially with the increase of voltage at low voltages and the reverse-biassed current was very small, almost unmeasurable. However the forward-biassed current was severely limited at higher voltages (greater than 1.0 V) by the high series resistance. The C^{-2}-V characteristic could not be obtained because of the high resistivity of this sample.

The carrier concentration, n, of this sample was roughly estimated by measuring the resistance, R, between two indium dots on a long stripe sample cut from the same epilayer. Using the equations $R=\rho L/hw$ and $1/\rho=e\mu n$, where h, w, L are the width of the stripe, the thickness of the epilayer and the distance between two indium dots respectively, ρ is the resistivity, μ is the electron mobility, the carrier concentration, n, is calculated to be about $3*10^{15}$ cm^{-3} by taking μ=200 $cm^2/Vsec$.

4.3.2 Apparatus for photocurrent measurements

The photocurrent measurements were carried out in a dark room at room temperature. The optical path arrangement was the same as that used in the photocapacitance measurements shown in Fig.3.5 in the last chapter. The measuring system was also basically the same, except that the DC current signal was measured with a Keithley electrometer 602 instead of the capacitance bridge.

4.4 Results

4.4.1 Barrier height

A single beam photocurrent measurement was first carried out in order to find out the photoemission threshold. A Fowler plot of photocurrent against photon energy is shown in Fig.4.2. The intercept of the straight line on the photon energy scale gives the barrier height of 0.84 eV ± 0.01 eV between the aluminium and the zinc sulphide.

4.4.2 The spectrum of photoionization cross-section

Since the photoemission threshold between the aluminium and the zinc sulphide is quite small, namely 0.84 eV, the DLSS photocurrent measurement could only be carried out in a narrow lower photon energy range. In order to investigate deep levels in the lower half of the band-gap, the photon energy of the pump light was chosen to be 410 nm (3.02 eV) to partially empty the deep level. When the photocurrent reached the steady-state in this initial condition, the probe light of photon energy hν (E_g-E_T<hν<E_T), was shone on the diode and the photocurrent change (in the order of 10^{-12} A) produced by the probe light was recorded at different photon energies. The relative photoionization cross-section spectrum was then obtained by correcting the photocurrent change for the photon flux. It is shown in Fig.4.3 with the results presented in the previous works. The spectrum in the energy range of

0.75 eV to about 1.1 eV, obtained in this work, is a sharp strong peak at 0.87 eV, with a threshold at about 0.78 eV. When the photon energy of the probe light was greater than 1.1 eV, the photoemission current could strongly affect the spectrum of deep levels because the absolute values of the single beam photoemission current and the dual-light beam photocurrent are comparable.

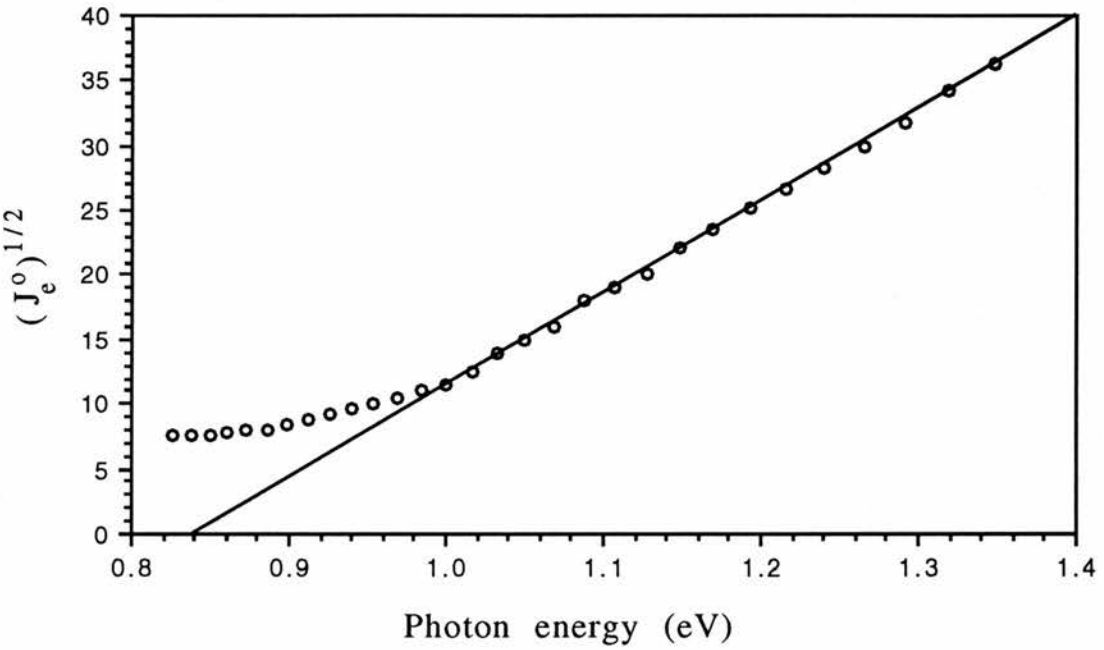

Fig.4.2: A Fowler plot of photocurrent against photon energy obtained in the epilayer ZnS diode with an aluminium Schottky contact. The Fowler rule is expressed by $(J_e^o)^{1/2}=C(h\nu-h\nu_o)$. The energy resolution of the monochromator at 0.84 eV is 0.01 eV. So the intercept of the straight line on the horizontal scale is 0.84 eV±0.01 eV.

For example, when the photon energy of the single beam or the probe light was 1.1 eV, the absolute value of the single beam photoemission current was about $0.25*10^{-12}$ A, and the absolute value of the dual-light beam photocurrent was about $0.44*10^{-12}$ A. Since the experimental conditions of the single beam and DLSS junction photocurrent measurements are not identical, the spectrum shown in Fig.4.3, obtained in this work by the DLSS

junction photocurrent measurement, could not be simply corrected by the single beam photocurrent spectrum.

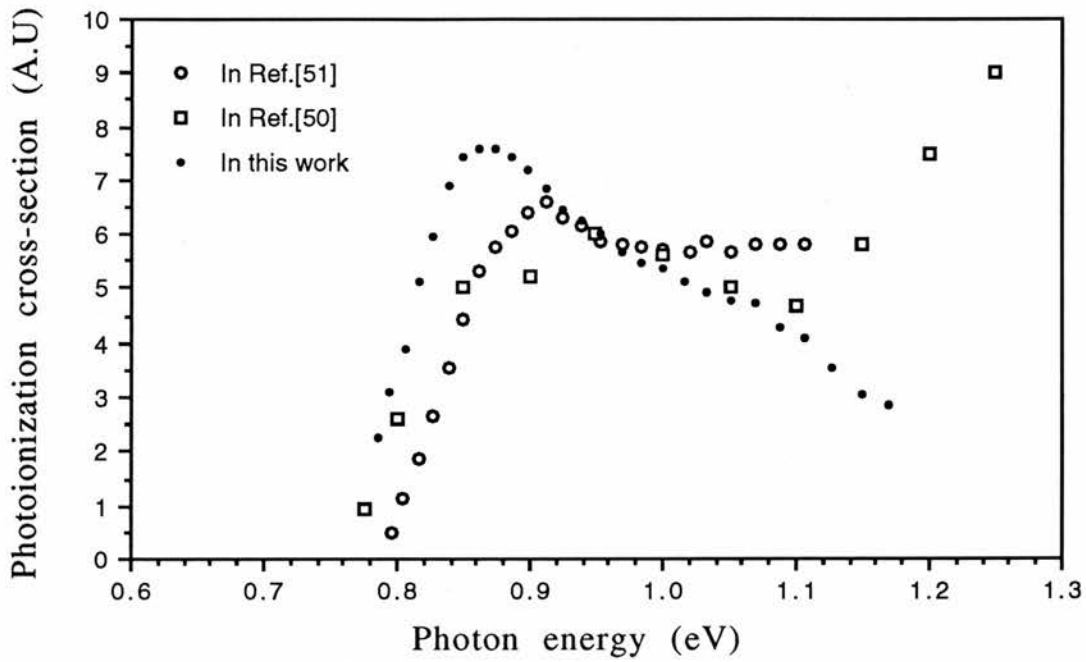

Fig.4.3: The photoionization cross-section spectrum obtained by the DLSS photocurrent measurement in this work, with the hole photoionization cross-section spectra, obtained by the junction capacitance technique in previous work, for comparison. They are normalized at about 0.92 eV. (•) for the spectrum obtained in this work; (o) for the spectrum in Ref.[51]; (□) for the spectrum in Ref.[50].

4.5 Discussion

Since the photocurrent measurement cannot tell which band is involved in the optical process, the photocurrent change produced by the probe light could be due to either free electrons, photoionized from deep levels in the upper half of the band-gap to the conduction band, or free holes, photoionized from deep levels in the lower half of the band-gap to the valence band or even both. However, it can be seen in Fig.4.3 that the feature

in the spectrum obtained in this work is similar to those peaked at about 0.9 eV with a sharp rise at lower photon energy observed in the hole photoionization cross-section spectra by the junction photocapacitance measurement in Ref.[50] and Ref.[51]. Therefore, the spectrum obtained in this work is more likely to be the hole photoionization cross-section one. The small shift of the peak positions to higher energies in Ref.[50] and Ref.[51] could be due to superposition of the optical cross-section of another centre. The centre responsible for this distinctive feature in the spectrum is labelled M' here. It seems that the M'-centre is a very common deep centre in ZnS. The position of the M'-centre in ZnS, estimated from the threshold of the spectra in Fig.4.3, is at about 0.78 eV above the valence band.

Comparing the hole photoionization cross-section spectrum of the M'-centre in ZnS with that of the M-centre in ZnSe, the remarkable similarities are obvious. Both hole photoionization cross-section spectra are characterized by a narrow strong peak at lower photon energy and both the M-centre and the M'-centre are common in these two materials respectively, whatever the growth method is. From the crystal structure and symmetry points of view, ZnSe and ZnS, which both belong to the II-VI compounds, have the same tetrahedral local symmetry when they are perfect crystals. Therefore, it is very likely that same kind of lattice defect is easily created in both ZnSe and ZnS during the growth process. Other measuring techniques are needed to reveal different properties of this defect in order to identify the origins of the M-centre and the M'-centre.

The feature with a less sharp rise at higher photon energy observed in the spectrum in Ref.[50], shown in Fig.4.1, could be due to another centre, which is labelled L4' here. However, it is difficult to do any comparison between the spectra of the L4'-centre in ZnS and the L4-centre in ZnSe because of the lack of a more complete spectrum of the L4'-centre. The energy position of the L4'-centre cannot be obtained either. In the spectrum observed in Ref.[51], shown

in Fig.4.1, there is also, certainly, another centre which has its spectrum overlapping that of the M'-centre. However, the experimental data on this centre is too limited to identify or associate it with other centres, such as the L4'-centre in ZnS or the centres in ZnSe.

4.6 Conclusions

In this work, the clearer hole photoionization cross-section spectrum of the M'-centre is observed in an epilayer ZnS sample grown by MOCVD. By comparing the spectrum obtained in this work with those in previous work, at least two deep centres in the lower half of the band-gap, i.e. the M'-centre and the L4'-centre, have been found in undoped ZnS. The similarities in the characteristic spectra of the M'-centre in ZnS and the M-centre in ZnSe suggest that the M'-centre and M-centre could be the same kind of lattice defects.

Chapter 5

The identifications of deep levels in ZnSe and ZnS

5.1 Introduction

In the last two chapters, the deep levels, especially in the lower half of the band-gap, in ZnSe and ZnS have been studied by the junction space-charge techniques. The results are now summarized. In undoped ZnSe (the meaning of "undoped" has been given in chapter 3), four deep levels in the lower half of the band-gap have been found. They are the L1-centre, the M-centre, the L2-centre and the L4-centre. They are distinguished by their distinctive photoionization cross-section spectra. The energy positions of the L1-centre and the M-centre are 0.50 eV and 0.68 eV above the valence band respectively. The accurate energy positions of the L2-centre and the L4-centre are still unknown. They could be close to the position of the M-centre. In undoped ZnS crystals, two centres, i.e. the M'-centre and the L4'-centre, in the lower half of the band-gap have been found. The energy position of the M'-centre is at about 0.78 eV above the valence band. The position of the L4'-centre could be close to that of the M'-centre. The origins of these centres in ZnSe and ZnS cannot be revealed by the junction techniques.

In the 1950's and the 1960's, ZnSe and ZnS semiconductors attracted the great interest of physicists because both of them are very good phosphors. A lot of effort was made in the investigation of the photoelectronic properties of ZnSe [55,56,42,57] and ZnS [58,59,60]. It was found that the luminescence from ZnSe and ZnS was often dominated by some broad emission bands at lower photon energies than their band-gaps. The typical broad emission bands in ZnSe and ZnS, observed by photoluminescence measurements, are the self-activated emission band and the emission bands related to the presence of copper impurity which are designated as the Cu-red and Cu-green emission

bands in ZnSe and the Cu-red, the Cu-green and Cu-blue emission bands in ZnS. It has been found that ZnSe [42] and ZnS [59] are easily contaminated by copper impurity from the environment. However, the atomic structures and the accurate level positions of these luminescent centres within the band-gaps cannot be obtained from their broad emission bands.

Prener and Williams [61] proposed a model for the centre responsible for the self-activated emission band, which is that a zinc vacancy associated with a substitutional coactivator, such as Cl, I, Al in the third or seventh columns in the periodic table, at a nearest-neighbor site constitutes a singly-ionizable acceptor. This model was first supported by the electron paramagnetic resonance (EPR) experiments performed by Kasai and Otomo [62,63]. The similar EPR experiments were further made by Schneider et al [64,65] and Watkins [66]. In halogen-doped ZnS, at 77°K under the photoexcitation condition those authors observed an EPR signal which was identified as the neutral state of the zinc vacancy-halogen donor pair by the anisotropy of the g-value and the dependence of the signal shape upon the kind of halide ion used as a coactivator. The centre responsible for this EPR signal was labelled A. Watkins [66] confirmed the identity of this EPR A-centre and the self-activated luminescent centre in ZnS: Cl by the good agreement between the wavelength dependence of the defect alignment observed with polarized light generation of the EPR A-centre and that for the polarized self-activated luminescence observed by Koda and Shionoya [58].

Since several deep levels have been found in ZnSe and ZnS by junction techniques and several luminescent centres have been found in the same materials by photoluminescence measurements, one would like to identify those centres or associate them with each other. In principle, the optical quenching experiment could offer information about the energy level of a luminescent centre and the photoionization cross-section of this centre when the system of deep levels within the band-gap is simple, for example, the case

of one deep level. Therefore, the comparison of the spectra obtained by the optical quenching experiment and the junction techniques could be used for identification of deep levels.

Suppose that the luminescence process is the reverse one of the excitation process, which means that the excited electrons in the conduction band recombine radiatively to the emptied deep centres where they are excited from. The luminescence intensity, L, of a luminescent centre is proportional to the number of free electrons, n, in the conduction band and bound holes, p_T, at this luminescent centre, i.e. $L \propto np_T$. Therefore, when either n or p_T is decreased, the quenching process will occur; when either n or p_T is increased, the stimulation process will occur. Under illumination with the infrared light, n and p_T could be changed in different ways depending on the system of deep levels. In the simple case of a single luminescent deep level in the lower half of the band-gap, the infrared light can only cause the release of the holes from the deep level to the valence band so that p_T is decreased and the optical quenching of luminescence could be observed. However, if there are more than one deep level within the band-gap, the optical quenching of one luminescence band could be a complicated process with the involvement of many deep levels. For example, in an insulating semiconductor where the photo-excited electrons in the conduction band are much more than the intrinsic free electrons in the dark, the optical quenching could occur due to reduction of free electrons in the conduction band by recombination through other deep levels with the holes, produced by the infrared light, in the valence band.

In the literature, some experimental data of the optical quenching of luminescence obtained in ZnSe and ZnS has been reported. In ZnSe, most of the data is focused on the optical quenching of the copper luminescence. For example, Grimmeiss et al [37] and Zheng [39] observed the optical quenching of the Cu-red luminescence in ZnSe: Cu. They also compared the optical

quenching spectra with the hole photoionization cross-section spectra obtained by junction techniques. Their results are shown in Fig.5.1. Good agreement, especially at lower photon energy, was found. Grimmeiss et al [37] therefore interpreted this agreement as evidence that the hole photoionization cross-section spectrum in Fig.5.1 observed by junction techniques was due to the Cu-red centre. This is not correct because it has been found, as discussed in chapter 3, that the hole photoionization cross-section spectrum in Fig.5.1 is the superposition of spectra of two centres. The optical quenching of the self-activated luminescence has been measured in undoped ZnSe by Stringfellow and Bube [55] and Iida [42]. However, the data obtained by Stringfellow and Bube is only in a narrow lower photon energy

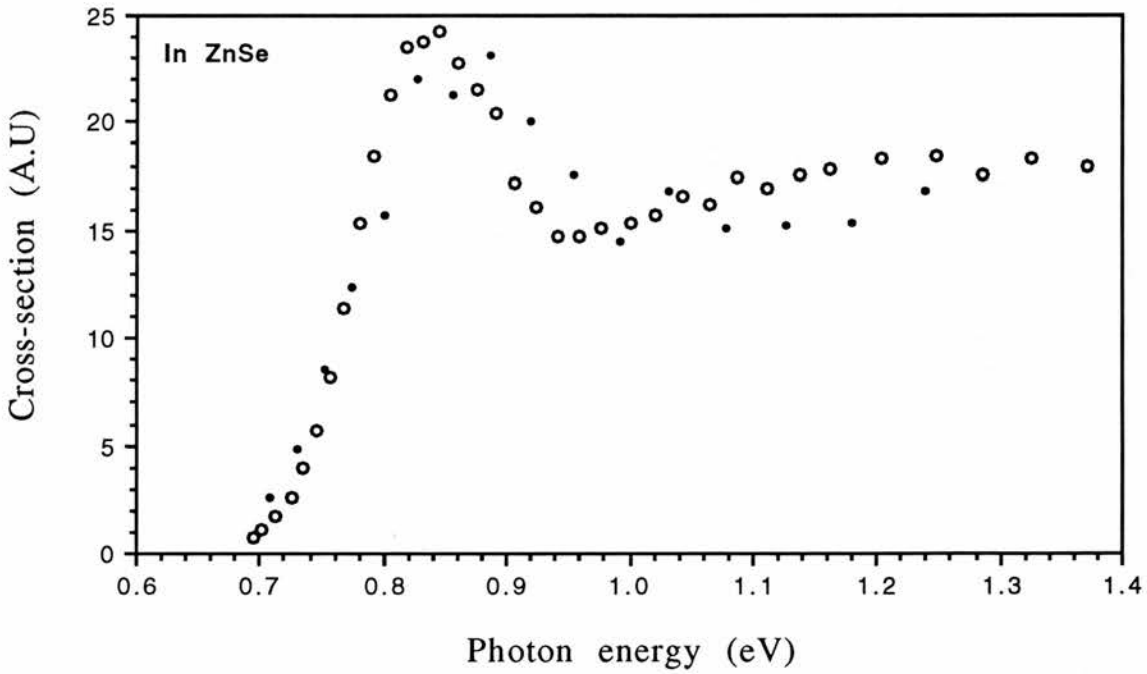

Fig. 5.1: The comparison of the optical quenching spectrum (•) of the Cu-red luminescence with the hole photoionization cross-section spectrum (o) obtained in ZnSe: Cu by Grimmeiss et al [37]. They are plotted on a linear scale.

range. Copper impurity was found in Iida's samples by photoluminescence measurement. Therefore, to get more complete data on the optical quenching of the self-activated luminescence in ZnSe is one of the aims in this work. In ZnS, Koda and Shionoya [58] observed the optical quenching of self-activated luminescence in ZnS: Cl.

In this chapter, we will concentrate on the identification and association of the self-activated luminescent centres in both ZnSe and ZnS with those centres found in undoped ZnSe and ZnS by the junction techniques. The experiment of the optical quenching of the self-activated luminescence was first carried out with an undoped ZnSe sample at liquid nitrogen temperature. The optical quenching spectrum is a single feature peaked at about 1.20 eV. By comparing this result with those in the literature, two phenomena are found in the optical quenching spectrum in ZnSe. The first is that the optical quenching spectra observed in previous work have more than one feature, which means that they could arise from two centres or even more centres. The second is that one of these features is often observed in the optical quenching spectra and its spectrum is similar to the distinctive hole photoionization cross-section spectrum of the M-centre. The similarities are also found in ZnS. Therefore, a model involving three deep levels is proposed to interpret the optical quenching processes of the luminescence arising from one luminescent centre in terms of hole transfer between different centres.

5.2 Experiments

The bulk ZnSe sample used for the optical quenching experiment in this work was treated in a molten-Zn bath for 70 hours.

The photoluminescence measurement was first carried out at liquid nitrogen temperature where thermal quenching is not important. The photon energy of the excitation light was 3.40 eV (365 nm). The luminescence

spectrum is shown in Fig.5.2. It was not corrected for the photomultiplier response. It has been found [55,57] that a typical self-activated luminescence spectrum and a typical Cu-red luminescence spectrum in ZnSe at liquid nitrogen temperature are broad emission bands peaked at about 2.03 eV (610 nm) and 1.97 eV (630 nm) respectively. The half-widths of their emission bands are also respectively about 0.26 eV and 0.18 eV. Therefore, it can be seen from Fig.5.2 that the spectrum with a strong peak at 2.07 eV (600 nm) and a half-width of 0.25 eV is dominated by the self-activated emission band. The weak hump at lower photon energy of about 1.98 eV could be due to another emission band, for example the Cu-red emission band. So the self-activated centres may be dominant rather than any other luminescent centres in this sample.

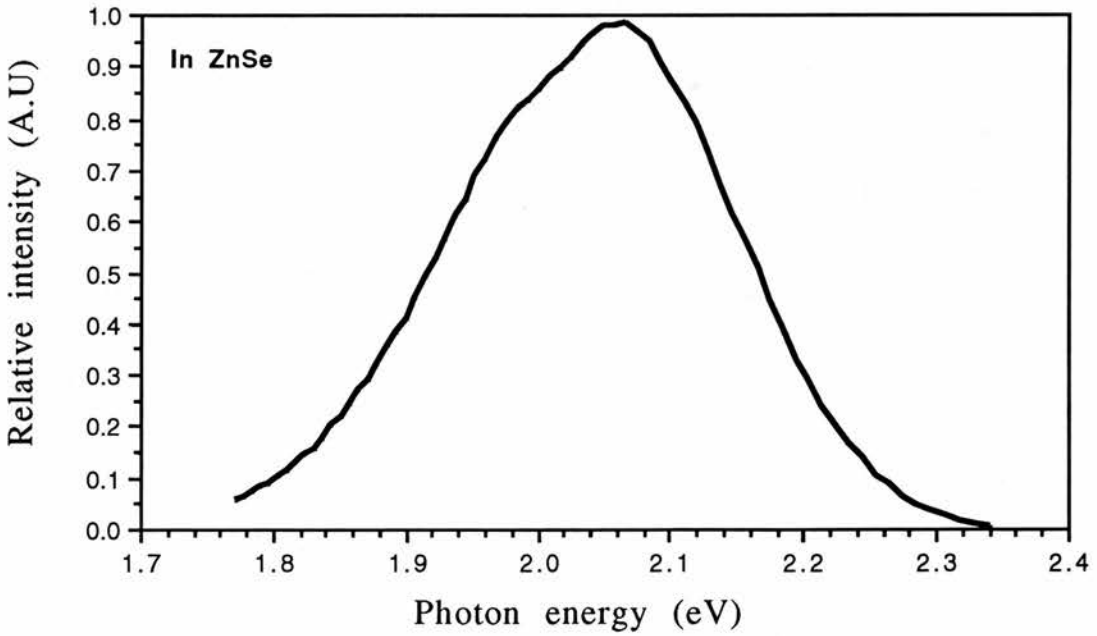

Fig.5.2: The photoluminescence spectrum obtained in the bulk ZnSe 18B1 at liquid nitrogen temperature in this work.

The optical quenching of the self-activated luminescence was then performed also at liquid nitrogen temperature. The experimental set-up is

shown in Fig.5.3. The sample was mounted on a metal finger with a hole in the centre and placed inside a gas-flow cryostat where the temperature was controlled. The excitation light was chosen to be 460 nm (2.70 eV), which was filtered from a 200 W mercury lamp, in order to get strong enough luminescence and to have a sufficiently penetrative depth in ZnSe. The infrared light came from a 100 W tungsten lamp, went through a grating monochromator with 5.0 mm slits and an appropriate filter (either Si filter or GaAs filter) and lenses, and finally was well focused on the same part of the sample as where the excitation light was focused. The luminescence, coming out from the opposite side of the sample, was detected through a 600 nm ± 20 nm filter fixed on the window of a S-20 photomultiplier. Therefore, only the self-activated luminescence in the range of 580 nm (2.14 eV) to 620 nm (2.0 eV) was detected, but not any other out of this range. When the chopper, running at 8 Hz where the signal was bigger than that at higher frequency, was located in the excitation light path, a decrease in the luminescence signal could be observed after the infrared light was switched on. This is why it is called "quenching". The largest decrease due to introduction of the infrared light of a certain photon energy was 2.5% in this experiment. When the chopper was located in the infrared light path, the self-activated luminescence change, perturbed by the infrared light, was detected and recorded. Photon fluxes of the infrared light were measured by a thermopile at room temperature.

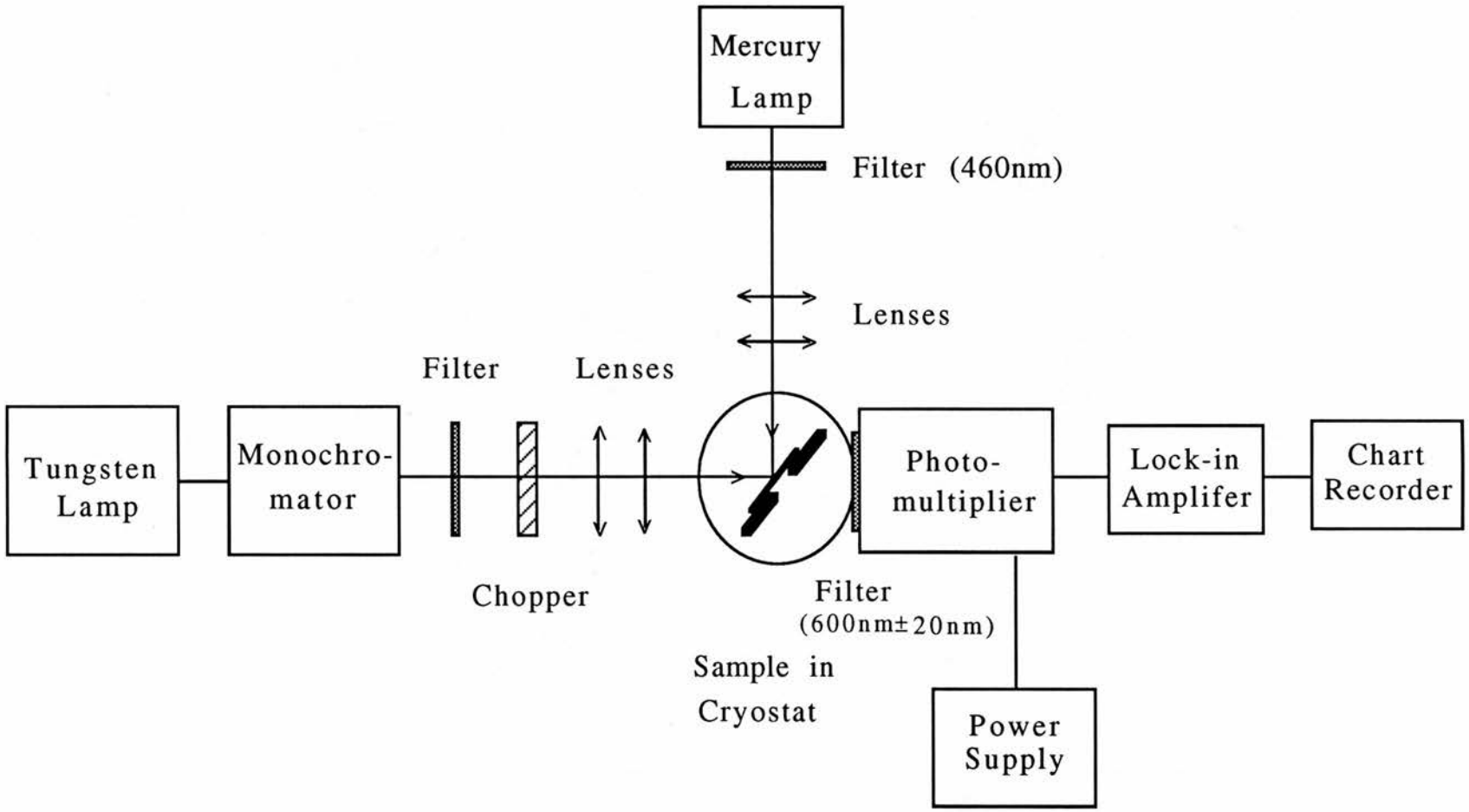

Fig.5.3: The schematic diagram of the optical quenching experiment.

5.3 Experimental results

The optical quenching spectrum of the self-activated luminescence is shown in Fig.5.4. It has been corrected for the photon flux. The dots are the experimental data. The line is drawn to guide the eye. (Some other graphs below in this chapter are drawn in the same way.) It can be seen that only a single feature peaked at about 1.20 eV has been observed.

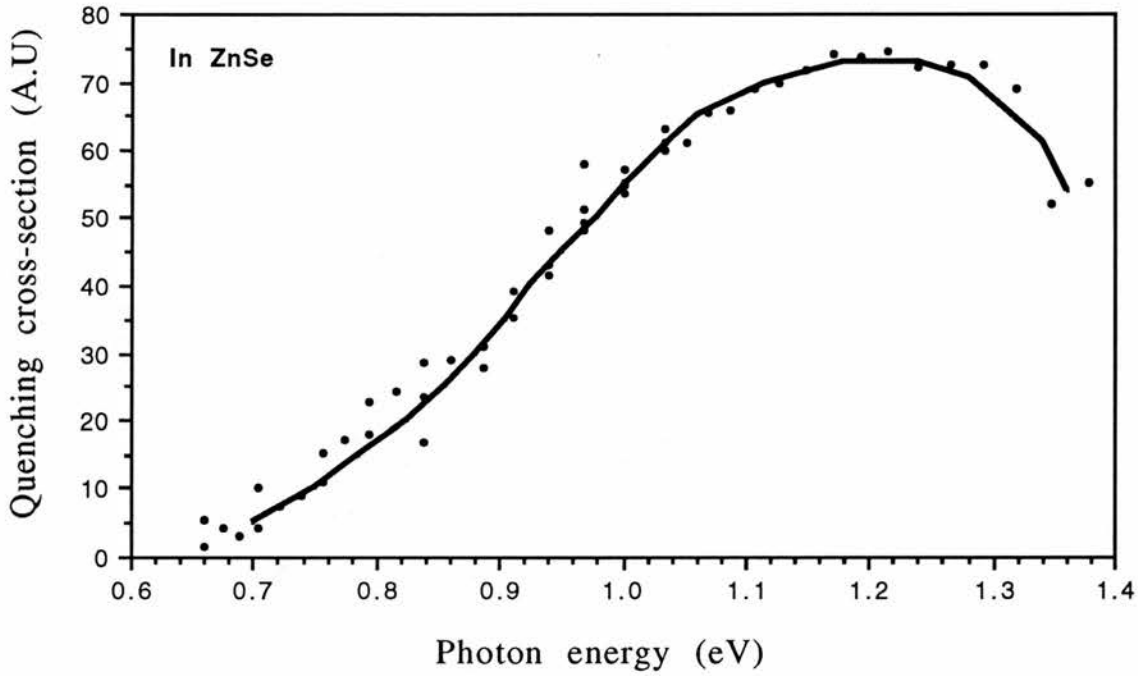

Fig.5.4: The optical quenching spectrum of the self-activated luminescence obtained in bulk ZnSe 18B1 at liquid nitrogen temperature in this work. The dots are the experimental dots. The line is drawn to guide the eye.

5.4 Comparisons with other works in ZnSe and ZnS

5.4.1 In ZnSe

In the literature, there have been only a few works which have presented the optical quenching spectra in quite wide energy ranges. They are the optical

quenching spectra of the Cu-red luminescence observed in ZnSe: Cu by Grimmeiss et al [37] and Zheng [39] and the optical quenching spectrum of the self-activated luminescence observed in as-grown ZnSe containing copper impurity by Iida [42]. For comparison, they are all shown in Fig.5.5 and normalized at about 0.8 eV. It is seen in Fig.5.5 that the spectra are in fairly good agreement at lower photon energies in the range of 0.7 eV to 0.84 eV, followed by obvious departure at higher photon energies from sample to sample. This phenomenon shows that the features in agreement at lower

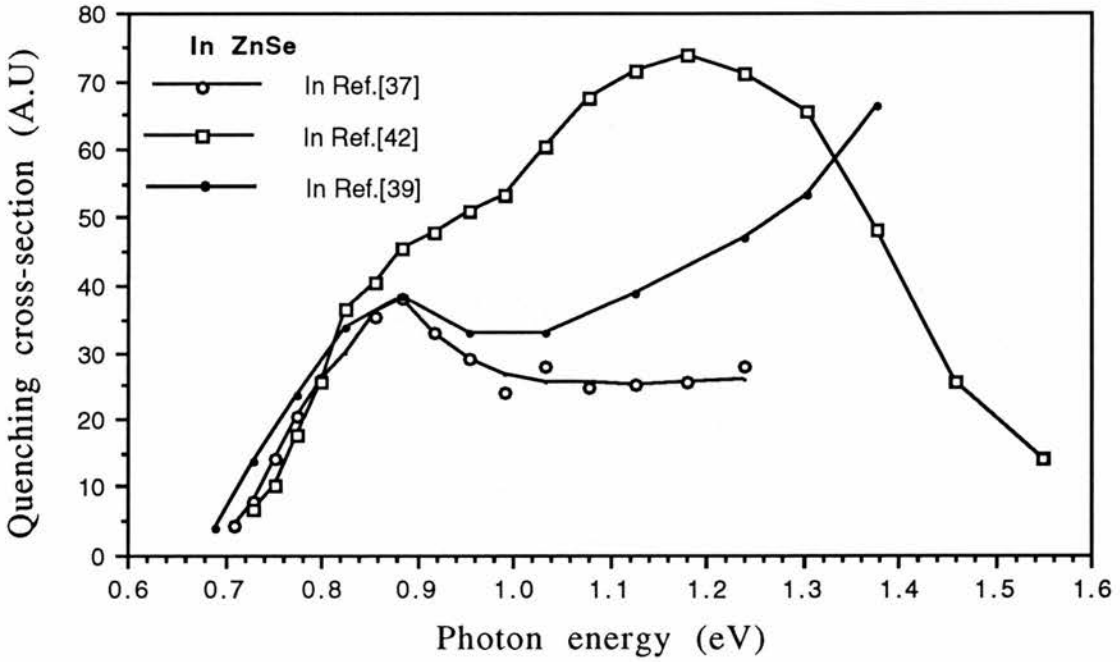

Fig.5.5: The optical quenching spectra obtained in the previous works. They are normalized at about 0.8 eV. They are the optical quenching spectra of the Cu-red luminescence obtained in ZnSe: Cu by Zheng [39] (•) and Grimmeiss et al [37] (o), and the optical quenching spectrum of the self-activated luminescence obtained in as-grown ZnSe containing copper impurities by Iida [42] (□).

photon energy could arise from the same centre, labelled OM here, but the features in disagreement at higher photon energies could arise from different centres in different samples.

In Fig.5.6, the comparison of the optical quenching spectra of the self-activated luminescence obtained in this work and Ref.[42] is shown. The common feature at lower photon energy, observed in Fig.5.5, is missing in the spectrum obtained in this work. However, they are in very good agreement at higher photon energy in the range of 1.0 eV to 1.36 eV. Therefore, the feature peaked at about 1.20 eV observed in this work and Ref.[42] could be due to the same centre which is different from the OM-centre responsible for the feature in agreement at lower photon energy in Fig.5.5. This centre is then labelled OSA.

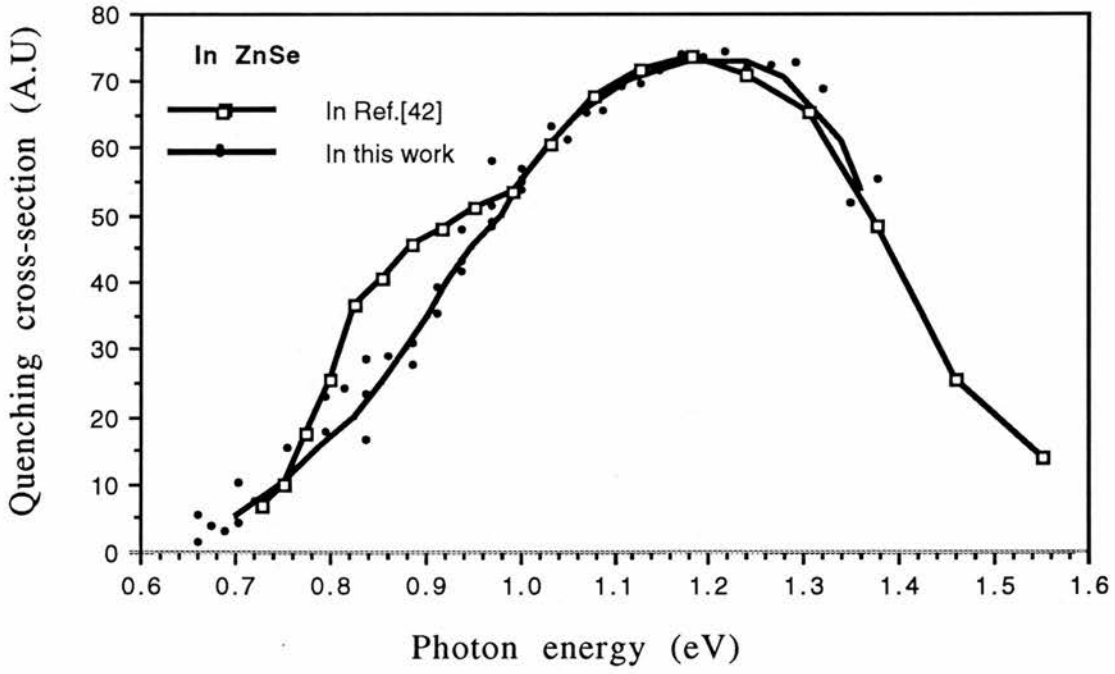

Fig.5.6: The comparison of the optical quenching spectra of the self-activated luminescence. (•) for the one obtained in this work; (□) for the one obtained in Ref.[42]. The spectra are normalized at about 1.02 eV.

The comparisons of the optical quenching spectra with those of hole photoionization cross-section obtained by junction techniques are shown in Fig.5.7 and Fig.5.8. In Fig.5.7, the spectra are normalized at lower photon energy in order to compare the optical quenching spectra of the OM-centre with the hole photoionization cross-section spectra of the M-centre, which have been well studied in chapter 3. It can be seen that they are in very good agreement in the energy range of 0.7 eV to 0.84 eV, showing that the OM-centre seen in the optical quenching spectra could be the same centre, i.e. the M-centre, observed in the photoionization cross-section spectra. In Fig.5.8, the

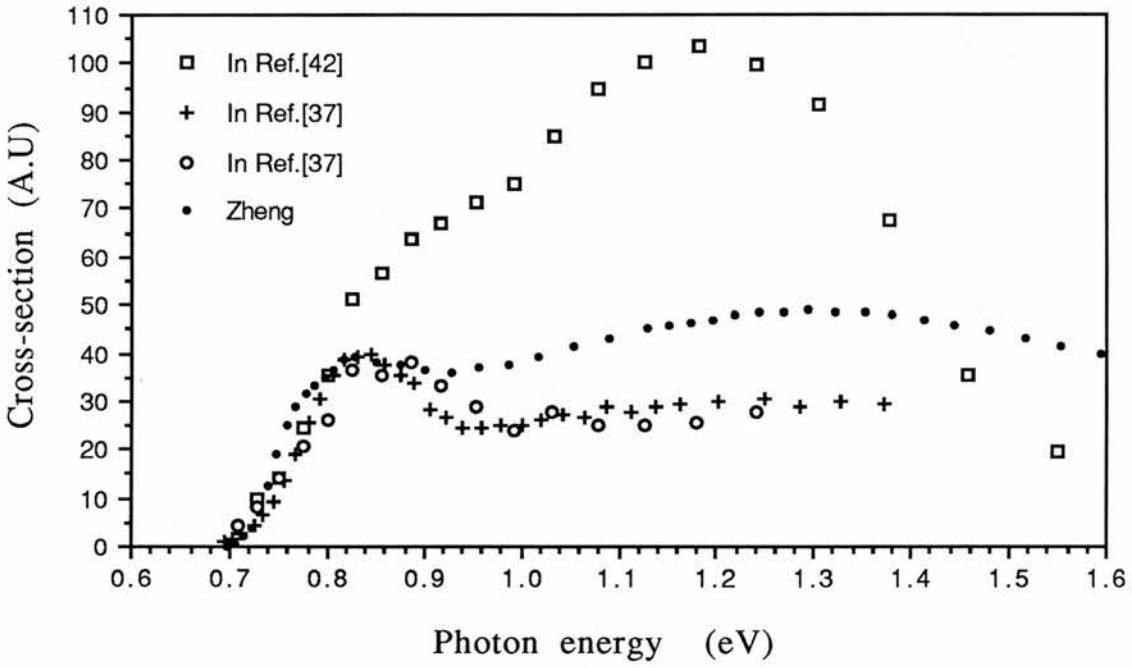

Fig.5.7: The comparison of the optical quenching spectra with the hole photoionization cross-section spectra of the M-centre obtained by junction techniques. They are normalized at lower photon energy of about 0.75 eV. The optical quenching spectra were obtained in Ref.[42] (❑) and Ref.[37] (o). The hole photoionization cross-section spectra were obtained in Ref.[37] (+) and measured in an undoped ZnSe epilayer sample H814 by Zheng (•) (from the private communication).

spectra are normalized at higher photon energy in order to compare the optical quenching spectrum of the SA-emission with the hole photoionization cross-section spectra of the L4-centre. They are only in good agreement in the energy range of 1.0 eV to 1.25 eV. At higher photon energy, the optical quenching cross-section decreases more quickly than the hole photoionization cross-section. Even so, it seems that they come from the same centre. The reason for the disagreement at higher photon energy will be discussed in the next section.

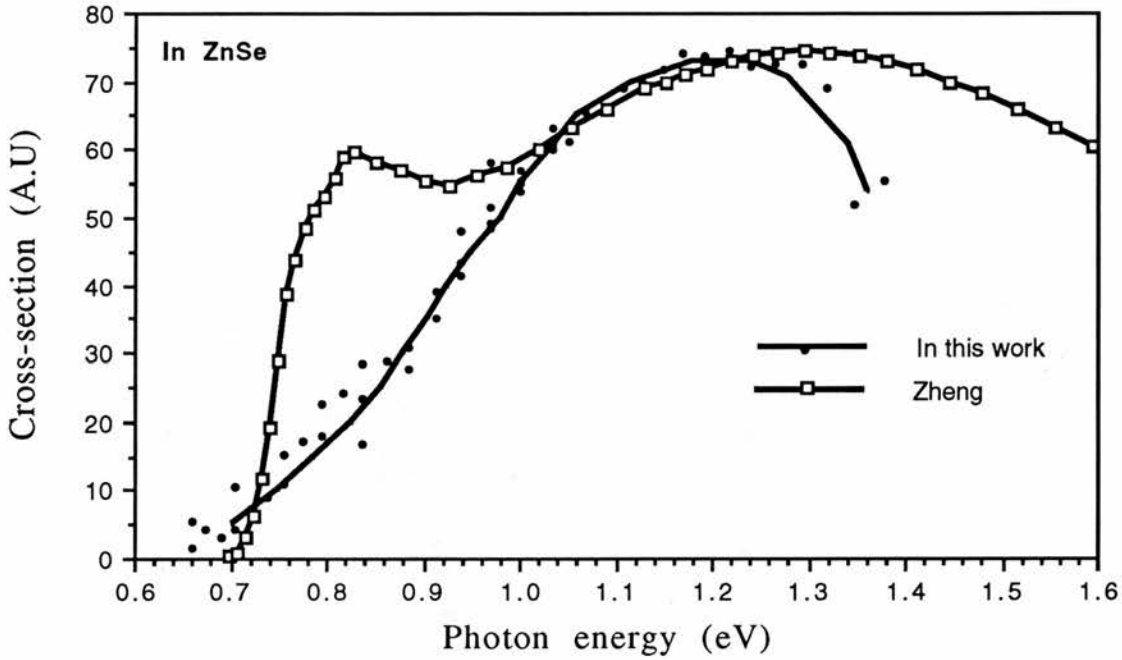

Fig.5.8: The comparison of the optical quenching spectrum of the self-activated luminescence, obtained in this work (•), with the hole photoionization cross-section spectrum of the L4-centre, obtained in ZnSe H814 sample by Zheng (□). They are normalized at higher photon energy of about 1.04 eV.

From the above comparisons, it can be seen that there are two, such as the OM-centre and the OSA-centre, or more centres involved in the optical

quenching processes. The OM-centre and the OSA-centre observed in the optical quenching spectra could be, respectively, corresponding to the M-centre and the L4-centre found by the junction techniques.

5.4.2 In ZnS

Koda and Shionoya [58] measured the optical quenching spectrum of the self-activated luminescence in ZnS: Cl, which is shown in Fig.5.9. In the spectrum, there are two features. One is a weak hump peaked at about 0.87 eV. The other is a strong wide feature peaked at about 1.43 eV. This spectrum is quite similar in shape to the one observed in ZnSe by Iida [42] (see Fig.5.6). Two features in the spectrum might come from two different centres or even more centres. Similarly, the centre responsible for the feature at lower photon

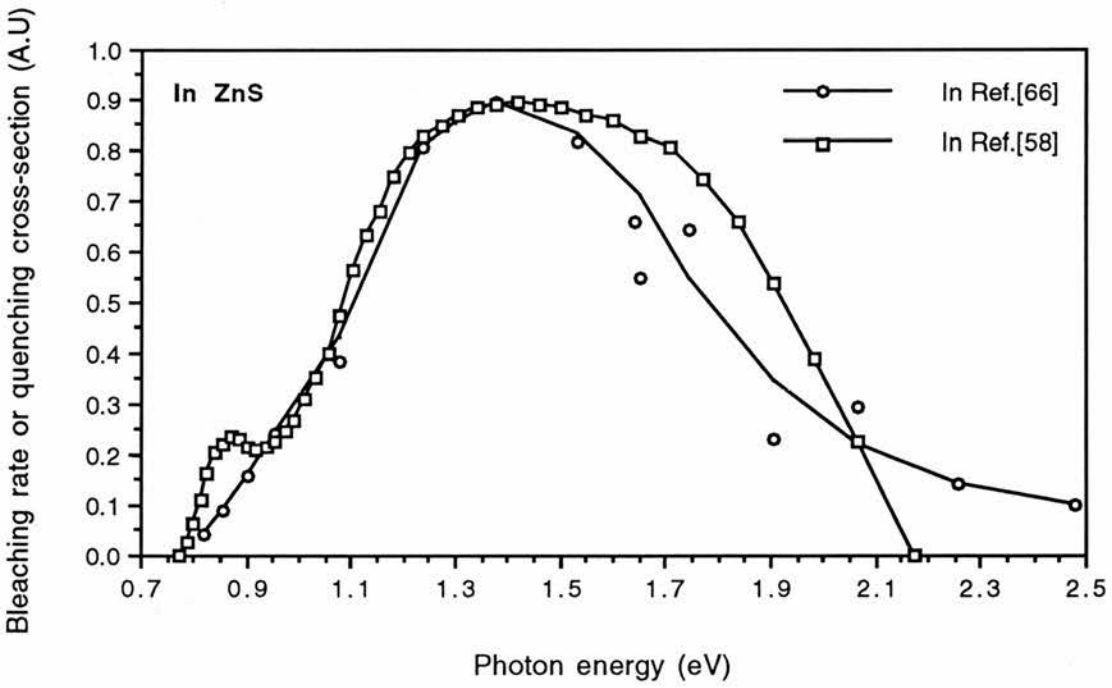

Fig.5.9: The comparison of the optical quenching spectrum of the self-activated luminescence with the EPR bleaching rate spectrum. They were obtained in ZnS: Cl by Koda and Shionoya [58] (□) and Watkins [66] (o). They are normalized at 1.32 eV.

energy in the spectrum is then labelled OM' here, and the centre responsible for the feature at higher photon energy is labelled OSA'.

In ZnS: Cl, Watkins [66] identified unambiguously the self-activated (SA) luminescent centre and the A-centre by the agreement of their polarization characteristics, and presented the bleaching rate spectrum of polarized light of the EPR signal associated with the A-centre, which is also shown in Fig.5.9. The single feature peaked at about 1.38 eV in the bleaching rate spectrum is also believed to be due to the A-centre, that is the SA-centre. It can be seen in Fig.5.9 that the single feature in the bleaching rate spectrum is in fairly good agreement with that at higher photon energy in the optical quenching spectrum, which suggests that the OSA'-centre responsible for the feature peaked at about 1.43 eV in the optical quenching spectrum could be the SA-centre.

The optical quenching spectrum is then compared with those of hole photoionization cross-section studied in the last chapter. In Fig.5.10, they are normalized at lower photon energy of about 0.88 eV in order to compare the feature at low photon energy in the optical quenching spectrum with the hole photoionization cross-section spectrum of the M'-centre. The pretty good agreement is found, showing that they could have the same origin, i.e. the M'-centre could be the same as the OM'-centre. This phenomenon is similar to the observation of the M-centre involved in the optical quenching process in ZnSe consistent with the suggestion in the last chapter that the M-centre in ZnSe and the M'-centre in ZnS could have the same kind of origin. However, no agreement is found at higher photon energies in the spectra. Actually, the lack of the hole photoionization cross-section spectrum at higher photon energy limits this comparison.

In ZnS, similarities are found in the optical quenching spectrum as they have been observed in ZnSe. There must be also two, such as the OM'-centre and the OSA'-centre, or more centres involved in the optical quenching

process. The OM'-centre could be the M'-centre found by the junction techniques, and the OSA'-centre could be the SA luminescent centre.

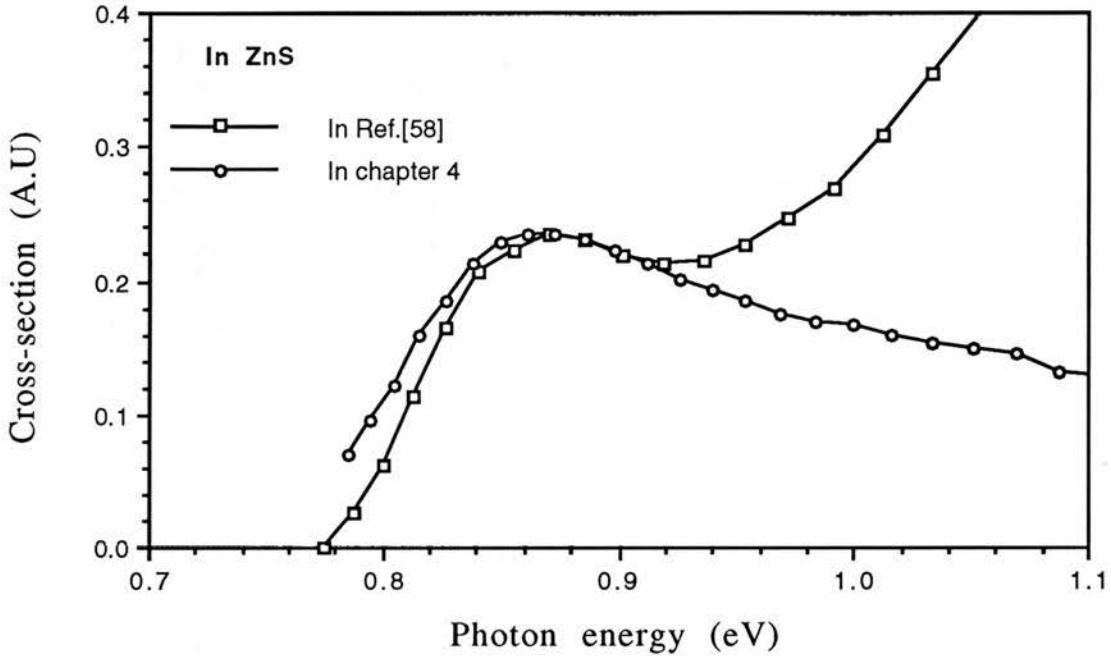

Fig.5.10: The comparison of the optical quenching spectrum of the self-activated luminescence with the hole photoionization cross-section spectrum of the M'-centre. They are normalized at about 0.87 eV. The optical quenching spectrum of the self-activated luminescence was obtained in ZnS: Cl by Koda and Shionoya [58] (□); The hole photoionization cross-section spectrum was obtained in an ZnS epilayer in chapter 4 (○).

5.5 Discussion

First of all, a summary of the deep levels found by different experimental methods is given in Table 5.1. In the last section, by comparing different quenching spectra obtained in different samples and comparing those quenching spectra with the photoionization cross-section spectra of different centres, it is found that there must be two or more centres involved in the

optical quenching processes of the self-activated luminescence in ZnSe and ZnS. The centres responsible for the optical quenching processes are identified with those found by junction techniques, as seen in the last column in Table 5.1. In ZnS, the OSA'-centre is suggested to be the SA-centre. In ZnSe, there is no evidence that the OSA-centre is the SA-centre. However, since there are great similarities found in the shapes and the origins of the optical quenching spectra in ZnSe and ZnS and the dominant centre observed in ZnSe 18B1 by the photoluminescence measurement is the SA-centre, as seen in Fig.5.2, the analogous conclusion for ZnSe is then suggested which is that the OSA-centre could be the SA-centre.

Table 5.1 The deep levels found in ZnSe and ZnS by different experimental methods.

Methods	Junction techniques		Photoluminescence method		Quenching method	
Materials	ZnS	ZnSe	ZnS	ZnSe	ZnS	ZnSe
Centres		L1				
	M'	M			OM'(M')	OM(M)
		L2				
	L4'	L4	SA	SA	OSA'(SA)	OSA(L4)
			Cu-red	Cu-red		
			Cu-green	Cu-green		
			Cu-blue			

A model is then proposed to interpret the optical quenching phenomenon of the self-activated luminescence in ZnSe and ZnS. The energy level diagram of this model is schematically shown in Fig.5.11. In this model, there

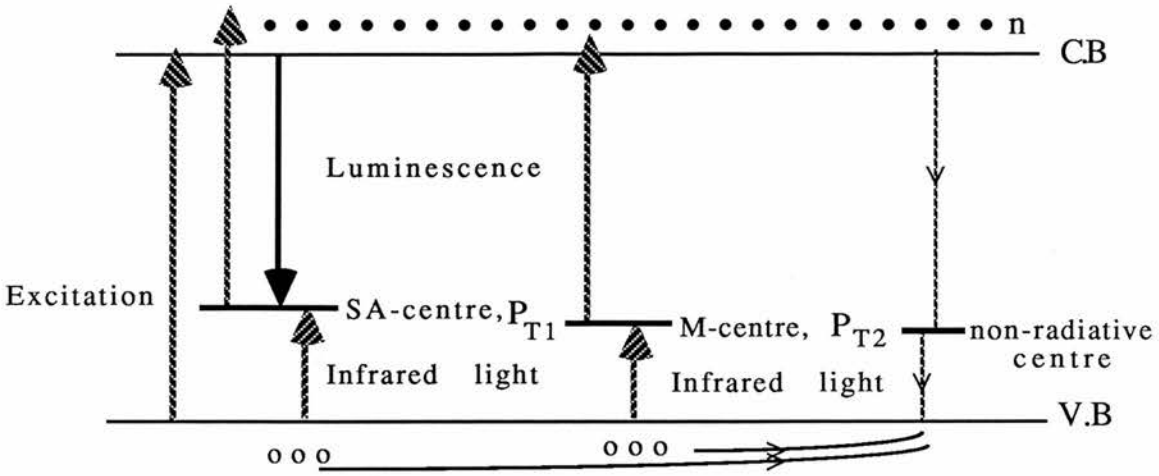

Fig.5.11: A model of the energy level diagram to explain the optical quenching process of the self-activated luminescence when there are two or more centres introduced in the process. The upward arrow stands for the electron excitation; the downward arrow stands for the electron recombination.

are at least three centres involved in the optical quenching process. The infrared light in the photon energy range of 0.7 eV to 0.96 eV in ZnSe and 0.78 eV to 0.94 eV in ZnS could dominantly release the bound holes from the OM-centre in ZnSe or the OM'-centre in ZnS to the valence band because the hole photoionization cross-sections σ_p of these two centres could be large enough in these energy ranges, as seen in the hole photoionization cross-section spectra of these two centres shown in the last two chapters. Then the released holes Δp, in the amount of about $\Delta p \propto p_{T2}\sigma_{p2}\phi$ (where ϕ is the photon flux, p_T is the concentration of the emptied deep centres, and suffixes "1" and "2" stand for the OSA-centre and the OM-centre in ZnSe or the OSA'-centre the OM'-centre in ZnS, respectively), would be left behind in the valence band. These holes could recombine with the freed electrons in the conduction band through a non-radiative centre with a very high hole capture coefficient. So an equal number of free electrons in the conduction band, i.e. $\Delta n \propto p_{T2}\sigma_{p2}\phi$, would be decreased. Therefore, the self-activated luminescence intensity L ($L \propto np_{T1}$) would be quenched by the same amount of $\Delta n \propto p_{T2}\sigma_{p2}\phi$, which is

proportional to the hole photoionization cross-section of the OM-centre in ZnSe or the OM'-centre in ZnS when the electron occupancy of deep levels is mainly established by the strong excitation light, namely p_{T1} is approximately constant. So the feature in the lower energy range in the quenching spectrum arises from the OM-centre in ZnSe or the OM'-centre in ZnS, as suggested in section 5.4. When the photon energy of the infrared light is higher, the hole photoionization cross-section of the OSA-centres in ZnSe or the OSA'-centre in ZnS becomes greater than that of the OM-centre in ZnSe or the OM'-centre in ZnS. In this case, the released holes would be mainly released from the OSA-centre or OSA'-centre to the valence band by the amount of about $\Delta p \propto p_{T1}\sigma_{p1}\phi$. The number of the emptied OSA-centre or OSA'-centre would be decreased by the same amount. The holes left behind in the valence band could also recombine with free electrons in the conduction band through the same non-radiative centre by the same amount. Therefore, the self-activated luminescence intensity would be quenched by the decreases of free electrons in the conduction band and the bound holes at the OSA-centre or OSA'-centre by about $2p_{T1}\sigma_{p1}\phi$, which is proportional to the hole photoionization cross-section of the OSA-centre in ZnSe or OSA'-centre in ZnS respectively. So the feature in the higher energy range in the quenching spectrum arises from the OSA-centre in ZnSe or the OSA'-centre in ZnS, as also suggested in section 5.4. When the OSA-centre concentration is much higher than that of the OM-centre in ZnSe, i.e. $p_{T1} >> p_{T2}$, the total number of the holes released from the OSA-centre and the OM-centre to the valence band, i.e. $\Delta p \propto p_{T1}\sigma_{p1}\phi + p_{T2}\sigma_{p2}\phi$, could be dominant by the holes released from the OSA-centre so that the optical quenching spectrum is mainly affected by the OSA-centre in a wider photon energy range, as seen in Fig.5.4. In a word, this model can interpret what has been observed in experiments.

The existence of some non-radiative centre in both ZnSe and ZnS is obvious in photoluminescence measurements because the intensity of

photoluminescence is often much weaker than that of excitation light. However, its origin is still unknown.

According to this model, it can be seen that whether a deep centre would affect the quenching of a luminescence band depends on the competition of emission rates of different centres at photon energies of the infrared light. The emission rate is proportional to the product of deep-level concentration p_T and photoionization cross-section σ_p. If deep-level concentrations could be known or controlled, then this model could be tested. The quenching of a luminescence band would be dominated by the deep level with the largest product of $p_T \sigma_p$. The centre responsible for an optical quenching spectrum of one luminescence does not have to be the luminescent centre.

Actually, the infrared irradiation can lead either to raising an electron trapped at a centre in the upper half of the band-gap to the conduction band or to release of a hole trapped at a centre in the lower half of the band-gap to the valence band. In both undoped ZnSe and ZnS, it has been found that there are some deep levels in the upper half of the band-gap. The electron transition from deep centres in the upper half of the band-gap to the conduction band, produced by the infrared irradiation, will create more free electrons in the conduction band so that the stimulation of luminescence can occur. Then the total luminescence quenching rate could be reduced. This is a possible reason for the departure at higher photon energy between the optical quenching spectrum of the self-activated luminescence and the hole photoionization cross-section spectrum of the L4-centre in ZnSe, seen in Fig.5.8.

Since the optical quenching of one luminescence band could involve many deep centres, the optical quenching spectrum could be very different from sample to sample. Since the characteristic optical quenching spectrum of different deep centres cannot be simply separated from each other in the way that the photoionization cross-section spectrum of each deep centre can be

separated by using different pump light in the DLSS photocapacitance measurements, the optical quenching experiment cannot be used, in general, to identify centres with any certainty. It should be also kept in mind that photoluminescence could be due to a very small concentration of centres which is not necessarily seen in the photocapacitance measurements.

The similar phenomenon, when a hole released from one deep centre is captured by another deep centre, has been observed in the transient stimulation spectrum of the Cu-green luminescence in ZnSe: Cu in Ref.[55]. It was observed that when crystals were excited with 2.5 eV radiation such that the Cu-red but not the Cu-green emission was excited, the optical quenching of the Cu-red emission caused a transient stimulation of the Cu-green emission. The spectra of the quenching of the Cu-red and the stimulation of the Cu-green are identical. This effect can be interpreted thus: after the holes are freed from the Cu-red centres by the infrared light, they can be captured by the Cu-green centres. This is followed by recombination of the free electrons with the holes captured at the Cu-green centres. This process gives the stimulation of the Cu-green luminescence. Räuber, Schneider and Matossi [67] also observed hole transfer between the A-centre and the Fe^{3+}-centre in ZnS doped with iron impurity by the EPR measurement under the photo-excitation condition. It was observed that the EPR Fe d^5 signal could be increased by the Fe d^6 centres capturing the free holes released from the A-centre by the infrared light while the EPR A-centre signal was decreased. In these two examples, both the Cu-green centre and the Fe d^5 centre played a role in capturing the holes released from another deep centre. The difference is that the Cu-green centre is a luminescent one, the Fe d^6 centre is a non-radiative one.

5.6 Conclusions

The optical quenching spectra and photoionization cross-section spectra obtained in ZnSe and ZnS in this work and in previous works are compared. It is found that there are more than one feature, in the optical quenching spectra, due to different centres. They are the OSA-centre and the OM-centre in ZnSe and the OSA'-centre and the OM'-centre in ZnS. The OM-centre and the OM'-centre are, respectively, identified to be the M-centre and the M'-centre. The OSA'-centre is identified to be the self-activated luminescent centre by its characteristic polarization property in ZnS. Similarly, the OSA-centre is suggested to be the SA luminescent centre in ZnSe. A model involving three deep centres is then proposed to successfully explain these optical quenching processes in terms of hole transfer between different centres.

Since there could be many deep centres to affect the optical quenching process of one luminescence band, the optical quenching experiment does not allow us to identify centres with any certainty without further information.

Chapter 6

Investigation of n-ZnSe/n-GaAs heterojunctions grown by MOCVD

6.1 Introduction

There has been a considerable interest in growing high quality ZnSe material due to its potential application in optoelectronic devices. In recent years, it has been found that the growth by both metalorganic chemical vapour deposition (MOCVD) and molecular beam epitaxy (MBE) can give an opportunity for low temperature deposition resulting in a great improvement in the optoelectronic properties of the ZnSe epitaxial layers. Because large perfect single crystals of ZnSe are very difficult to grow, GaAs has become the most commonly used substrate for the growth of ZnSe by MOCVD and MBE due to its availability, very good quality of crystal, well-established surface cleaning and preparation procedures. However, with a combination of two materials, such as the ZnSe/GaAs structure, with different band-gaps, different lattice constants, different thermal expansion coefficients etc, there can be many factors affecting the electrical and optical properties of the heterojunction.

In theory, there are a lot of modelings of heterojunctions, for example, the quantum mechanical heterojunction barrier models of Harrison and of Frensley-Kroemer [68,69], the electron-affinity Anderson-Shockley model [70,71], the dipole-minimization Tersoff model [72] and so on, to calculate the conduction and valence band discontinuities at heterojunctions. However, so far there is still not any very successful theory to give close agreement with the experimental results in a wide range of materials, such as III-V compounds and II-VI compounds. For the ZnSe/GaAs system, their band-gaps of ZnSe and GaAs are, respectively, 2.7 eV and 1.43 eV at room

temperature. It is suggested that the main band discontinuity may occur in the valence band at the interface. The theoretically predicted offsets of the conduction and valence bands, which in this case are in fairly good agreement with experimentally measured values, are about 0.3 eV and 1.0 eV respectively [73,74].

In practice, the well established successes of heterojunctions are mainly based on the lattice-matched structures of AlGaAs/GaAs and InP/InGaAs which have been used to produce commercially various electron devices including high quality lasers and optical detectors.

For the lattice mismatched heterojunctions, such as ZnSe/GaAs where the lattice constant of ZnSe is 0.25% larger than that of GaAs, it has been found that the lattice mismatch can result in the formation of misfit dislocations and threading dislocations which can propagate through the whole epilayer structure [75]. Many efforts to overcome this obstacle have been made by improving or developing the growth techniques [76,77]. For example, the defect density can be reduced by grading the composition of the epitaxial layer so that the lattice parameter changes gradually as the layer is grown. A more attractive approach is the use of strained layer superlattices (SLS) to accommodate misfit dislocations and also to act as dislocation filters, where the SLS is used to intercept and bend over threading dislocations. A chemical reaction could also occur on the substrate surface during the growth. A thin interfacial layer of Ga_2Se_3, which is thermodynamically the most stable of the compounds of gallium and selenium, has been found at the ZnSe/GaAs interface [78,79,80]. Therefore, careful control of the growth process including the temperature, the purification of growth sources and so on can efficiently reduce cross diffusions and dislocations so as to improve the quality of epitaxial layers.

The techniques used to investigate the structure and optoelectronic properties of epitaxial layers, such as in the ZnSe/GaAs system, are various.

For example, transmission electron microscopy (TEM) [75], reflection high-energy electron diffraction (RHEED) [81], Auger electron spectroscopy [82], Raman spectroscopy [80,83], x-ray photoelectron spectroscopy (XPS) [79] and so on have been mainly employed in the investigation of dislocations and structures at the interfaces and on the epitaxial layers. Photoluminescence measurements, Hall effect measurements [84], capacitance-voltage (C-V) and current-voltage (I-V) measurements [81,85,86] and so on have been mainly employed in the investigation of optoelectronic properties of heterojunctions. However, each of them can only offer one aspect of properties of heterojunctions and some of them cannot separate the information about whole epitaxial layers from the information about interfaces.

In this study, we have investigated the nonlinear I-V characteristics of n-ZnSe/n-GaAs heterojunctions grown by MOCVD and the effect of post-growth annealing on the heterojunction interfaces. An insulating layer formed at the heterojunction interface has been characterized by capacitance-voltage (C-V) measurements and space-charge-limited current phenomena. The thickness increases with the increase of the annealing temperature. When the thickness of the insulating layer is greater than several thousand angstroms, the space-charge-limited current through the heterojunction interface can be observed. The possible band-bendings at the interfaces were investigated by the open-circuit photovoltage measurement. A model is then tentatively proposed to describe the situation of the heterojunctions in the samples in this work.

6.2 Materials and experiments

6.2.1 Sample conditions

Two sets of ZnSe epilayer samples, labelled ZnSe K and ZnSe HL1, were investigated. They were all grown on very conducting n-type GaAs substrates

by MOCVD in the Solid State Chemistry Group of the University of Manchester Institute of Science and Technology (UMIST). The growth was at atmospheric pressure using dimethylzinc and hydrogen selenide, at a substrate temperature 280°C. For the ZnSe K, one conducting epilayer with a thickness of about 5 μm and carrier concentration of $1.0*10^{18}$ cm^{-3} was grown on the n-GaAs substrate. For the ZnSe HL1, there were two ZnSe epilayers grown on the n-GaAs substrate as schematically depicted in Fig.2.5. The top ZnSe epilayer is about 5 μm thick, with a carrier concentration between 10^{15} cm^{-3} and 10^{16} cm^{-3}, the middle ZnSe epilayer is about 4.6 μm thick with the carrier concentration of about $1.0*10^{18}$ cm^{-3}. The samples of each set were cut from the same slice (i.e. either the ZnSe K or the ZnSe HL1) by using a wire saw followed by cleaning with three organic solvents (toluene, acetone and propanol). The size of each dice is about 2 mm x 2 mm x 0.4 mm.

6.2.2 The post-growth annealing and the making of ohmic contacts

Zheng and Allen [29] have found that post-growth annealing between 300°C and 450°C is a useful method to control the resistivity of MOCVD grown ZnSe. In order to further apply this annealing method in practice, it is necessary to know the effect of the post-growth annealing on the n-ZnSe/n-GaAs heterojunction interfaces.

The annealing procedure has been described in section 2.3.1 (A) in chapter 2. After cleaning dice with three organic solvents (as mentioned above) and dilute HCl, they were placed in a container made from high-purity germanium which was then placed in a spectrosil silica tube. In this way, the copper contamination is believed to be minimized during heat treatments. The samples used were heat treated between 350°C and 400°C in air for 30 minutes. The detailed annealing temperature for each sample can be found in Table 6.1 and Table 6.2.

The technique of making ohmic contacts has also been described in section 2.3.2. Ohmic contacts were made respectively on the ZnSe and GaAs surfaces with at least two indium dots by heating at about 310°C in 90% N_2/10% H_2 atmosphere for 30 seconds. The locations of indium dots on different samples were nearly the same in order to compare the results of the I-V measurements among the samples.

6.2.3 The experimental measurements

Conventional I-V and C-V measurements were performed in the dark. The capacitance characteristics were measured with the Wayne-Kerr 601 Bridge at a frequency ranging from 60 kHz to 1.2 MHz with a peak-to-peak signal of about 30~60 mV. For the temperature dependent measurement, the samples were placed in a temperature-controlled oven to be heated to a temperature which was higher than room temperature, but lower than 100°C. The steady-state temperature was measured with a digital thermometer.

The open-circuit photovoltage measurement was employed at room temperature to investigate the band-bendings of heterojunctions. A wide spectral band tungsten halide lamp was used as the excitation source. The light was passed through a prism monochromator and appropriate lenses, then was focused on the ZnSe surfaces. A micro-voltmeter was directly connected to the ohmic contacts on the different sides of the samples, i.e. the ZnSe side and GaAs side, to measure the open-circuit photovoltages. No applied voltage was used. The photon flux was measured by a thermopile at room temperature.

6.3 Results

6.3.1 The results of the I-V measurements

First of all, the I-V characteristics of two indium dots on the same side, such as the ZnSe side or the GaAs side, were measured in both current directions to check the quality of ohmic contacts. They were straight lines and the same in both current directions. This indicated that the indium contacts were good ohmic contacts. As the annealing temperature increased the resistance of the ZnSe epilayers increased as well. The data of the resistance, $R_{I\text{-}V}$, between two indium dots on the ZnSe side are listed in Table 6.1 for the samples HL1 and Table 6.2 for the samples K respectively. The resistance between two indium contacts on the GaAs substrate was about 3.0 Ω and it remained a constant value after heat treatments.

The I-V characteristics between two indium dots on different sides (i.e. one on the ZnSe side, the other on the GaAs side) were also measured in both current directions. They were not linear and not the same in different current directions. For the set of the ZnSe K epilayer samples, the I-V characteristics in two current directions are shown in Fig.6.1 and Fig.6.2 where the signs "ZnSe-" and "ZnSe+" represent respectively that the ZnSe side is connected with the negative or positive polarity of the power supply. These two signs are also used in the following figures with the same meaning, except in Fig.6.9 and Fig.6.10. The sample K001 was not heat treated. The samples K002 and K003 were heat treated at 390°C and 400°C respectively. For the set of the ZnSe HL1 epilayer samples, the I-V characteristics of the sample HL1-002 without heat treatment are shown in Fig.6.3. When the ZnSe side was biassed positively, there was a critical voltage V_0 below which the current was very small, as shown in Fig.6.3 (a). When the applied voltage was increased to a few volts above V_0, the heterojunction interface broke down. In this case, the electrical behaviour was completely changed. The I-V characteristic at room temperature, shown in Fig.6.4, is a typical one for the samples HL1 annealed at a temperature between 350°C and 395°C. The currents with the ZnSe side biassed positively were too small (less than 1.0 nA) to be measured over a

wide range of applied voltage up to 15 V. Typical I-V behaviours at different temperatures for the samples HL1 annealed are shown in Fig.6.5.

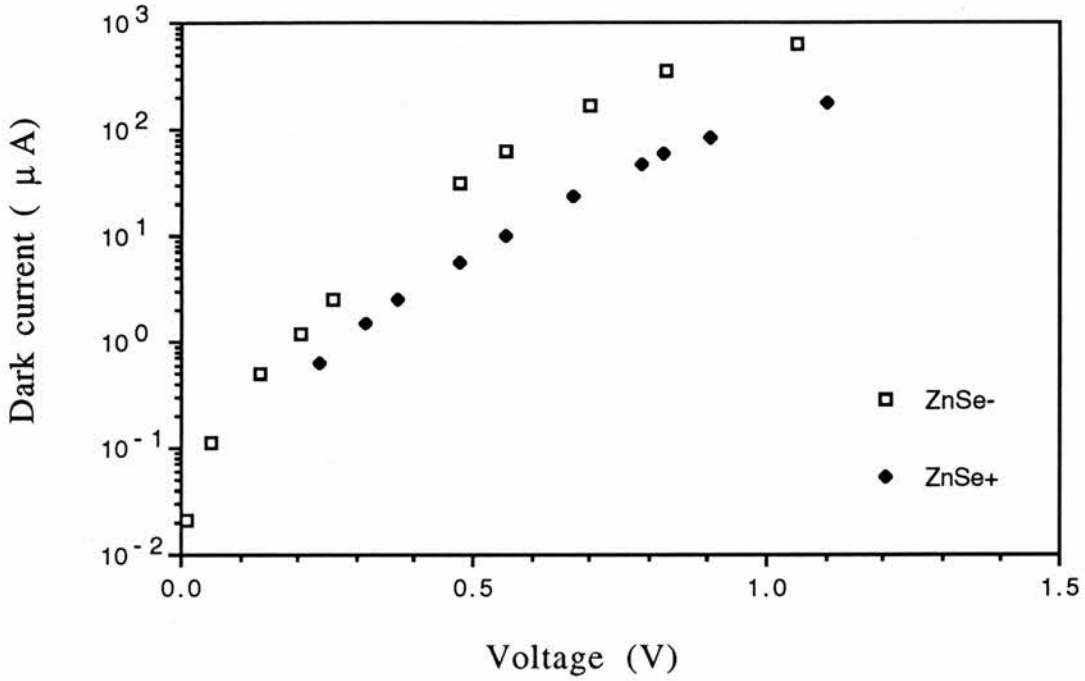

Fig.6.1: The I-V characteristics of the sample K001 without heat treatment. They were obtained at room temperature between two indium dots on different sample surfaces, i.e. one is on the ZnSe side, the other is on the GaAs side, for both current directions.

6.3.2 The results of the C-V measurements

The C-V measurement was carried out between two indium dots on the different surfaces of each sample. So it gives information about the heterojunction interfaces. However, it is difficult to interpret the measured capacitance, which might consist of several components. The capacitance may depend on the band-bendings of ZnSe and GaAs, and the insulating layer which possibly exists at the heterojunction interfaces. The capacitance of each component would have a different dependence on the bias and frequency.

Fortunately, in our samples, the dependences of capacitances on the frequency and bias show simple behaviours so that the C-V measurement can be a useful analytic tool in this study. This point will be further discussed in detail in section 6.4.2 and section 6.5.

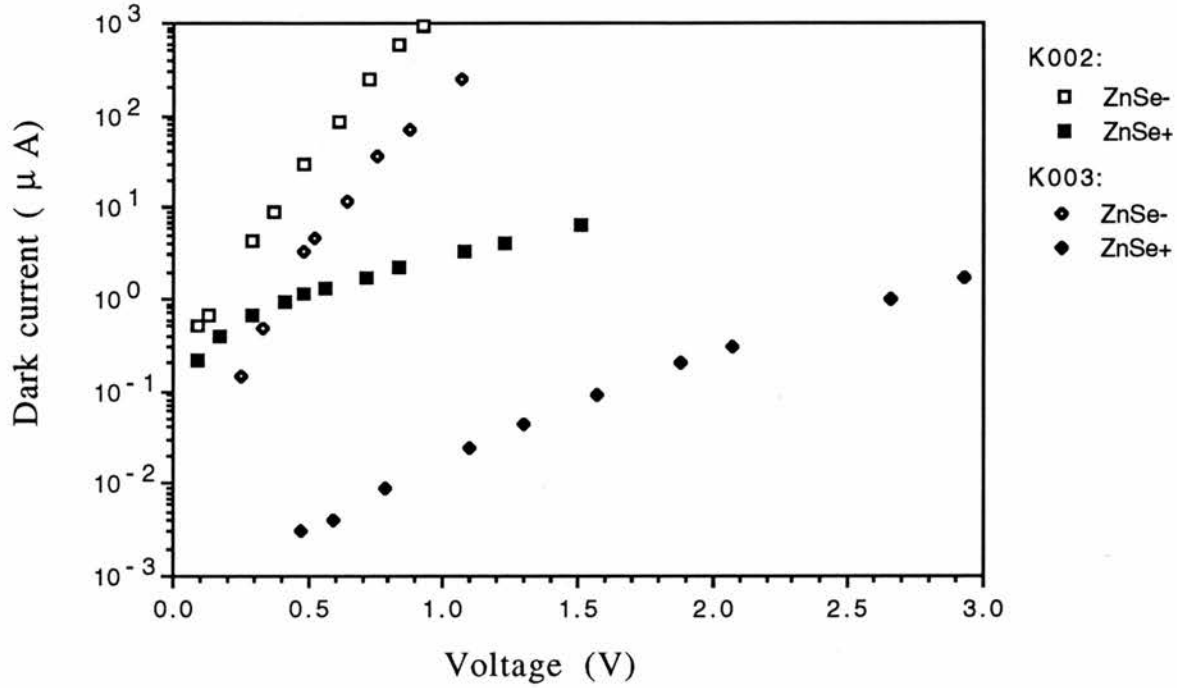

Fig.6.2: The I-V characteristics of the samples K002 and K003 annealed at 390°C and 400°C respectively. They were obtained at RT between two indium dots on different sample surfaces in both current directions.

For the samples ZnSe K, the C-V characteristics measured at a frequency of 1 MHz or 60 kHz are shown in Fig.6.6 and Fig.6.7. For the samples ZnSe HL1, the C^{-2}-V characteristics of the sample HL1-002 measured at different frequencies are shown in Fig.6.8. The capacitance measured at a given frequency for other samples with heat treatments did not change with an increase of applied voltage. The results of the constant capacitances are listed in Table 6.1, where the capacitance C_s and resistance R_s represent those of an

equivalent circuit of a capacitor and a resistor in series. They were evaluated from the equations

$$R_s = \frac{R}{1+\omega^2 C^2 R^2} \tag{6.1}$$

$$C_s = C + \frac{1}{\omega^2 C R^2} \tag{6.2}$$

$$\omega = 2\pi f \tag{6.3}$$

where C and R were read from the bridge because the equivalent circuit of the bridge is a capacitor and a resistor in parallel. f is the frequency of the ac signal.

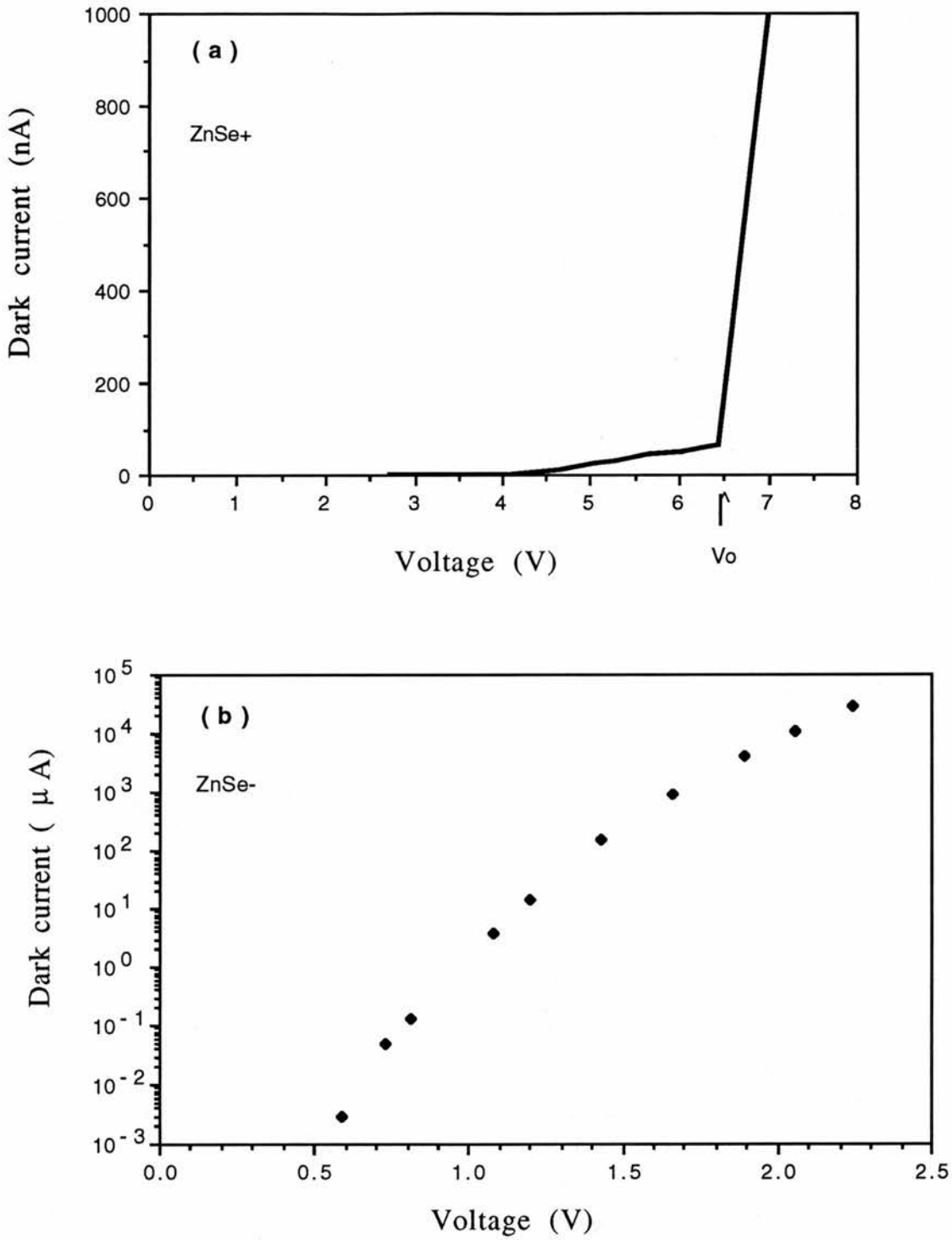

Fig.6.3: The I-V characteristics of the sample HL1-002 without heat treatment. They were obtained at RT between two indium dots on different sample surfaces in both current directions. (a) the ZnSe side was biassed positively; (b) the ZnSe side was biassed negatively.

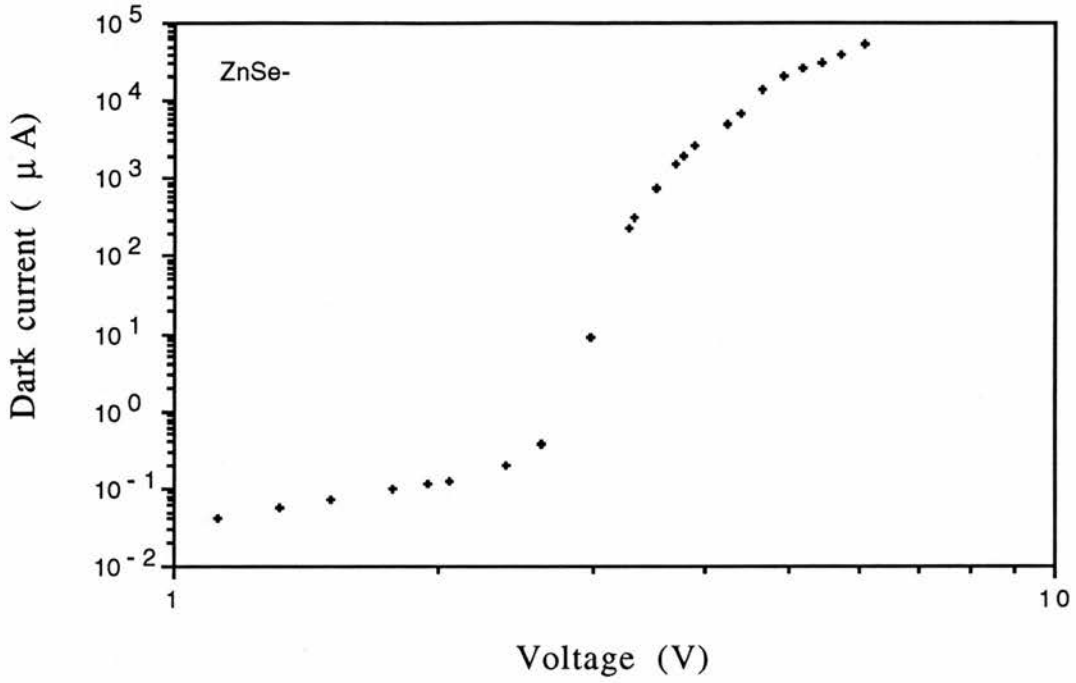

Fig.6.4: The I-V characteristic of the sample HL1-003 annealed at 380°C. It was obtained at RT between two indium dots on different sample surfaces when the ZnSe side was biassed negatively.

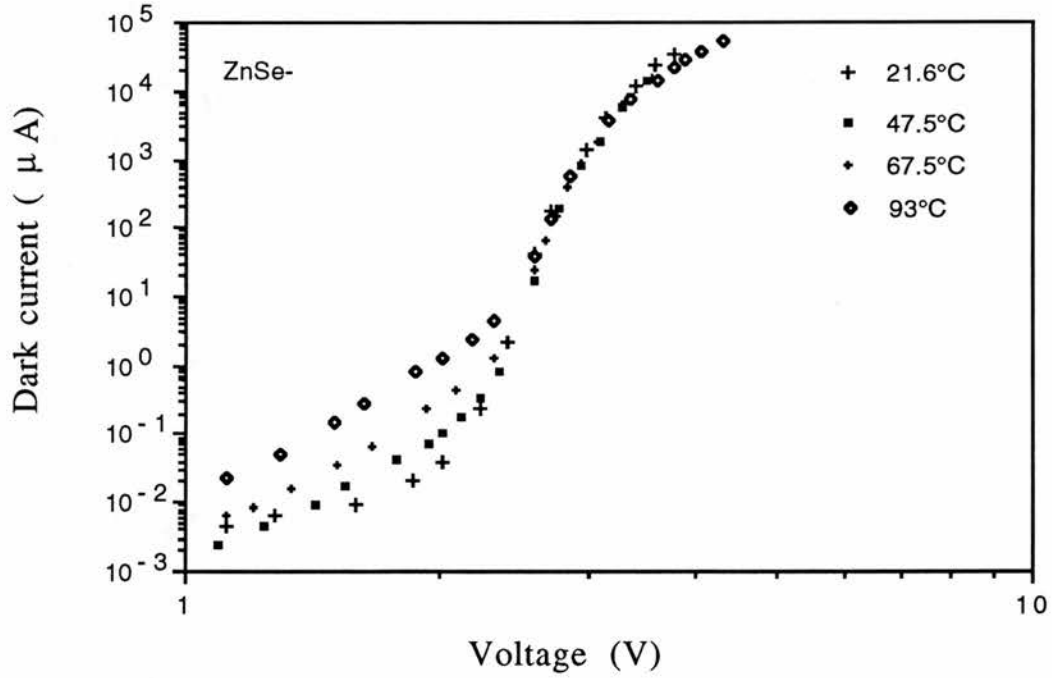

Fig.6.5: The I-V characteristics of the sample HL1-004 annealed at 370°C. They were measured at different temperatures between two indium dots on different sample surfaces when the ZnSe side was biassed negatively.

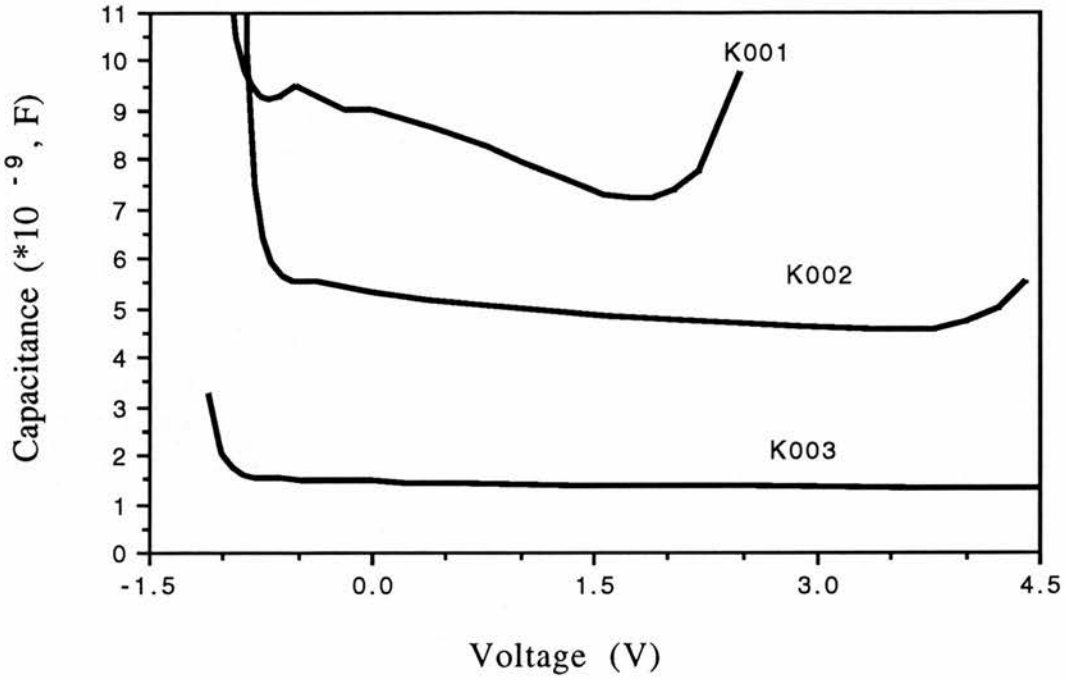

Fig.6.6: The C-V characteristics of the samples ZnSe K measured at a frequency of 1 MHz. The positive voltage corresponds to the ZnSe side biassed positively.

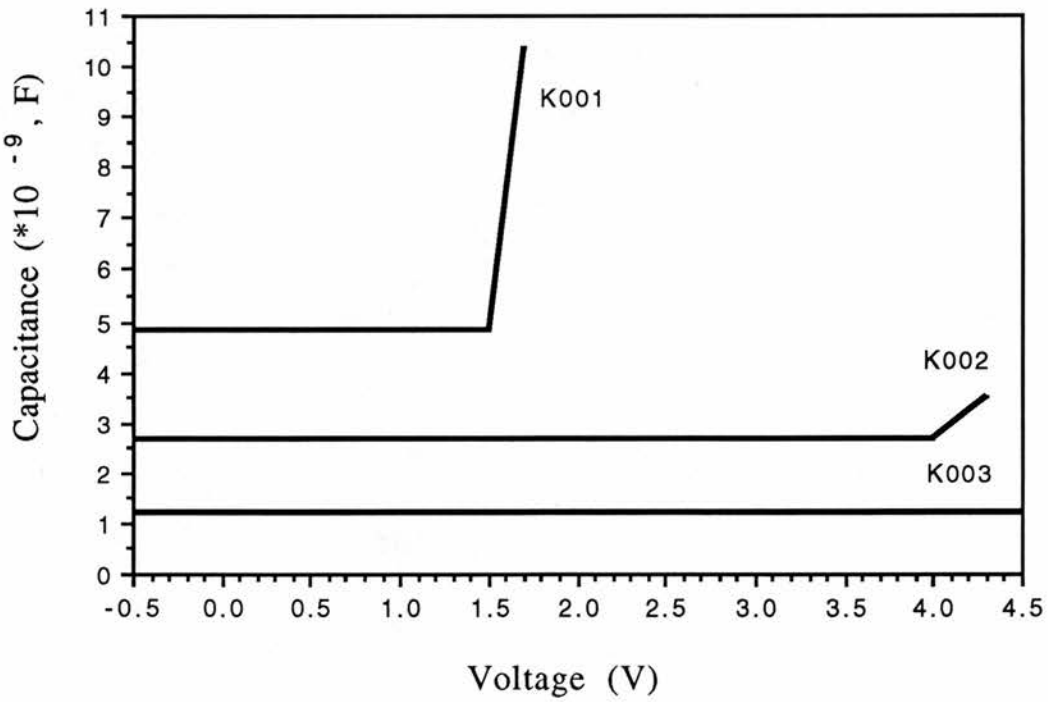

Fig.6.7: The C-V characteristics of the samples ZnSe K measured at a frequency of 60 kHz. The positive voltage corresponds to the ZnSe side biassed positively.

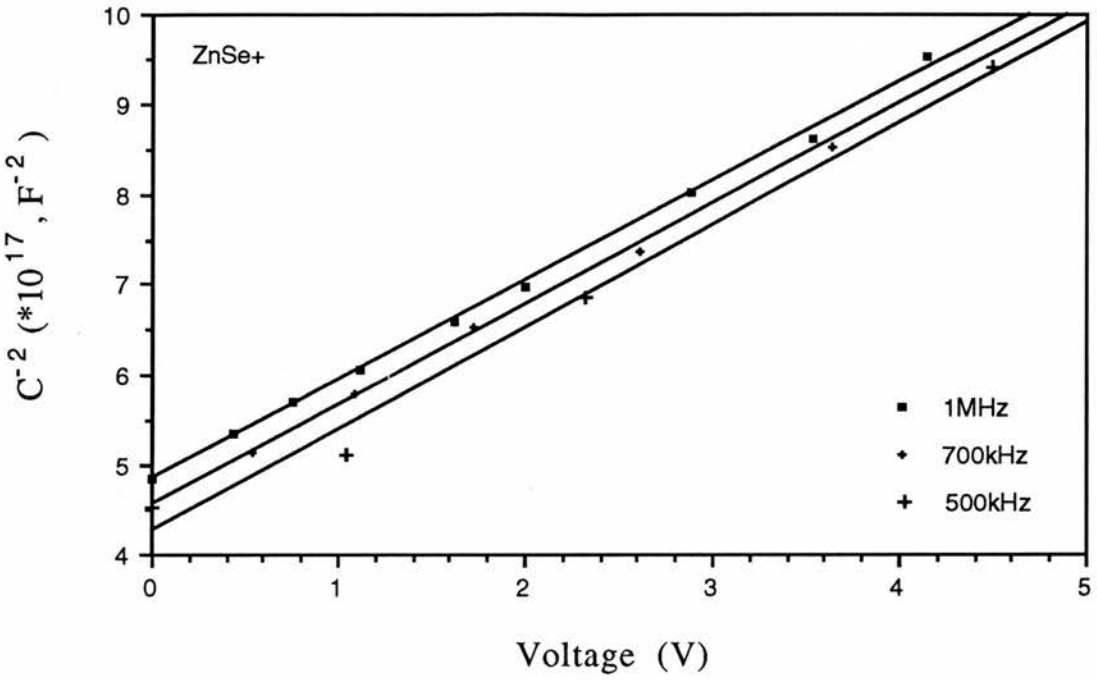

Fig.6.8: The C-V characteristics of the sample HL1-002 measured at different frequencies.

6.3.3 The results of the open-circuit photovoltage measurements

Fig.6.9 shows the characteristics of the open-circuit photovoltage against the photon energy for the samples ZnSe K. For the samples without and with annealing at 390°C, the positive polarity of the open-circuit photovoltage is on the ZnSe side, as labelled "ZnSe+" in the figure. It had no change when the photon energy varied from 1.35 eV to 2.82 eV. However, after annealing at 400°C, the polarity of the open-circuit photovoltage changed in different regions of photon energy. From 1.35 eV to 1.55 eV the ZnSe side was positive; above 1.55 eV its polarity became negative, as labelled "ZnSe-". The same phenomena were observed in other samples as well, and the photon energy at which the polarity started to change seemed slightly different from sample

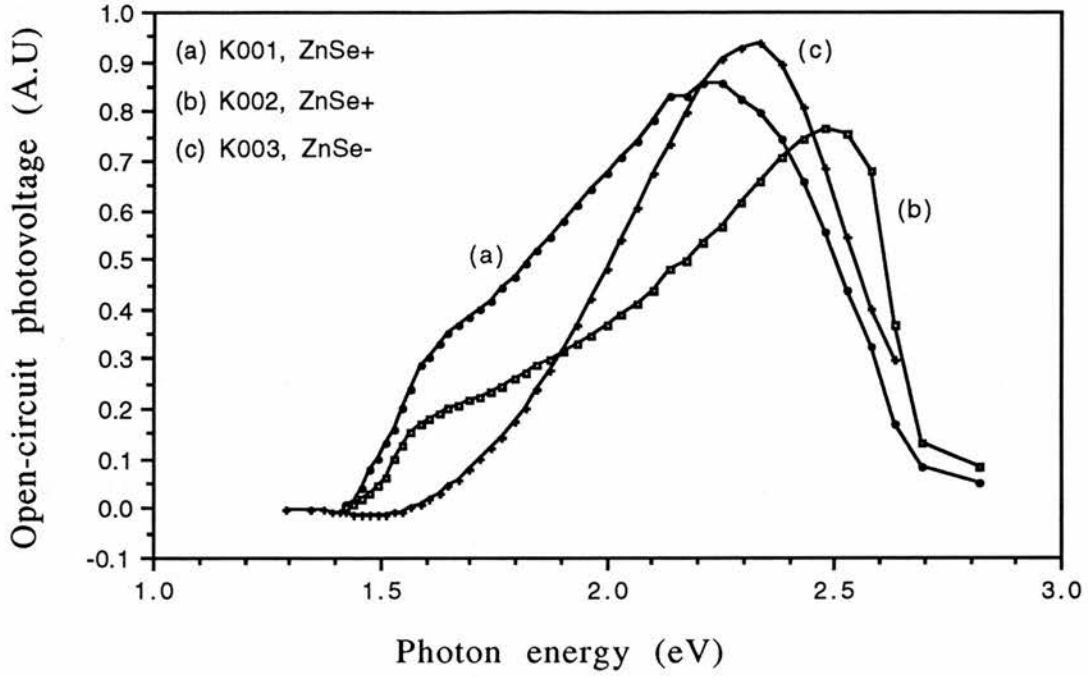

Fig.6.9: The dependences of the open-circuit photovoltage on photon energy for the samples K. (a) and (b) for the samples K001 and K002. The polarity of their open-circuit photovoltages is positive on the ZnSe side; (c) for the sample K003 and the polarity of the open-circuit photovoltage has been changed from positive to the negative on the ZnSe side when the photon energy is greater than about 1.55 eV.

to sample. The characteristic of the open-circuit photovoltage against the photon energy for the sample HL1-003 annealed at 380°C is shown in Fig.6.10 where the negative polarity is on the ZnSe side in the measured energy range (from 1.35 eV to 4.00 eV). In Fig.6.9 and Fig.6.10, the spectra of the open-circuit photovoltages are corrected for the photon flux and plotted on an arbitrary scale. In practice, the magnitude of the open-circuit photovoltages in Fig.6.9 was much greater than that in Fig.6.10.

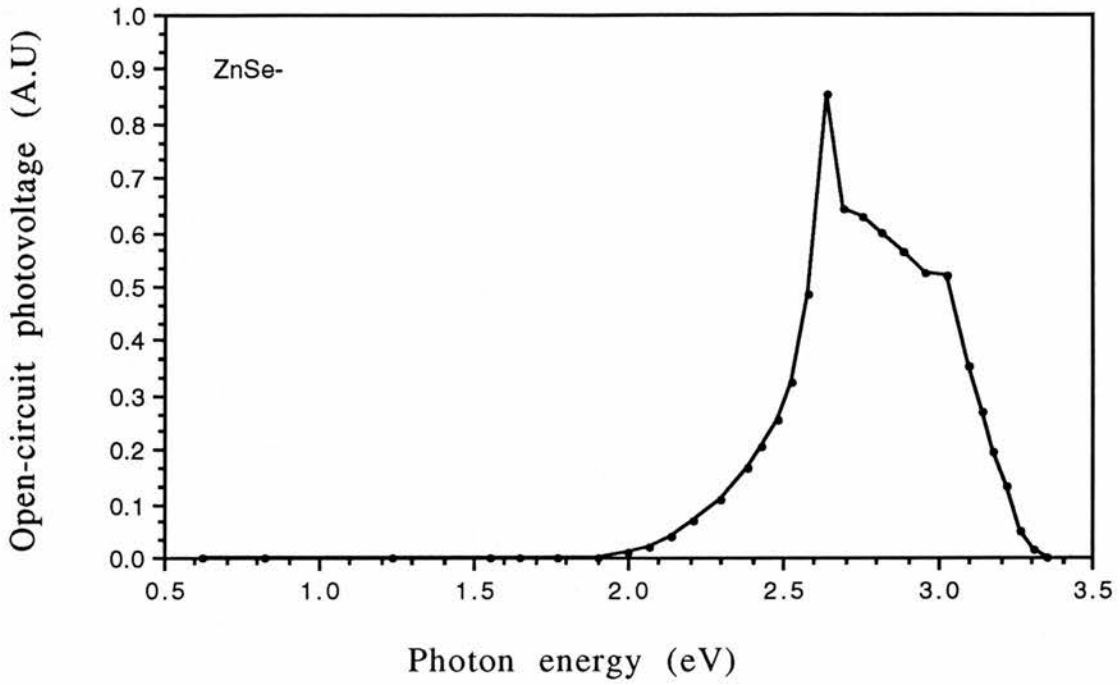

Fig.6.10: The dependence of the open-circuit photovoltage on photon energy for the sample HL1-003. The polarity of the open-circuit photovoltage is negative on the ZnSe side.

6.4 The background theories

6.4.1 The space-charge-limited current through an insulator

Before we discuss the results of the I-V measurements, it is necessary to review the knowledge of space-charge-limited current briefly, especially in the phenomenological analysis.

In 1940, on the basis of the energy-band viewpoint, Mott and Gurnney [25] pointed out that an insulator should be able to carry an electronic current if electrons were injected into it by a suitable contact. Such currents were first observed experimentally by Smith and Rose in CdS in the early 1950's [87]. The theoretical analysis of space-charge-limited current is very complicated. The I-V characteristics due to the space-charge-limited current are not unique. They vary from material to material which have different energy-level

positions and different distributions of trap centres, which can result in a greatly reduced current at lower injection levels. In addition, they will show different characteristics in high field conditions because of the field-dependent drift mobility. For simplicity, we only take the simplest situation, in which all the trap centres lie at a discrete energy level, to understand the key features of the relevant I-V characteristics.

The equations that govern the behaviour of steady-state, one carrier space-charge-limited current are the current continuity equation, Poisson's equation and the steady-state equilibrium equation relating the free-electron concentration to the trapped-electron concentration in the different traps at the same position in space. By the simplified theory in one dimension [88], they are

$$J = en\mu E \tag{6.4}$$

$$(\frac{\varepsilon}{e})(\frac{dE}{dx}) = n - n_o + \Sigma_j (n_j - n_{Tj,o}) \tag{6.5}$$

where j denotes the jth set of traps. Here $n=n(x)$ and $n_{Tj}=n_{Tj}(x)$ are the actual, spatially varying free electron concentration and trapped electron concentration in the jth set of traps respectively, and n_o, $n_{Tj,o}$ are the corresponding, constant, thermal equilibrium values in the bulk, neutral insulator far away from the contacts and surfaces. E is the electric field. ε is the dielectric constant of the insulator.

For the perfect trap-free insulator, there are neither thermal free carriers nor trapping states in the solid, that is n_o and all the n_{Tj} are identically zero in equation (6.5). So we obtain

$$(\frac{\varepsilon}{e})(\frac{dE}{dx}) = n. \tag{6.6}$$

Taking the boundary condition as E(0)=0, and integrating the equation, it gives the current-voltage characteristic

$$J = (\frac{9}{8})\,\varepsilon\mu\,(\frac{V^2}{L^3}) \tag{6.7}$$

where μ is the mobility and L is the thickness of the insulator. It is referred to as the trap-free square law.

For the perfect insulator with a single set of traps shallow enough to be in thermal equilibrium with the conduction band, the equation (6.5) can be written as

$$(\frac{\varepsilon}{e})(\frac{dE}{dx}) \approx (\frac{1}{\theta})(n-n_o). \tag{6.8}$$

Here θ is given by

$$\theta = \frac{n(x)}{n_T(x)} = \frac{N_c}{N_T}\exp(-\frac{E_T}{kT}) \tag{6.9}$$

where N_c is the effective density of states in the conduction band, E_T is the trap position with respect to the conduction band, N_T is the total trap concentration. Then the square law is obtained as follows

$$J = (\frac{9}{8})\,\theta\varepsilon\mu\,(\frac{V^2}{L^3}). \tag{6.10}$$

As the voltage is continuously increased, this square law region will terminate in a steeply rising current which increases to the trap-free curve of equation (6.7) as the traps at E_T are filled. In this case, the density N_T of traps can be determined from the voltage V_{tfl} at which the traps are filled and the current rises abruptly, that is

$$N_T = \frac{2\varepsilon V_{tfl}}{L^2 e}. \tag{6.11}$$

If the square law portion of SCLC (space-charge-limited current) curve obeying equation (6.10) is measured as a function of temperature so that a plot of $\ln\theta$ vs $\frac{1}{T}$ is possible, then E_T and N_T can be obtained without reference to the value V_{tfl} in the light of the equation (6.9).

For an insulator with a single set of deep traps, the equation (6.9) will not hold further. Ohm's law will be obtained up to the voltage V_{tfl} required to fill the set of deep traps. It is followed by a steeply rising current. After all deep traps have been filled, the characteristic merges with the trap-free square law. In this case, we cannot get the density of deep traps directly. Instead, we can get

$$p_{T,o} = \frac{2\varepsilon V_{tfl}}{L^2 e} \qquad (6.12)$$

where $p_{T,o}$ is the unfilled trap density.

In summary, in a logJ-logV plot, the most important feature related to the space-charge-limited current is a nearly vertical current rise due to the filling of trap centres.

6.4.2 The capacitance of the heterojunction interfaces

Before discussing the interpretation of the data, the expected properties of heterojunctions are discussed. Because the band-gaps of ZnSe and GaAs are very different, there might exist some kinds of band-bendings taking place at both sides of the heterojunction interface. So for the MOCVD grown n-ZnSe/n-GaAs epilayers, the capacitance could come from the depletion layer capacitance, due to the band-bending, and the interfacial layer which possibly exists.

For an ideal, single depletion layer, as in an ideal metal-semiconductor structure, the capacitance C_d is related to the applied voltage V by the expression

$$\frac{1}{C_d^2} = \frac{2}{\varepsilon_s \varepsilon_o en} (V+V_d) \qquad (6.13)$$

where n is the carrier concentration, and V_d the built-in barrier potential. If the experimental results have this form, a graph of C_d^{-2} vs V will be a straight line with the intercept on the voltage axis equal to V_d. The carrier concentration n can be calculated from the slope of the line.

For the mixed structure of an insulating layer and a depletion layer, such as the MIS structure, the capacitance expression is no longer as simple as equation (6.13). There could be some kinds of charged states in the insulating layer or at the interfaces. The time response of these charged states can cause dispersion of the observed capacitance. When the insulating layer is thin, these charged states are usually called the interface states. The capacitance calculation for a MIS structure, even with a thin insulating layer, is complicated when the presence of interface states cannot be ignored. It has been investigated by many physicists [89-93]. When the interface state is a single level, the equivalent circuit of a MIS structure can be simplified [93] as shown in Fig.6.11. It is the depletion layer capacitance C_d in parallel with the

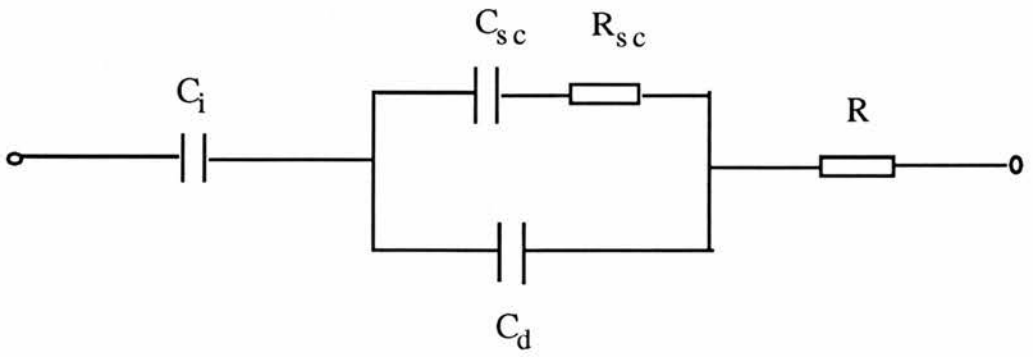

Fig.6.11: The equivalent circuit of the MIS structure. C_d is the depletion layer capacitance; C_{sc} is the interface state capacitance; C_i is the insulating layer capacitance; R is the bulk resistance; R_{sc} is the interface state resistance.

interface state capacitance C_{sc} and that combination then in series with the insulating layer capacitance C_i. The depletion layer capacitance still obeys equation (6.13). The insulating layer capacitance behaves like a plate capacitor which follows $C_i = \frac{A\varepsilon_s\varepsilon_o}{L}$, where L is the thickness of the insulating layer. If the insulating layer is very thin, C_i can be neglected in this equivalent circuit. Shockley and Read [94] have calculated the interface state capacitance in this case, which is

$$C_{sc} = \frac{C_{sc}'}{1+\omega^2\tau^2} \tag{6.14}$$

and

$$C_{sc}' = e^2 N_s f_0(1-f_0)/kT \tag{6.15}$$

where e is the electronic charge, N_s is the interface state density, f_0 is the Fermi function, k is Boltzmann's constant, T is the absolute temperature, ω is the angular frequency of the ac signal and τ is the time constant. This capacitance is time dependent. If the time constant of the interface states is slow compared with the time response of the depletion layer, it can be seen from equation (6.14) that the total parallel capacitance may be dominated by C_d when the frequency of the ac signal is high. This is why, in practice, the carrier concentration can be obtained in a Schottky diode by the C-V measurement performed at high frequency when the inevitable oxide layer between the metal and the semiconductor is thin enough.

However, if the thickness of the insulating layer is big enough, the total capacitance of this equivalent circuit is then dominated by the insulating layer capacitance C_i no matter what the frequency of an ac signal is.

6.5 Discussion

Because the I-V characteristics between two indium dots on the same side (either the ZnSe side or the GaAs side) are linear in both current directions, it indicates that the indium contacts are good ohmic contacts. The resistances (listed in Table 6.1 and Table 6.2) between two indium dots on the ZnSe side are not very high for the samples with and without heat treatments except for the sample HL1-005. Although the exact resistivities of the ZnSe epilayers cannot be calculated from these values, they show clearly that the ZnSe epilayers are still conducting after different heat treatments. So the nonlinear I-V characteristics and C-V characteristics measured between two indium dots on different sides must only come from the heterojunction interfaces.

For the sample HL1-002 without annealing, the C^{-2}-V characteristic, as shown in Fig.6.8, is a very good straight line and it is slightly dependent on frequency in the high frequency range of 0.5~1.2 MHz. It indicates that the capacitance of the heterojunction interface is dominated by a depletion layer capacitance, as discussed in the last section. So there might be a depletion layer, which is possibly due to a conduction band-bending at the n-ZnSe/n-GaAs interface. At a frequency of 50 kHz or less than 50 kHz the capacitance of the heterojunction interface remains a constant as the applied voltage increases. This phenomenon suggests that there might be also an insulating layer at the heterojunction interface. In this case, the insulating layer capacitances C_i becomes dominant. It will be seen below that this suggestion is consistent with other results. The thickness L of the insulating layer can be evaluated by $L=\frac{A\varepsilon_s\varepsilon_o}{C_i}$ where A is the area of the ZnSe surface. It has been listed in Table 6.1. The I-V characteristics of this sample, as seen in Fig.6.3, show that the current with the ZnSe biassed positively is strongly rectified with a current breakdown at a voltage V_0 of about 6.5 V. It is difficult to estimate how many volts are dropped in the insulating layer and how many volts dropped in the depletion layer. If one supposes that the voltage V_0 is

mainly droped in the insulating layer then the electric field in the insulating layer is about $5*10^5$ Vcm^{-1} at which the impact ionization processes may occur (discussed in chapter 2). So the current breakdown might be due to impact ionization processes in the insulating layer. The thickness of the insulating layer is too big for tunneling to take place.

The C-V measurements of the samples HL1 with the post-growth annealing have more obvious evidence that an insulating layer exists at the heterojunction interfaces. Because their capacitances are independent of the bias and frequency in a certain range as seen in Table 6.1 with "less than" signs, the equivalent circuit, in this case, must be just a capacitor C_i and a resistor R in series. The thickness L of the insulating layer can be obtained by the same equation as the above one. They have been listed in Table 6.1 as well. As we can see in Table 6.1, the thickness of insulating layers increases with the increase of annealing temperature.

For the I-V characteristics of the samples HL1 with the post-growth annealing, such as the examples shown in Fig.6.4 and Fig.6.5 for HL1-003 and HL1-004 respectively, there is a steeply rising current region at different applied voltages for different samples with different heat treatments. This is the typical feature of space-charge-limited current as described in section 6.4.1. The voltage at which the current rises abruptly is the so-called trap filled limit voltage V_{tfl}. The voltages, V_{tfl}, for different samples are listed in Table 6.1. The phenomenon indicates that an insulating layer could exist with trap centres at the heterojunction interfaces. This conclusion is consistent with that from the C-V measurements. In Fig.6.5, in the lower applied voltage region, the current increases with the increase of the temperature of measurement. The slope of the line in the logI-logV plot, measured at 21.6°C, is 2.6. At higher temperatures, the slope of the lines remains 6.0 approximately. It means that the ratio θ of the free-electron concentration to the trapped-electron concentration in thermal equilibrium at different

temperatures, as seen in the equation (6.9), has measurable changes. The origin of these trap centres is unknown. However, above the voltage V_{tfl}, the current varies independently of temperature. It is very difficult to analyse the situation of trap level distribution because the present data do not follow any simplified model in theory. It can be seen in Table 6.1 that the voltage V_{tfl} increases as the thickness of the insulating layers increases. The electric fields E_{tfl}, obtained by dividing the voltage V_{tfl} by the thickness, are also listed in Table 6.1. They are all less than $4*10^4$ V/cm which is also less than the threshold field at which the impact ionization takes place in ZnSe, as found in chapter 2. Therefore, the sharp rise in current at V_{tfl} cannot be due to the impact ionization processes. The thickness of the insulating layers is too wide for the tunneling effect to take place.

For the samples ZnSe K, it is difficult to outline the situation of the heterojunction interface from the I-V and C-V characteristics as shown in Fig.6.1, Fig.6.2 and Fig.6.6. Their nonlinear I-V characteristics also show a rectification trend. As the annealing temperature increases, currents become larger in one current direction compared with that in the other direction. Fortunately, the capacitances remain nearly a constant (as shown in Fig.6.7) in a range of applied voltages at a frequency of 60kHz though the currents are not very small. These phenomena are quite similar to what has been observed in the samples HL1 in the I-V and C-V measurements. According to the analysis of the electrical behaviours of the samples HL1, we can, similarly, draw the conclusion that there is an insulating layer and some kind of band barriers at the interfaces. In Table 6.2, the values of C_s are taken from the flat regions in Fig.6.7. They are used to roughly calculate the thicknesses of insulating layers which are listed in Table 6.2 as well. The thicknesses of the insulating layers of the samples K are thinner compared with those of the corresponding samples HL1.

The difference of the I-V characteristics in the two current directions might be due to the existence of a depletion layer or an accumulation layer in either the ZnSe side or the GaAs side, or both adjacent to the insulating layer. When ZnSe is biassed positively or negatively, part of the applied voltage will be dropped in these depletion or accumulation layers which have a different capability to inject electrons into the insulating layer in different current directions.

To further investigate properties of the insulating layer and potential barriers at the heterojunction interfaces, the open-circuit photovoltage measurement was carried out. When electrons or holes are excited to the conduction band or to the valence band by illumination, they can form photocurrents by moving along the built-in electric field produced by the band-bendings at the interfaces. In this case, an open-circuit photovoltage can be measured. Because ZnSe and GaAs have different band-gaps, when the photon energy is greater than the GaAs band-gap 1.43 eV, but less than the ZnSe band-gap 2.7 eV, the ZnSe epilayer will act as "a window" transparent to the incident light on the ZnSe surface unless the ZnSe contains deep centres with high absorption. This allows us to get information about the band-bending in the GaAs side in principle.

Considering a simple Schottky diode on a n-type semiconductor with a single depletion layer, the open-circuit photovoltage can be expressed as

$$V_{oc} = \frac{kT}{q} \ln\left(\frac{qAL_n}{I_0} g_{op} + 1\right) \qquad (6.16)$$

where I_0 is the dark saturation current in reverse bias, g_{op} is the optical generation rate, L_n is the electron diffusion length, A is the area of the Schottky contact. Accordingly, the variation of the open-circuit photovoltage with photon energy depends on the photon energy dependence of the optical generation rate g_{op}. When the photon energy hν is greater than the band-gap

of a direct gap material, the optical generation rate g_{op} is proportional to $\phi(h\nu - E_g)^{1/2}$ where ϕ is the photon flux. So V_{oc} will increase with the increase of photon energy if ϕ is constant. However, V_{oc} cannot increase forever. It is limited by the built-in potential barrier V_d. Therefore, the spectrum of the open-circuit photovoltage vs photon energy can vary from sample to sample because V_d varies.

For the samples K001 and K002, positive open-circuit photovoltages were observed. As can be seen in the spectra in Fig.6.9 (a) and (b) there is a steep rise when the photon energy is near the GaAs band-gap. As the photon energy increases the photovoltage increases as well until the photon energy is near the ZnSe band-gap. It means that when the photon energy is near the GaAs band-gap, the incident light is mainly absorbed by the GaAs region at the interfaces where the band-bending may take place. Then the electron-hole pairs produced by the incident light will move along the electric field due to this band-bending in GaAs to contribute to the positive open-circuit photovoltages. When the photon energy is near the ZnSe band-gap, the incident light is mainly absorbed near the ZnSe surface, away from the interface, where there might be no band-bending if the thickness of the epilayer is thick enough, and then the positive open-circuit photovoltage is rapidly decreased.

In Fig.6.9 (c), as the photon energy increases the polarity of the open-circuit photovoltage changes from positive to the negative at about 1.55 eV, then the photovoltage decreases again when the photon energy is near the band-gap of ZnSe. The observation of the opposite, i.e. the negative, open-circuit photovoltage shows evidence that there might be another opposite band-bending at the interface. Since the negative open-circuit photovoltage was only observed in the energy range less than the band-gap of ZnSe, it seems that the responsible, opposite band-bending is not in the ZnSe side at the

interfaces. There could be another layer, for example the insulating layer, with a band-bending at the interfaces in the opposite direction.

In Fig.6.10, a negative open-circuit photovoltage on the ZnSe side was also observed. However, the spectrum is in the energy range near or greater than the band-gap of ZnSe, especially the spectrum has a maximum at a photon energy corresponding to the band-gap of ZnSe. This feature indicates that in the sample HL1-003 the open-circuit photovoltage might arise from the band-bending in the ZnSe side. In this case, the region of the band-bending should be fairly thick compared with the situation in the samples K.

It seems that the band-bendings at the interfaces of the ZnSe/GaAs system are very complicated. There could be more than one band-bending. The spectrum of the open-circuit photovoltage vs photon energy is actually the sum of contributions of several band-bendings. For the n-ZnSe/n-GaAs structure, if there is an insulating layer at the interface, in thermodynamic equilibrium the Fermi levels of ZnSe and GaAs and the insulating layer between them should be same. In this case, if the Fermi level of the insulating layer is lower than those of n-ZnSe and n-GaAs when they are separated from each other, two back-to-back electron depletion layers would be expected to be formed in the ZnSe side and GaAs side of the interfaces when they are in contact. The band of the insulating layer at the interface can also be slightly bent. Therefore, the spectrum of open-circuit photovoltage could vary from sample to sample depending on the degree of band-bending of different layers. The model of the heterojunctions in the samples in this work is diagrammed in Fig.6.12.

There are two possibilities contributing to the origin of the insulating layer at the interface. One is that lattice defects produced by dislocations could produce a ZnSe insulating region in the ZnSe, but as discussed above it cannot explain the observation of the negative open-circuit photovoltage in the energy range less than the band-gap of ZnSe, as shown in Fig.6.9 (c). The

second one is that a compound of gallium and selenium, such as Ga_2Se_3, produced by chemical reactions is formed at the interfaces. It could be an insulating semiconductor and have a band-bending in the same direction as in the ZnSe. The formation of a Ga_2Se_3 layer at the ZnSe/GaAs interfaces has been recently detected [78,79,80]. In the present work, it has been found that the thickness of the insulating layer increases with an increase of the annealing temperature. However, the techniques used in the present work cannot directly establish the existence of the Ga_2Se_3 compound.

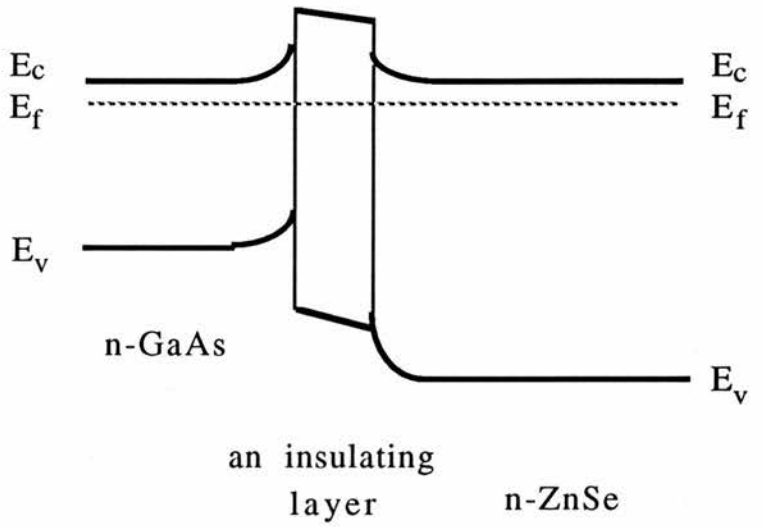

Fig.6.12: A model of the band-bendings at the n-ZnSe/n-GaAs heterojunctions of the samples in this work. Two back-to-back depletion layers occur in the ZnSe side and GaAs side adjacent to the insulating layer at the interface.

Walsh and Mazuruk et al [96] found that there was an electron accumulation layer in the ZnSe side and an electron depletion layer in the GaAs side at the interface in their sample. This might be possible if there is no insulating layer at the interface, depending on the quality of the epilayer.

From this study, the fact is clear that the electrical properties of devices can be affected seriously by the presence of heterojunctions. It could cause new

phenomena, such as the space-charge-limited current, and play an important part in the design of devices. For example, for the purpose of producing blue LED's using the ZnSe/GaAs structure, the problem of heterojunctions could be very important, even when a conducting p-ZnSe epilayer can be readily grown [95].

Table 6.1: The relevant experimental parameters and results for the samples HL1. They are, respectively, sample, annealing temperature, series capacitance of heterojunction, measurement frequency, series resistance of heterojunction, resistance of ZnSe epilayer, thickness of insulating layer, trap-filled-limit voltage and corresponding electric field.

Sample	Annealing	C_S(pF)	f(MHz)	R_S(Ω)	$R_{I\text{-}V}$(kΩ)	L (μm)	V_{tfl}(V)	E_{tfl}(V/cm)
HL1-001	350°C	1000	< 0.08	450	0.80	0.40	1.50	$3.75*10^4$
HL1-002	-----	2000	< 0.05	90	0.65	0.13		
HL1-003	380°C	193	< 0.5	2000	3.80	1.70	2.85	$1.68*10^4$
HL1-004	370°C	350	< 0.5	600	1.40	1.10	2.10	$1.90*10^4$
HL1-005	395°C	165	< 1.0	∞	20000	1.90	> 4.00	$2.10*10^4$

Table 6.2: The relevant experimental parameters and results for the samples K. They are, respectively, sample, annealing temperature, series capacitance of heterojunction, resistance of ZnSe epilayer and thickness of insulating layer.

Sample	Annealing	C_S (pF)	$R_{I\text{-}V}$ (Ω)	L (A)
K001	----	4800	2.6	680
K002	390°C	2650	21.0	1780
K003	400°C	1200	53.0	2510

6.6 Conclusions

The electrical properties of the n-ZnSe/n-GaAs structure can be affected seriously by the presence of an insulating layer at the heterojunction interface. The width of this insulating layer increases with the increase of the annealing temperature. The band-bendings at the interface can be qualitatively interpreted with a model of two back-to-back electron depletion layers in the ZnSe side and GaAs side at the interface.

This work shows an example of how to outline some electrical properties of heterojunctions with conventional experimental methods. Solving problems related to the heterojunction interfaces might be one of the most important steps towards the applications of ZnSe/GaAs structure devices.

Chapter 7

Conclusions

The work in this thesis is mainly focussed on three aspects. They are the impact ionization processes, the deep levels in ZnSe and ZnS and the n-ZnSe/n-GaAs heterojunctions. In this chapter, the main conclusions in each aspect are reviewed in order to see what progress has been achieved and a prospect of future work is given.

We have re-examined theoretically and experimentally the theories of two-stage impact ionization and band-to-band impact ionization. As a carrier production mechanism, theoretically, there is not much difference in these two theories which means that once both impact ionization processes take place the multiplicative current increases very rapidly (almost double exponentially) with the electric field. Accordingly, both multiplication processes are difficult to control in practice, even though the threshold electric field for the two-stage impact ionization process to take place is expected to be smaller than that for the band-to-band impact ionization process. However, in fact, the present theories are over-simplified. For example, the band structure is often treated theoretically as parabolic which is not true, especially at high energies. Therefore, the two-stage impact ionization is expected to have special features due to the band structure and the state density distribution, such as in the familiar impact excitation process of a luminescent centre in ZnSe: Mn. It is hoped that more precise models will be used in future to describe the impact ionization processes.

Experimentally, we have presented the behaviour of the photocurrent in a wide range of electric fields on various ZnSe samples, such as epilayer and bulk samples. The photoconductivity process with recombination at lower fields followed by a photoconductivity process without recombination at higher field have been identified by calculating more accurately the electric

field in good Schottky diodes. Only one multiplication process was observed in our samples at higher fields. It is attributed to the band-to-band impact ionization. For the two-stage impact ionization, it is found that the required deep level concentration is very high. For an active layer of 1 μm, in order to obtain a multiplication factor of 2, the deep level concentration is required to be at least 10^{19} cm^{-3} if we suppose the ionization cross-section is about 10^{-16} cm^2 which is of the order of the geometrical cross-section. Such a high deep level concentration is difficult to be realised generally by doping impurities because of the impurity solubility in a solid. This high-concentration requirement raises a severe challenge for the application of two-stage impact ionization.

In the aspect of the investigation of deep levels in ZnSe and ZnS, first of all we have made the extensive measurements on a ZnSe bulk sample, deliberately doped with cobalt impurity, by the DLSS photocapacitance method. It has been demonstrated that the DLSS photocapacitance method has its peculiar advantage when more than one deep level are present within the band-gap of the same sample. It is known that deep levels can be distinguished by their distinctive photoionization cross-section spectra. By choosing different pump light photon energies, we have successfully separated the different deep levels by separating their characteristic photoionization cross-section spectra.

By analysing the results obtained in our work and previous work, four unintentionally-doped deep centres have been further distinguished in the lower half of the band-gap in ZnSe. They are the L1-centre, the L2-centre, the M-centre and the L4-centre. The energy positions of the L1-centre and the M-centre are 0.50 eV and 0.68 eV above the valence band respectively. The accurate energy positions of the L2-centre and the L4-centre are still unknown. They could be close to the position of the M-centre. A new centre, labelled L3, is also found in our work. Its origin is unknown. However, it is

suggested to be related to the presence of the cobalt impurity because so far it has been only observed in the Co-doped ZnSe samples. The Co d^7 ground level in ZnSe is then estimated to be at about 2.4 eV below the conduction band by the analysis of the previous spectra obtained by photocapacitance measurements.

In ZnS, in previous work, several deep levels have been found in unintentionally-doped bulk ZnS samples. In our work, a deep centre is found in the lower half of the band-gap in a MOCVD grown ZnS epilayer sample by the junction photocurrent measurement. The characteristic hole photoionization cross-section spectrum of this deep centre, which is clearer than in previous work, shows a similarity in shape to that of the M-centre in ZnSe. This deep centre is then labelled M'. Its energy position is at about 0.78 eV above the valence band. It is very possible that the M-centre in ZnSe and the M'-centre in ZnS have the same kind of origin because of the similarity of their spectra.

It has been known for a long time that ZnSe and ZnS are good phosphors with wide band-gaps which can cover the whole visible band up to ultra-violet light. However, it is difficult to get strong near-band-edge luminescence because of the presence of unintentionally-doped deep centres. These are either non-radiative centres or luminescent centres. One of the common luminescent centres in ZnSe and ZnS is the self-activated (SA) centre. It gives a broad emission band.

Using optical quenching of the self-activated luminescence, we have concentrated on the identification of the self-activated centres in both ZnSe and ZnS with those deep centres found in undoped ZnSe and ZnS by junction techniques. The optical quenching spectra of the self-activated luminescence and the photoionization cross-section spectra obtained in ZnSe and ZnS in our work and in the literature are compared. It is found that there are more than one deep centre involved in the optical quenching process of

the self-activated luminescence. They are the OSA-centre and the OM-centre in ZnSe and the OSA'-centre and the OM'-centre in ZnS. The OM-centre and the OM'-centre are, respectively, identified with the M-centre and the M'-centre by the agreements between their optical quenching spectra and their photoionization cross-section spectra. The OSA'-centre is identified with the self-activated (SA) centre in ZnS by the agreement between its optical quenching spectrum and its EPR bleaching rate spectrum. Since great similarities have been found in both the optical quenching spectra and photoionization cross-section spectra in ZnSe and ZnS, the OSA-centre in ZnSe is then suggested to be the SA-centre. The OSA-centre is also suggested to be the L4-centre in ZnSe because of the fairly good agreement between its optical quenching spectrum and its photoionization cross-section spectrum.

We have proposed a model involving three deep centres to successfully explain these optical quenching processes in terms of hole transfer between different centres. According to this model, there could be many centres to affect the optical quenching process of one luminescence band. In this case the optical quenching spectra of different centres cannot be separated from each other. So, generally, an optical quenching experiment does not allow us to identify centres with any certainty without further information.

From the studies of deep levels in ZnSe and ZnS, it can be seen that the M-centre in ZnSe and the M'-centre in ZnS are ubiquitous. Although we have suggested that they may have the same kind of origin, their origins are still unknown. Further investigation of the M-centre in ZnSe and the M'-centre in ZnS, including their accurate concentrations and their absolute photoionization cross-sections, will be an important task in future.

Finally, we have used conventional I-V and C-V measurements to test the properties of n-ZnSe/n-GaAs heterojunctions grown by MOCVD and the effect of the post-growth annealing on these heterojunctions. An insulating layer has been found in most of our samples. The electrical properties of the

heterojunctions, therefore, are severely affected by this insulating layer. The I-V characteristics are nonlinear and the current in one direction is larger than that in the other direction. The effect of the post-growth annealing is to increase the thickness of the insulating layer at the interfaces.

The existence of the heterojunction at the interface will increase the voltage which is required for driving devices. To minimize this heterojunction effect and grow crystals with minimized defects, a lot of effort is being made to improve the MOCVD and MBE growth techniques. They include the purification of the growth sources, the surface etching and preparation procedures, the growth temperature, the gas flux ratios and so on. Recently, the breakthroughs in blue-green lasers, made of $ZnSe_xS_{1-x}$ epilayers grown on p-GaAs or n-GaAs substrates by MBE, have been achieved at 3M Corporate Laboratories in St. Paul, Minnesota, and a collaboration from Brown and Purdue universities in the US. However, there is still a long way to reach the goal of the commercial availability of blue LED's and visible semiconductor lasers.

Reference

[1]. H. J. Round, Electl. Wld. 19, 309 (1907).

[2]. G. Destriau, J. Chim. Phys. 33, 587 (1936).

[3]. T. Inoguchi, M. Takeda, Y. Kakihara, Y. Nakata and M. Yoshida, SID Intern. Symp. Dig. page 86 (1974).

[4]. A. G. Fischer, Radiation Recombination in Semiconductors, page 259, Dunod, Paris (1964).

[5]. A. W. Livingstone, K. Turvey and J. W. Allen, Solid-State Electronics, 16, 351 (1973).

[6]. A. G. Fischer and H. J. Moss, J. Appl. Phys. 34, 2112 (1963).

[7]. T. D. Thompson and J. W. Allen, J. Cryst. Growth, 101, 981 (1990).

[8]. J. W. Allen, Physica Polonica A, 77, 5 (1990).

[9]. P. A. Wolff, Phys, Rev. 95, 1415 (1954).

[10]. W. Shockley, Solid-State Electronics, 2, 35 (1961).

[11]. G. A. Baraff, Phys. Rev. 128, 2507 (1962).

[12]. A. W. Livingstone and J. W. Allen, J. Phys. C: Solid St. Phys. 6, 3491 (1973).

[13]. T. D. Thompson, "Impact Ionization By Hot Electron And Luminescence In ZnS And Other Wide Bandgap Semiconductors", Ph.D. thesis, The University of St. Andrews (1989).

[14]. J. W. Allen, J. Luminescence, 23, 127 (1981).

[15]. K. G. McKay, Phys. Rev. 94, 877 (1954).

[16]. A. G. Chynoweth, Phys. Rev. 109, 1537 (1958).

[17]. J. L. Moll and R. Van Overstraeten, Solid-State Electronics, 6, 147 (1963).

[18]. J. L. Moll, "Physics of Semiconductors", McGraw-Hill, New York (1964).

[19]. S. L. Miller, Phys. Rev. 99, 1234 (1955).

[20]. R. A. Logan and S. M. Sze, J. Phys. Soc. Japan, 21 Suppl. 434 (1966).

[21]. R. A. Logan, A. G. Chynoweth and B. G. Cohen, Phys. Rev. 128, 2518 (1962).

[22]. H. Kressel and G. Kupsky, Internat. J. Electronics, 20, 535 (1966).

[23]. R. A. Logan and H. G. White, Phys. Rev. 134, A761 (1964).

[24]. R. Mach and W. Ludwig, Phys. Stat. Sol. (a), 23, 507 (1974).

[25]. N. F. Mott and R. W. Gurney, "Electronic Processes In Ionic Crystals", Oxford University Press, London and New York (1940).

[26]. J. L. Heaton, G. H. Hammond and R. B. Goldner, Appl. Phys. Lett. 20 (9), 333 (1972).

[27]. A. Etcheberry, M. Etman, B. Fotouti, J. Gautron, J. Appl. Phys. 53, 8867 (1982).

[28]. H. R. Szawelska and J. W. Allen, J. Phys. C: Solid St. Phys. 10, 2115 (1977).

[29]. J. Z. Zheng and J. W. Allen, J. Crystal Growth, 101, 850 (1990).

[30]. N. Gordon, "Luminescence And Its Electrical Excitation In ZnSe And ZnS", Ph.D. thesis, The University of St. Andrews (1982).

[31]. K. Brennan, J. Appl. Phys. 64(8), 4024 (1988).

[32]. J. R. Chelikowsky, T. J. Wagener, J. H. Wraver and A. Jin, Phys. Rev. B, 40(14), 9644 (1989).

[33]. K. Kosai, J. Appl. Phys. 53, 1018 (1982).

[34]. P. Besomi and B. W. Wessels, J. Appl. Phys. 53, 3076 (1982).

[35]. K. Yoneda, Y. Hishida and H. Ishii, Appl. Phys. Lett. 47, 702 (1985).

[36]. H. G. Grimmeiss, C. Ovrén and J. W. Allen, J. Appl. Phys. 47, 1103 (1976).

[37]. H. G. Grimmeiss, C. Ovrén, W. Ludwig and R. Mach, J. Appl. Phys. 48, 5122 (1977).

[38]. H. G. Grimmeiss, C. Ovrén and R. Mach, J. Appl. Phys. 50, 6328 (1979).

[39]. J. Z. Zheng, "Optical Characterization And Device Application Of The Semiconductors ZnSe And ZnS", Ph.D. thesis, The University of St. Andrews (1990).

[40]. J. W. Allen and J. Z. Zheng, Phys. Rev. B, 44, 9039 (1991).

[41]. J. Z. Zheng, J. W. Allen, H. M. Yates and J. O. Williams, J. Crystal Growth, 117, 358 (1992).

[42]. S. Iida, J. Phys. Soc. Japan, 26, 1140 (1969).

[43]. J. M. Noras, H. R. Szawelska and J. W. Allen, J. Phys. C: Solid State Phys. 14, 3255 (1981).

[44]. H. G. Grimmeiss and C. Ovrén, J. Phys. E: Sci. Instrum. 14, 1032 (1981).

[45]. A. P. Radlinski, Phys. Stat. Sol. (b) 84, 503 (1977).

[46]. J. M. Noras J. Phys. C: Solid St. Phys. 13, 4779 (1980).

[47]. A. G. O'Neill and J. W. Allen, Solid State Commun. 46, 833 (1983).

[48]. P. J. Dean, Phys. Status Solidi, A81, 625 (1984).

[49]. H. Kukimoto, S. Shionoya, T. Koda and R. Hioki, J. Phys. Chem. Solids, 29, 935 (1968).

[50]. J-O Fornell, H. G. Grimmeiss, R. Mach and G. O. Muller, Semicond. Sci. Technol. 3, 511 (1988).

[51]. J. Z. Zheng and J. W. Allen, Semicond. Sci. Technol. 5, 1013 (1990).

[52]. C. R. Crowell, W. G. Spitzer, L. E. Howarth and E. E. LaBate, Phys, Rev. 127, 2006 (1962).

[53]. H. G. Grimmeiss, Ann. Rev. Mater. Sci. 7, 341 (1977).

[54]. S. Braun and H. G. Grimmeiss, J. Appl. Phys. 44, 2789 (1973).

[55]. G. B. Stringfellow and R. H. Bube, Phys. Rev. 171, 903 (1968).

[56]. G. B. Stringfellow and R. H. Bube, J. Appl. Phys. 39, 3657 (1968).

[57]. S. Iida, J. Phys. Soc. Japan. 25, 177 (1968).

[58]. T. Koda and S. Shionoya, Phys. Rev. 136, A541 (1964).

[59]. G. H. Blount, A. C. Sanderson and R. H. Bube, J. Appl. Phys. 38, 4409 (1967).

[60]. C. S. Kang, P. B. P. Phipps and R. H. Bube, Phys. Rev. 156, 998 (1967).

[61]. J. S. Prener and F. E. Williams, J. Chem. Phys. 25, 361 (1956).

[62]. P. H. Kasai and Y. Otomo, Phys. Rev. Letters, 7, 17 (1961).

[63]. P. H. Kasai and Y. Otomo, J. Chem. Phys. 37, 1263 (1962).

[64]. J. Schneider, A. Räuber, B. Dischler, T. L. Estle and W. C. Holton, J. Chem. Phys. 42, 1839 (1965).

[65]. J. Schneider, B. Dischler and A. Räuber, J. Phys. Chem. Solids, 31, 337 (1970).

[66]. G. D. Watkins, Solid State Communications, 12, 589 (1973).

[67]. V. A. Räuber, J. Schneider and F. Matossi, Z. Naturforschg. 17 a, 654 (1962).

[68]. W. A. Harrison, J. Vac. Sci. Technol. 14, 1016 (1977).

[69]. W. R. Frensley and H. Kroemer, J. Vac. Sci. Technol. 13, 810 (1976).

[70]. R. J. Anderson, Solid-St. Electron. 5, 341 (1962).

[71]. W. Shockley, Bell Syst. Tech. J. 28, 435 (1949).

[72]. J. Tersoff, Phys. Rev. B30 4874 (1984); see also Phys. Rev. Lett. 52, 465 (1984).

[73]. H. Unlu and A. Nussbaum, Solid State Electronics, 30 (11), 1095 (1987).

[74]. H. Kroemer, VLSI Electronics: Microstructure Science, 10, 121 (1985).

[75]. J. Petruzzello, B. L. Greenberg, D. A. Cammack and R. Dalby, J. Appl. Phys. 63, 2299 (1988).

[76]. H. M. Yates and J. O. Williams, Appl. Phys. Lett. 51, 809 (1987).

[77]. L. H. Shon, K. Inoue, O. Matsuda, K. Murase, T. Yokogawa and M. Ogura, Solid State Communication, 67, 779 (1988).

[78]. D. Li, J. M. Gonsalves, N. Otsuka, J. Qiu, M. Kobayashi and R. L Gunshor, Appl. Phys. Lett. 57, 449 (1990).

[79]. J. Qiu, D. R. Menke, M. Kobayashi, R. L. Gunshor, D. Li, Y. Nakamura and N. Otsuka, Appl. Phys. Lett. 58, 2788 (1990).

[80]. A. Krost, W. Richter, D. R. T. Zahn, K. Hingerl and H. Sitter, Appl. Phys. Lett. 57, 1981 (1990).

[81]. A. Nakagawa, H. Kroemer and J. H. English, Appl. Phys. Lett. 54, 1893 (1989).

[82]. D. W. Tu and A. Kahn, J. Vac. Sci. Technol. A3, 922 (1985).

[83]. D. Walsh, K. Mazuruk and M. Benzaquen, Phys. Rev. B, 36, 2883 (1987).

[84]. H. V. Houten, S. Colak, T. Marshall and D. A. Cammack, J. Appl. Phys. 66, 3047 (1989).

[85]. Q. D. Qian, J. Qiu, M. R. Melloch, J. A. Cooper, J. L. A. Kolodziejski, M. Kibayashi and R. L. Gunshor, Appl. Phys. Lett. 54, 1359 (1989).

[86]. T. Marshall, S. Colak, H. V. Houten, J. Petruzzello, B. Greenberg and D. Cammack, Mat. Res. Soc. Symp. Proc. 145, 441 (1989).

[87]. R. W. Smith and A. Rose, Phys. Rev. 97, 1531 (1955).

[88]. M. A. Lampert and P. Mark, "Current Injection In Solids", Academic Press, New York, London, Toronto, Sydney, San Francisco (1970).

[89]. A. M. Goodman, J. Appl. Phys. 34, 329 (1963).

[90]. A. M. Cowley, J. Appl. Phys. 37, 3024 (1966).

[91]. H. C. Card and E. H. Rhoderick, J. Phys. D, 4, 1589 (1971).

[92]. S. J. Fonash, J. Appl. Phys. 54(4), 1966 (1983).

[93]. E. H. Nicollian and A. Goetzberger, Bell Syst. Tech. J. 46 (3), 1055 (1967).

[94]. W. Shockley and W. T. Read, Phys. Rev. 87, 835 (1952).

[95]. M. A. Haase, H. Cheng, J. M. DePuydt and J. E. Potts, J. Appl. Phys. 67(1), 448 (1990).

[96]. D. Walsh, K. Mazuruk, M. Benzaquen and P. Weissfloch, Semicond. Sci. Technol. 3, 116 (1988).